University of Alberta

Automatic Test Data Generation Using Genetic Algorithm and Program Dependence Graphs

By

Hao Zhang 

A thesis submitted to the Faculty of Graduate Studies and Research in partial fulfillment of the requirements for the degree of Master of Science

Department of Electrical and Computer Engineering

Edmonton, Alberta

Spring 2004

Your file Votre référence
ISBN: 0-612-96573-2
Our file Notre référence
ISBN: 0-612-96573-2

Abstract

The complexity of software systems has been increasing dramatically in the past decade, and software testing as a most labor-intensive component becomes more and more expensive. Software costs at least 50% of the total expense of software development, so any techniques leading to automatic generation of test data will have great potential to considerably reduce the cost. Existing approaches of automatic test data generation have achieved some success of using evolutionary computation algorithms as their optimization techniques to transform problems of test data generation to optimization problems, but they are unable to deal with Boolean variables or enumerated types and they need to be improved in many other aspects. This thesis presents a new approach utilizing program dependence analysis technique and genetic algorithms (GAs) to generate test data. A set of experiments using the new approach is reported to show its effectiveness and efficiency based on the established criterion.

Acknowledgements

I would like to thank the following people:

To my parents, grandparents and brother I would like to thank you all for all your encouragement and support. I am extremely indebted to all of you for everything you have ever done for me.

Dr. Barry Patchett, your knowledge in the materials / welding engineering was and will continue to be an inspiration to me in the years to come. Thank you for your guidance and help over the past few years.

I would also like to thank the members of the IPSCO Inc. Research Center, in particular Brian McCrady and Jon Jackson.

Table of Contents

List of Tables

List of Figures

List of Symbols

Symbol	Meaning
A	area
C_M	compliance of Charpy impact machine
CP	center of percussion
CS	center of strike
CVP	Charpy constant upper shelf energy
CVT	Charpy test energy that corresponds to the full-scale test temperature
CV100	energy at the lowest temperature at which 100% shear is observed
DFP	ductile fracture propagation
DWTT	drop weight tear test
E	energy
E_B	energy consumed by Brinell type deformation at the specimen load points
E_{DIAL}	Charpy dial energy
E_i	initiation energy
E_I	increment of energy required to accelerate the specimen from rest to the velocity of the hammer
E_{INT}	instrumented tup energy
E_{ME}	stored elastic energy absorbed by the machine as a result of the interactions at the specimen load points
E_o	maximum kinetic energy of the hammer prior to impact
E_p	propagation energy

E_{SD}	total energy consumed by bending the specimen
E_{MV}	energy absorbed by the impact machine through vibrations after initial contact with the specimen
g	acceleration due to gravity
h_o	initial height of hammer
m	mass of hammer
P_a	load at the end of unstable crack propagation
P_τ	specific value of load at time τ
P_{gy}	general yield load
P_{iu}	load at the initiation of unstable crack propagation
P_m	maximum load
PN	pressed notch
QA	quality assurance
QC	quality control
SA	shear area
SATT	shear area transition temperature
sg	side groove
v_o	velocity prior to impact

1 INTRODUCTION

Difficulties in relating a full-scale fracture to a Charpy impact test has become an ongoing issue since the development of controlled rolled steels. Several investigators attempted to use the propagation energy relationships between drop weight tear tests (DWTT) and Charpy tests from conventionally rolled steels with rising shelf controlled rolled steels, but the relationship does not hold for Charpy impact energies greater than 104 J. The reason it does not hold for higher absorbed energies is because the relationship assumes the Charpy propagation energy is linearly related to the total absorbed energy, which is not the case for higher toughness steels. Therefore, a total absorbed energy measurement cannot be directly related to the propagation energy. However, instrumentation added to the DWTT and Charpy tests has enabled the differentiation of initiation and propagation energy directly from a load-displacement trace. Comparison of the propagation energy between the two may be possible, but the difference in specimen thickness between the two results in different stress conditions existing in each. The addition of side grooves to the traditional specimens can control the fracture path and change the stress conditions in the specimens, and enable the comparison of propagation energy between DWTT and Charpy impact tests.

To determine if a steady state propagation energy relationship between DWTT and Charpy impact tests can be made, strain gauges have been added to the Charpy's tup to measure the propagation energy from load – displacement data. Side grooves will be

added to the specimens to manipulate their crack front so they will simulate the steady state crack propagation conditions that exist in a pipeline failure.

A literature review of existing propagation energy measurement methods and measurement techniques is covered in Chapter 2. The experimental setup and procedure is covered in Chapter 3. The objective of this project is to assess the fracture propagation toughness in X70 and X80 pipeline steels by using instrumented impact tests and side grooved specimens. The measurement techniques and the effects of side grooves on traditional specimens are covered in Chapter 4. Conclusions and recommendations are given in Chapter 5 with regards to the accuracy of instrumentation and the effects of side grooving on impact testing.

Thus the areas to be examined in this study are:

1) Examine the relationship between Charpy and DWTT energy under plane strain conditions;
2) Examine the accuracy of the current accepted method of energy measurement (instrumented tup), and examine a newly developed measurement technique to assess upper shelf and rising shelf behavior.

2 LITERATURE REVIEW

A fracture issue that still has an uncertain solution in high strength pipeline steels is associated with long running shear cracks. According to Buzzichelli[1] traditional fracture parameters do not describe resistance to crack propagation correctly. Prior to the 1970's crack propagation was believed to occur only by means of a brittle fracture mode, and it was generally accepted that fracture could be controlled by ensuring that the DWTT or Charpy test would exhibit fully ductile behavior at temperatures equal to or less than the pipeline's design temperature. However, this assumption was proven to be wrong when a service failure of a 36 inch X65 pipe in the late 1960's when a ductile fracture propagated approximately 1000 feet.[2, 3] The running ductile crack is only a problem in line pipe[4] and this prompted the examination of the ductile fracture propagation problem in pipeline steels. Detailed examination of this problem led to the development of an equation that related Charpy energy to DWTT energy in the upper shelf region of conventionally rolled steels as shown in Equation 1.[5]

$$(E/A)_{DWTT} = 300 + 3.00\,(E/A)_{Charpy} \quad (ft{\cdot}lb/in^2) \qquad (1)$$

The energy measured by either of these tests was a measurement of total absorbed energy, and the total absorbed energy was subsequently related to the ductile fracture propagation (DFP) toughness in conventionally rolled pipeline steels. This equation is, however, only valid for pipeline steels with a total toughness less than 104 J of CVN as reflected in Figure 2-1.[6, 7]

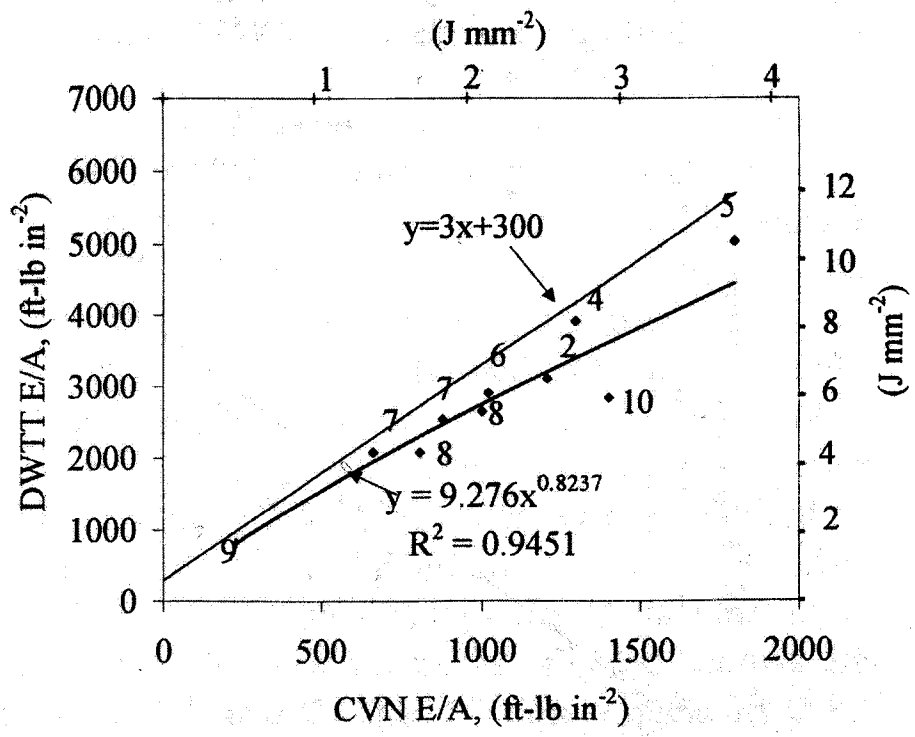

Figure 2-1. Relationship between Specific Energies from Charpy and PN DWTT Specimens[7]

At these lower energy levels the total energy absorbed is primarily the energy necessary to propagate the crack: thus E_{DIAL} can be a good indication of propagation energy for lower toughness materials. Since the correlations are only accurate for low toughness steels that were conventionally rolled, the recent development and extensive application of controlled rolled pipeline steels of high toughness have led to the need for different ductile fracture toughness measurements for steels with medium to high toughness (>100 J).

A quantitative value of propagation toughness in higher strength pipeline steels that has subsequently been used is the use of a crack tip opening angle(CTOA)[8, 9, 10, 11, 12, 13, 14, 15] which is inversely proportional to the crack velocity.

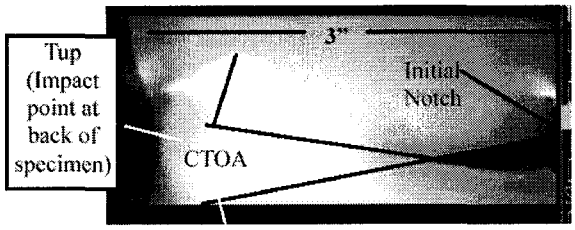

Figure 2-2. Schematic of CTOA[9]

Several investigators have attempted to relate the CTOA to Charpy and DWT test energy values for use as a simple quality assurance test. The CTOA does show promise as a measure to relate a quantitative value to ductile fracture propagation (DFP) toughness, but if a CTOA measurement is to be made with Charpy and DWTT specimens, the fracture stress conditions must be controlled so the energy absorbed by the two tests represent similar stress conditions to that present in full scale burst tests.

Controlling both the fracture path and the stress conditions can occur by side grooving the test specimens, and thus a relatively consistent material property can be measured as the result of minimizing the amount of plastic deformation in a specimen that occurs as the result of existing plane stress conditions in a specimen.

The ability to measure the propagation toughness energy in higher toughness specimens may be addressed by instrumented impact testing of both the Charpy and DWTT specimens. Instrumenting these machines may be a useful tool for separating the propagation energy from the total energy absorbed, but the accuracy and evolution of instrumented impact testing will be studied further.

2.1 Propagation Energy Measurement

A definable plateau exists in conventionally rolled steels, which makes it easy to compare DWTT plateau energy to Charpy plateau energy since CVP is equal to CV100 in this region as seen in Figure 2-3. Thus testing could be performed at any temperature in the upper shelf region and subsequently compared to DWTT plateau energy[16].

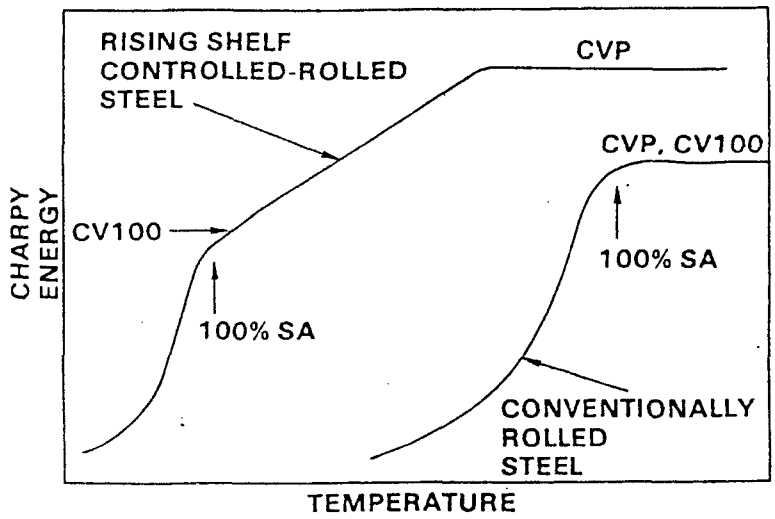

Figure 2-3. Transition curves for conventionally and controlled rolled steels[17]

However, today's controlled rolled steels have different absorbed energies and temperatures at CVP and CV100, which raises the question of at which temperature should both specimens be tested? Because of their rising shelf behavior and shifted transition temperature, Charpy specimens made from high toughness controlled rolled steels may require an appropriate testing temperature for the measurement of propagation toughness depending on where 100% SA fracture occurs. Since the transition curves of conventional DWTT and Charpy tests differ for controlled rolled steels as shown in Figure 2-4, propagation energies should be measured and compared at different points on

the rising and upper shelf regions, so long as 100% SA fracture occurs, to determine the effect of measuring propagation energy at different temperatures.

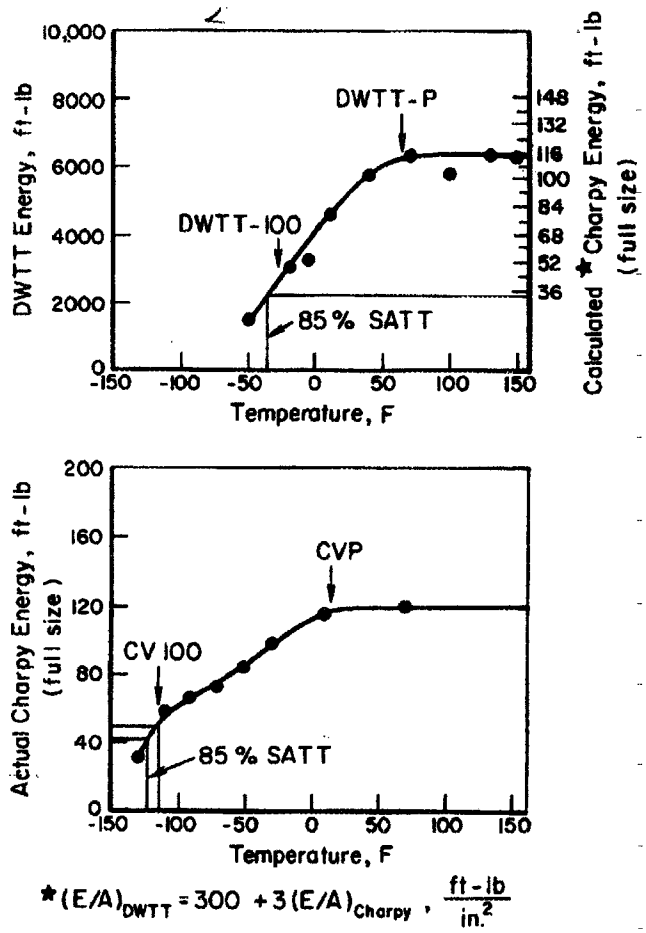

Figure 2-4. Comparison of DWTT and Charpy Energy in controlled rolled steels[5]

Maxey and Wilkowski have attempted to measure the energy using various measures of Charpy energy including CV100, CVP, and the CVT in attempts to extend the energy relationship for conventionally rolled steels to be valid for higher toughness materials as shown in Figure 2-5.

By using this relationship with controlled rolled steels, it was determined that CVP and CVT energies did not improve the correlations with full scale behavior but the CV100 energy did in a conservative way.[6]

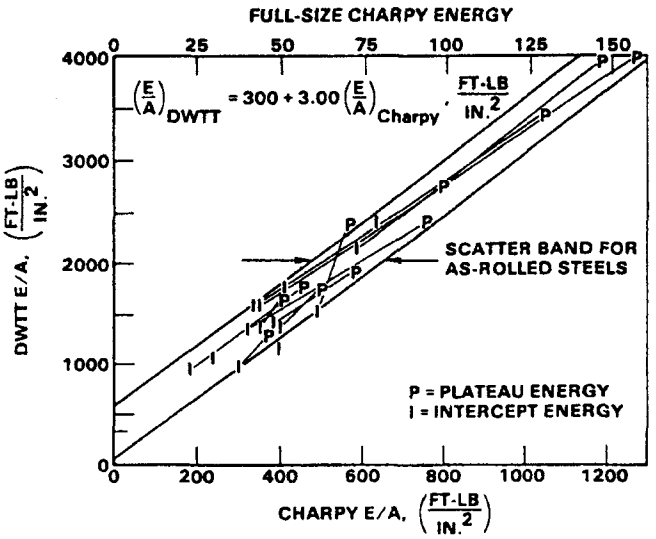

Figure 2-5. Pressed notch DWTT energy per unit area vs. Charpy V-notch energy per unit area for controlled rolled steels with rising shelf energy[6].

This work, by Maxey and Wilkowski was their attempt at trying to preserve the existing method of measuring propagation toughness by finding a Charpy testing temperature for controlled rolled steels that would allow Equation 1 to be functional for steels with rising shelf energies. Their work has shown that Equation 1 can thus be used if the PN-DWTT intercept energies are compared with the similar Charpy intercept energies, or if the plateau energies from each are compared with Equation 1, but only if the total energy absorbed by the Charpy specimens is less than 150 J. If the absorbed energy meets this criterion Charpy energy can be related directly to DWTT energies, otherwise it can not be used with confidence for the propagation toughness of controlled rolled pipeline steels. The reason that Equation 1 does not work with higher toughness materials has been

explained by Wilkowski.[17] This occurs because the energy necessary to initiate a crack does not increase in a linear fashion. This is because the initiation energy in high toughness pipeline steels is a considerable portion of the total energy absorbed. J_{Ic} values are directly proportional to Charpy energy up to about 68 to 95 J. The J_{Ic} values then increase nonlinearly and therefore crack propagation energy may be overestimated with the use of either Charpy or standard DWTT impact specimens for high toughness materials. Therefore, using Equation 1 to describe propagation errs with high toughness steels because of the non-linearity. However, instrumented impact testing can be utilized to differentiate propagation energy from initiation energy and thus the energy necessary to propagate a crack in DWTT and Charpy specimen will be measured with instrumentation.

2.1.1 Determining Ductile or Brittle Failure from load – displacement curves

Because we are concerned with the ductile propagation toughness, differentiating brittle fracture from ductile fracture needs to be addressed. Typically the fracture surface can be used to address this issue but the load-displacement curve also provides a plethora of information about the fracture process, which can be characterized by the load points listed in Figure 2-6 as P_{gy}, P_m, P_{iu}, and P_a.[18, 19]

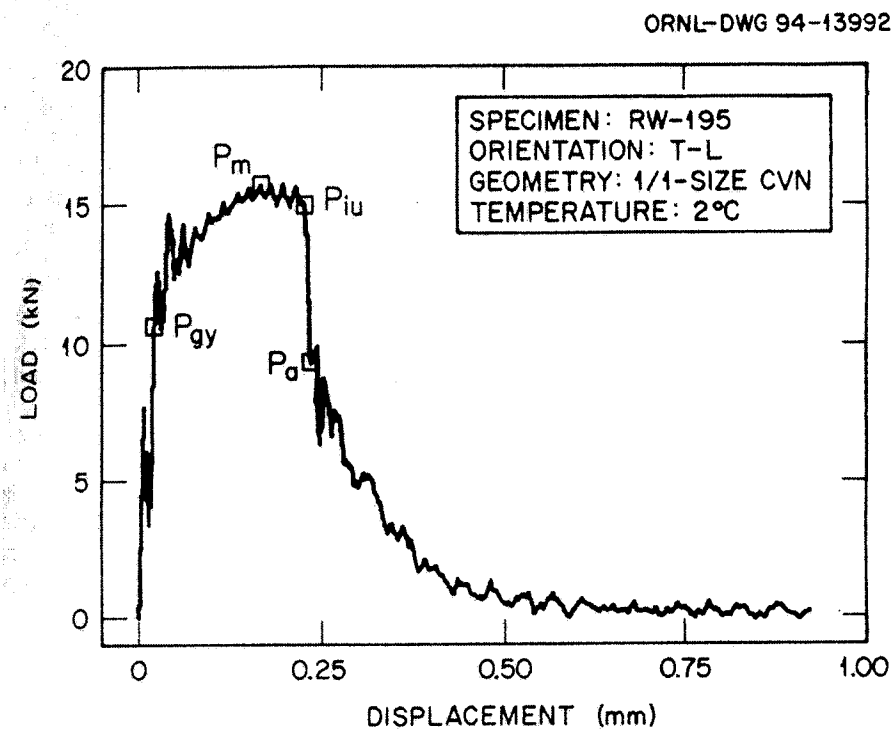

Figure 2-6. Characteristics of a Load vs. Displacement Curve[18]

Literature has characterized these points as general yield, maximum load, unstable crack propagation and finally arrest. A sudden drop in the load as seen in Figure 2-6 signifies that 100% SA fracture does not occur in a specimen but rather the specimen fails at least partially under a brittle fracture mode. The following equation can be used to approximate the percent shear area fracture that occurs in an impact specimen.

$$\% \text{ shear} = [1 - (P_{iu} - P_a)/0.5\,(P_{gy} + P_m)] \times 100\% \qquad (2)$$

Therefore, if a sudden drop is seen between P_{iu} and P_a, brittle fracture is the mode of failure, and hence it can be deduced that the test was not performed in the rising or upper shelf region about which we are concerned.

2.1.2 Specimen Thickness

In Charpy and DWT tests, specimens must reflect an equivalent degree of ductility as those obtained under actual failure conditions, and because the DWTT specimens are full pipe wall thickness they simulate full scale failure and thus their test temperature should be set at the pipeline design temperature for which ductile fracture propagation is a concern. The thickness difference that exists between traditional Charpy and DWTT specimens is the variable that gives rise to different transition temperatures for identical materials as shown by Towers[20, 21] in Figure 2-7. Towers' work was performed on sub-size Charpy specimens but this behavior or trend can be equally compared to a decrease in transition temperature observed between the DWTT and Charpy specimens since the decrease is the result of a transition from plane stress to plane strain conditions.

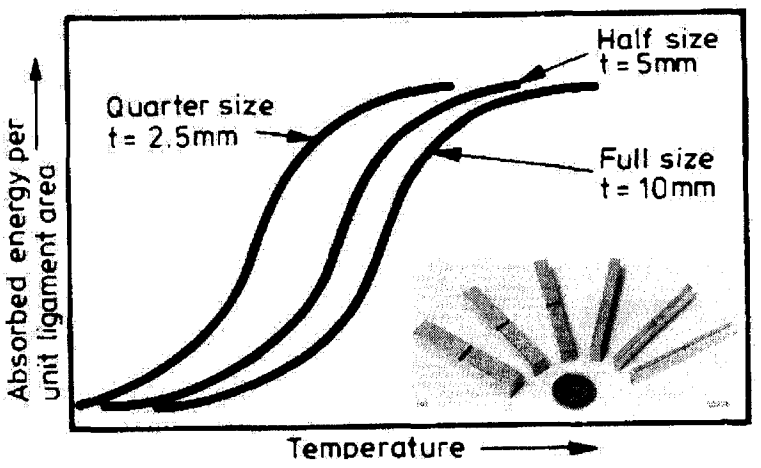

Figure 2-7. Absorbed energy per unit ligament area vs. Temperature[20]

These results again suggest that fracture toughness measurements of traditional Charpy and DWTT specimens may not be comparable at identical temperatures since the stress conditions in each will differ at identical temperatures.

Although Wilkowski and Maxey showed that either the intercept or plateau energies could be used in relationships that used total energy absorbed by the specimens for lower toughness specimens, the effect of intercept and plateau energy on propagation energy measured with instrumentation has not been thoroughly examined.

2.1.3 Stress Conditions and Side Grooves

A problem that arises when performing both Charpy and DWTT is the inability to control the propagation front and stress conditions. Side grooves can be added to both Charpy and DWTT specimens to control both the propagation front and the stress conditions in the specimens.[22, 23, 24, 25]

The stress fields present in traditional Charpy and DWTT specimens differ as a result of their different thickness. Plane strain conditions exist at the center of the specimen, while plane stress conditions exist at the surface of the specimen. Plane stress conditions result from the absence of constraining material at a specimen's surface and will change to plane strain values present at the center of the specimen as depicted in Figure 2-8. Figure 2-8 depicts the resulting plastic zone size in front of the crack tip as calculated by Von Misses yield criterion[26] as shown in Equation 3.

$$(\sigma_1-\sigma_2)^2 + (\sigma_2-\sigma_3)^2 + (\sigma_3-\sigma_1)^2 = 2(\sigma_{ys})^2 \qquad (3)$$

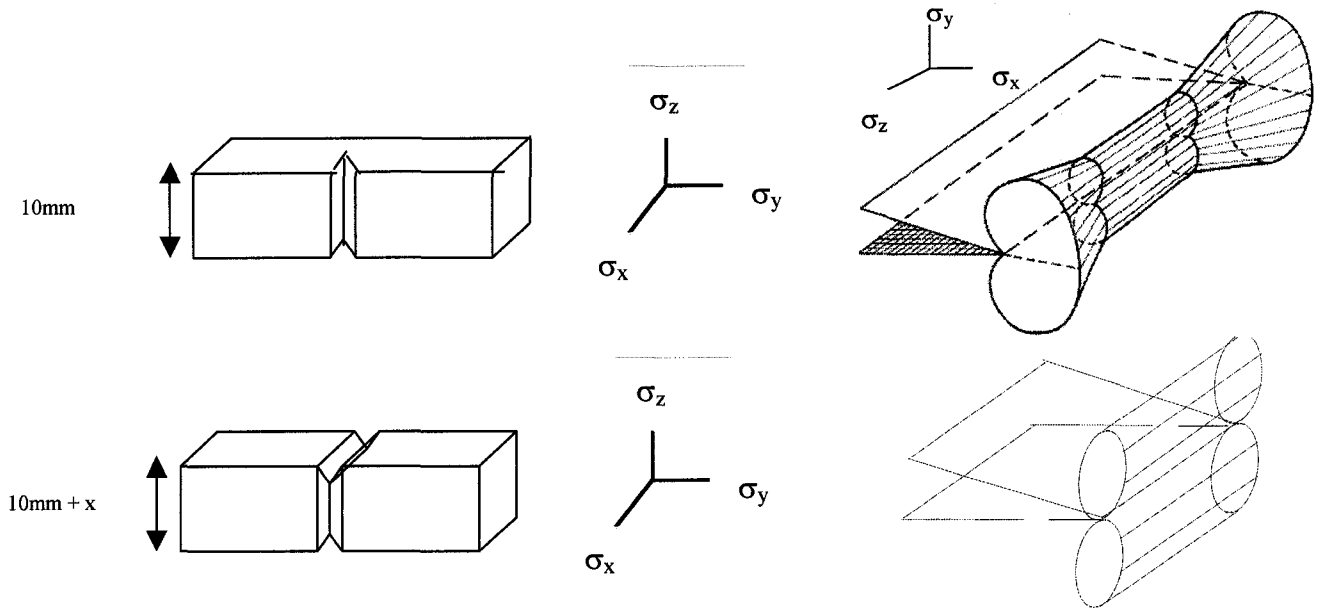

Figure 2-8. Three-dimensional plastic zone with and without side grooves

A different thickness between the two results in different plane strain to plane stress ratios and, as a result, energy relationships may be affected by a specimen's thickness. Full size Charpy samples do not appear to represent a full plane strain condition as evidenced by their much lower transition temperatures when compared with DWTT results for X70 and X80 steels, where much greater sample width and thickness generate much greater plastic constraint at the notch tip.[27] The addition of side grooves to both the Charpy and DWTT specimens may be used to alter the transition temperatures and stress conditions from those obtained with traditional specimens.

Smith and Patchett[23] noted that in traditional Charpy specimens quantitative data cannot be derived from specimens that are less than full wall thickness. The reduced amount of material ahead of the crack tip in addition to the blunt notch reduces the restraint at the base of the notch. Pre-cracking the specimens has been used in some instances to

manipulate the restraint condition at the base of the notch, but there is an uncertain effect of cracking on the remaining cross sectional area and the lack of material restraint in some areas. Smith and Patchett stated that this places some doubt on the use of fatigue pre-cracks in small specimens, and thus they questioned how to use small test specimens while achieving an accurate assessment of fracture toughness (especially in ductile fracture where the effectiveness of the sharp cracks is offset by blunting). Specimen design was a variable that Smith and Patchett considered when attempting to manipulate the restraint conditions from traditional Charpy specimens. Variables that were considered and manipulated when considering a specimens design were both notch acuity and artificial restraint techniques that used the addition of side grooves to the specimens.

Notch acuity was increased by using a 0.15 mm slit instead of a Charpy V notch, which affects the results in the following way:

1) raises the temperature at which low energy fracture occurs;
2) narrows the transition temperature range;
3) slightly reduces the scatter of the results;
4) considerably reduces both the energy absorbed and lateral expansion at higher temperatures.

Inducing an artificial restraint with the addition of side grooves was shown to be dependent on the depth of the side grooves, and it was concluded that the stress concentration at the ends of the notch become more severe as the side groove depth is

increased. The increase in material constraint induced by the side grooves affected the crack fronts in the following way:

1) 1mm side groove – produced full width cracks along the notch root at the point of fracture initiation
2) < 1mm side groove – cracks initiate first at the center of the specimen
3) > 1mm side groove - cracks initiate first at the edges

Artificial restraint with side grooves of appropriate depth therefore enables the formation and the propagation of a crack because the running fracture is less inhibited by the edges of the specimen because of the increased stress concentration at the edges of the specimen. Increasing the plane strain conditions results in an increased transition temperature.

Therefore, side grooving can create a constant stress concentration across the crack front, and the use of fatigue pre-cracks would not benefit fracture toughness tests of ductile materials because of effects of crack tip blunting and the inability to accurately measure the crack propagation area.

Wilkowski et al. has shown that PN-DWTT specimens do not need side grooves to achieve the characteristic properties of full scale DDF as these specimens fracture under steady state crack condition[9] and resemble full scale fracture in both crack tip opening angle and fracture morphology.[28] Steady state propagation is shown in the region where

both the velocity and the crack tip opening are constant, and thus the steady state region as shown in Figure 2-9 can be used as the reference value for energy absorbed by side grooved Charpy specimens.

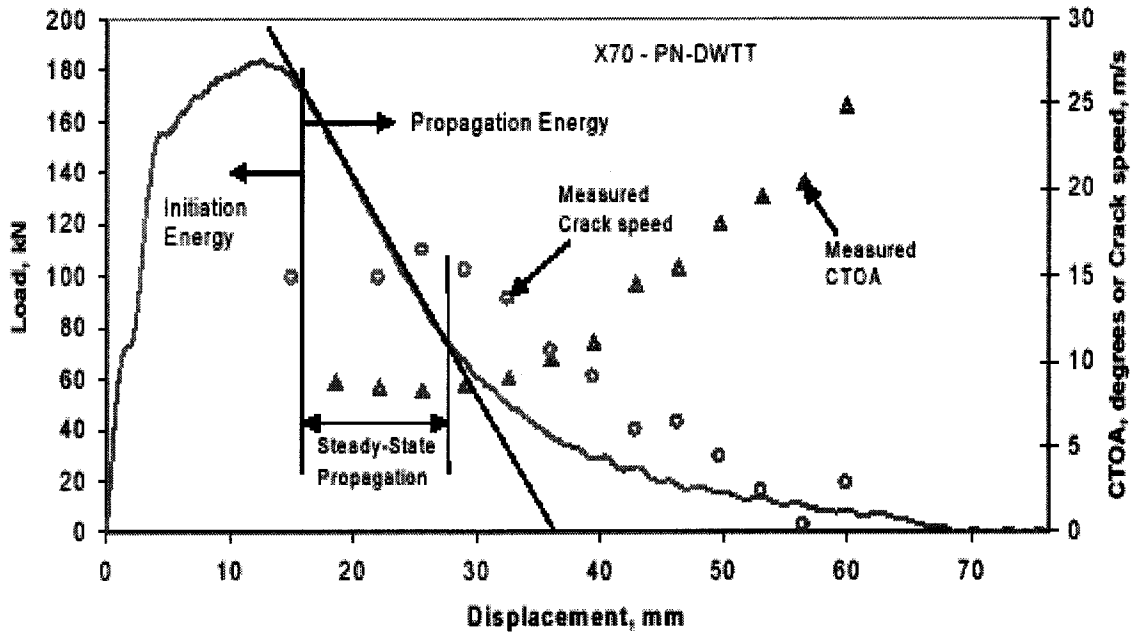

Figure 2-9. Steady State Propagation Region[28]

Steady state propagation energy from PN-DWTT specimen may therefore be used as the energy reference value. However, only PN-DWTT specimens with a thickness of 22 mm or less can be used as a reference value for steady state propagation according to Figure 2-10.

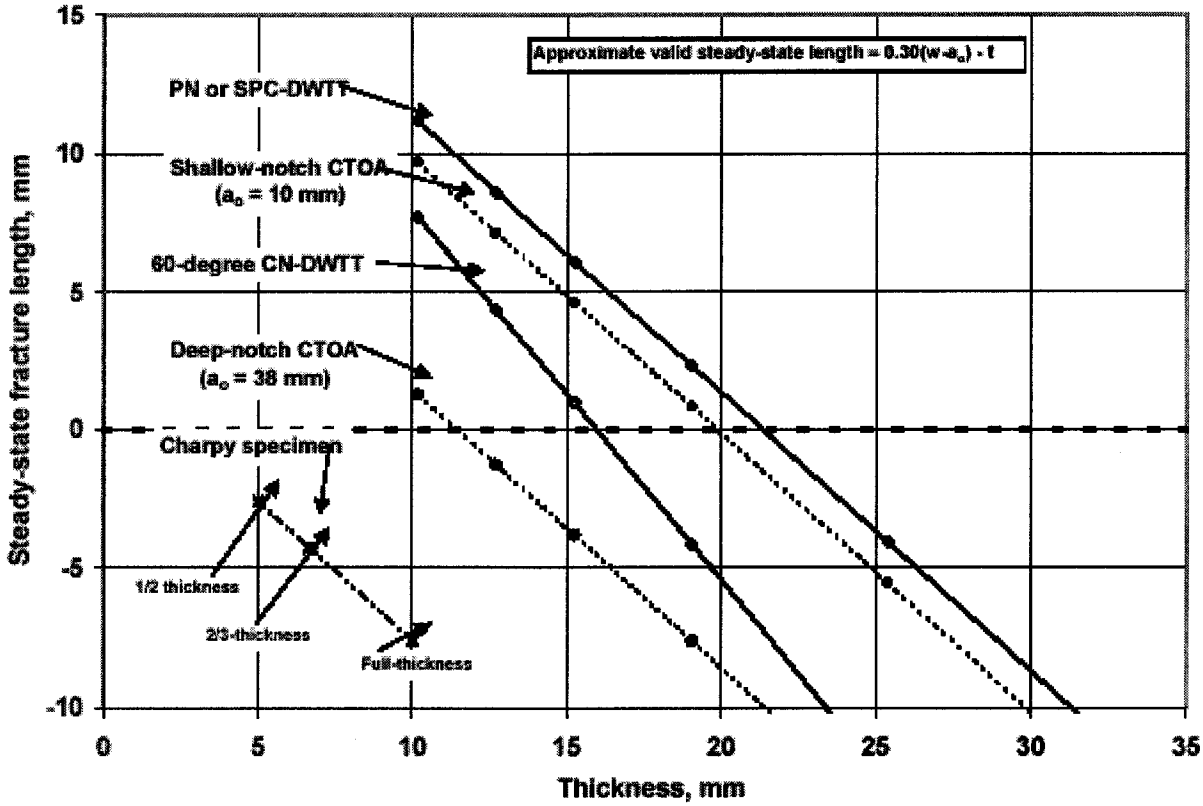

Figure 2-10. Length of Steady State Crack Propagation[9]

Leis and Eiber[29] stated that when very high toughness levels are measured using CVN specimens, the apparent fracture resistance becomes dominated by notch blunting, plastic deformation, and by other processes that do not contribute to DDF resistance: thus the addition of side grooves can minimize or eliminate these uncharacteristic properties of full scale DDF.[30] Since both Wilkowski et al.[9] and Leis and Eiber[30] suggest that steady-state crack propagation can not occur in traditional Charpy specimens, side grooves may be added to the specimens to eliminate notch blunting and reduce the amount of plastic deformation in the Charpy specimens which is uncharacteristic of DDF.

2.2 Instrumented Impact Testing

The equipment used with instrumented impact testing includes both a load sensor and a data acquisition system. Load sensors need to be a part of data measurement with DWTT, but it is a relatively new concept with Charpy impact testing. The necessity of a load sensor on a DWTT machine is the result of its inability, unlike a Charpy machine, to measure energy absorbed by measuring the changes in potential energy of the hammer. Although the changes in potential energy can be measured with the Charpy impact tester and this has been deemed the conventional way of measuring absorbed energy when ASTM's E-23 standard complies, the addition of an instrumented load sensor will be used with Charpy impact tests so the energy necessary to initiate a crack can be differentiated from the energy necessary to propagate it. This is particularly important in tough materials in which crack initiation absorbs a significant proportion of the total energy.

2.2.1 Measured Energy

2.2.1.1 Dial

The maximum energy that a Charpy impact tester can transfer under ideal conditions is equal to the kinetic energy of the hammer prior to impact as shown in equation 4.

$$E_o = \tfrac{1}{2} m v_o^2 \qquad (4)$$

$$v_o = (2gh_o)^{1/2} \qquad (5)$$

The change in potential energy from before and after impact is equal to the energy absorbed during a given impact test was separated into five parts by Ireland[31] as shown in equation 6.

$$E_{DIAL} = \Delta E_o(\text{measured}) = E_I + E_{SD} + E_B + E_{ME} + E_{MV} \quad (6)$$

where:

E_I = increment of energy required to accelerate the specimen from rest to the velocity of the hammer

E_{SD}=total energy consumed by bending the specimen

E_B =energy consumed by Brinell type deformation at the specimen load points

E_{MV}=energy absorbed by the impact machine through vibrations after initial contact with the specimen

E_{ME}=stored elastic energy absorbed by the machine as a result of the interactions at the specimen load points

The contribution of each component to total energy absorption will differ as the toughness of a material changes, and thus contribution of each is briefly examined and tabulated in Table 2-1.

Energy Component	
E_I	$E_I = \nu_o \int_0^{\tau} P dt$ - τ is the time associated with inertial loading - this is usually negligible for elastic-plastic fracture
E_{SD}	- $E_{SD} = \nu_{ave} \int_0^{\tau} P dt = E_a (1 - (E_a / 4 E_o))$ - when E_I and E_{ME} are small - this is where the majority of energy is absorbed
E_B	- increases with toughness - determined from secondary experiments - can be an accountable portion of ΔE_o
E_{MV}	- energy is small when ASTM E-23 standard comply
E_{ME}	$E_{ME} = \frac{1}{2} P_\tau^2 C_M$ - this is usually negligible

Table 2-1. Contribution of Energy Absorption

If a Charpy machine complies to ASTM standard E-23 or an equivalent ISO standard, the dial energy measured will consist primarily of all the energy necessary to fracture and deform the specimen (E_{SD}). When compliance to a standard is met the vibrational energy lost to the tester is minimal and thus the majority of the energy absorbed is consumed by the specimen (E_{SD}, E_B, E_{ME}).

2.2.1.2 Tup

If conservation of energy is considered during impact, the force that is measured by the Tup should then be equal to the force applied on the specimen, thus E_{DIAL} should equal E_{INT} when a machine complies with either the ASTM or ISO standards. However, the integrated energy values have been shown by Kalthoff et al.[32], Sreenivasan[33], Naniwa et al.[34], Kobayashi et al.[35] and Battelle[36] to differ from the dial gauge energies. Since Kalthoff et al., Sreenivasan, and Naniwa et al. have shown that E_{DIAL} is less than E_{INT} in their tests, and Kobayashi et al. and Battelle observed the opposite, examination of calibration procedures and other potential sources of error need to be examined.

2.2.2 Early Calibration Procedures

Several different calibration procedures have been used in the past in attempt to equate both E_{DIAL} and E_{INT}. Since E_{DIAL} is assumed to be the correct energy value if compliance to ASTM E-23 is met, all the calibration procedures that have been used are used to correct E_{INT}.

2.2.2.1 Velocity

The earliest calibration procedure used was developed by Ireland[31], initially used on low toughness materials. It involved adjusting the gain until E_a as shown in Figure 2-11 equaled E_{DIAL}.

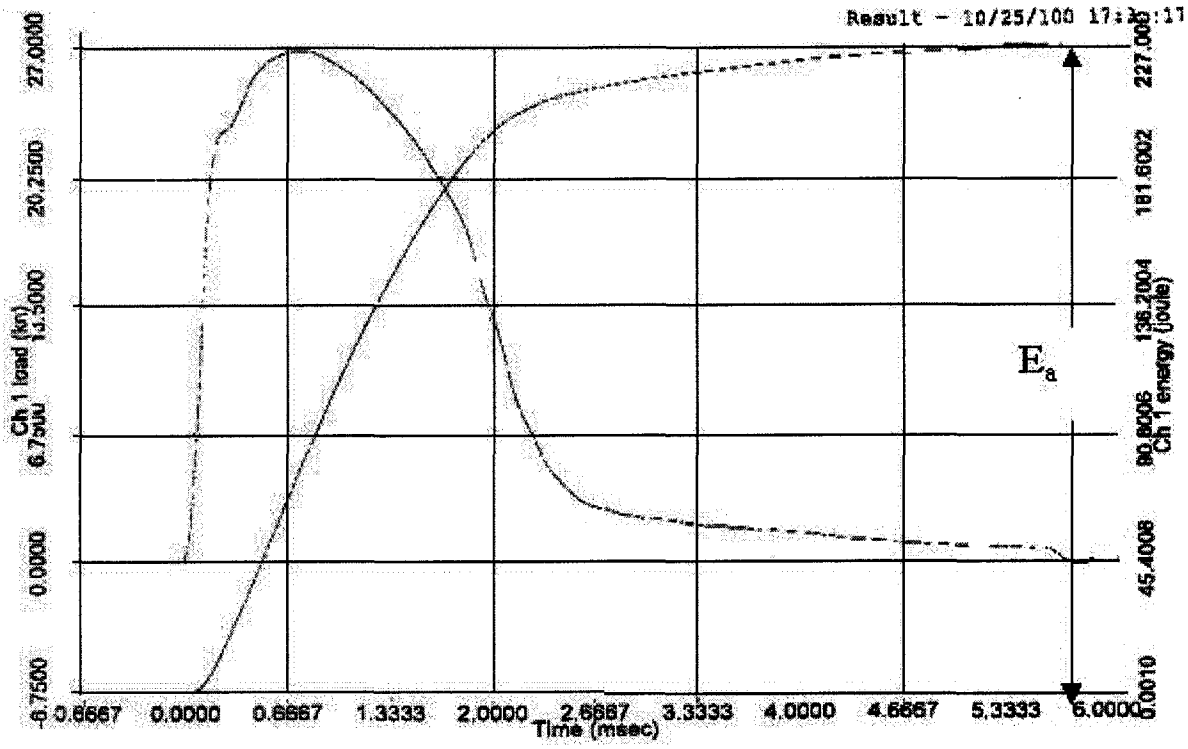

Figure 2-11. Load vs. Time plot for a X-70 Charpy V-notch specimen

Determining the maximum allowable toughness that could be used with this calibration process was subsequently determined by using some mild steel test blocks that had been notched with a saw to varying depths. After adjusting the gain, the validity of the integration energy was checked by performing a slow rate bend test on the identical material (both geometry and composition) that was used in the impact test, and calibration was considered successful if the maximum loads were within 3% for both tests. This led to peak energy level where the instrumented tup energy could be used without deviating from its 1:1 relationship with the dial gauge energy as shown in Figure 2-12 where Equation 5 was used to measure E_a.

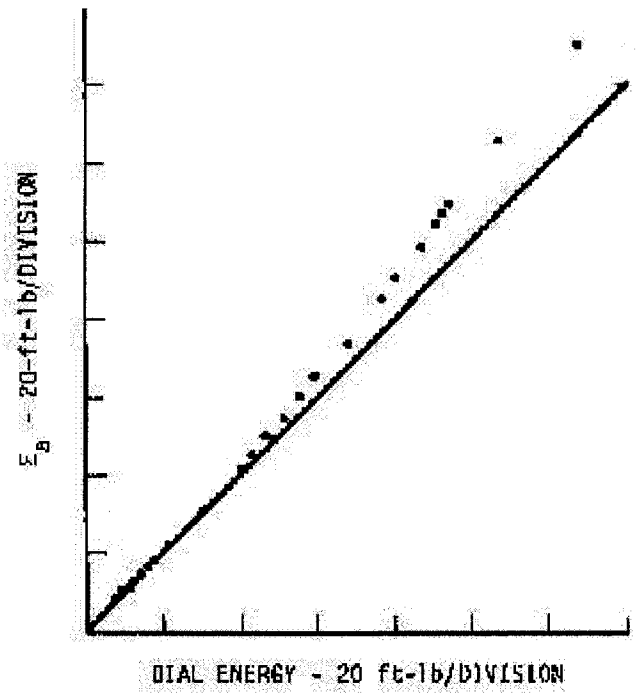

Figure 2-12. Comparison of E_{DIAL} to E_a where the impact velocity is assumed to be constant.

$$E_a = v_o \int_0^t P dt \qquad (7)$$

This region only existed because there was a minimal change in velocity in low toughness specimens through impact, but as the toughness of a specimen increased the energy measured by the strain gauges deviated from the linear relationship as a result of the increased change in velocity.

The linear region only occurred up to 55 J (40 ft·lb) when using a 325 J impact tester and therefore Ireland corrected Equation 7 to account for the problem in measuring E_a in higher toughness materials. The equation was altered such that the average impact

velocity, as shown in Equation 8 was used to measure E_a, which produced a 1:1 relationship with E_{DIAL} as shown in Figure 2-13.

$$E_a = v_{ave} \int_0^t P dt \qquad (8)$$

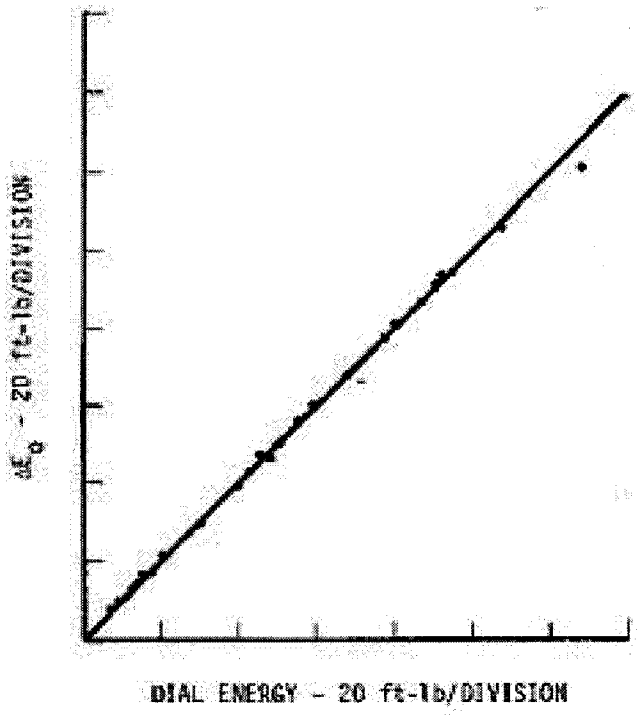

Figure 2-13. Comparison of E_{DIAL} to E_a where the impact velocity is assumed to be the average value.

This early work by Ireland shows how the development of instrumented energy measurement has progressed through the years as the toughness of materials increased. Although he ended up using the average velocity, calculation of E_a needed to be improved upon further. In addition to the incorrect energy calculations when using equations 7 and 8, his first generation "home-made" instrumented impact testers that

were used in the early 1970's were also technologically restricted and therefore more prone to energy measurement errors (reproducibility) than today's fabricated tups.

Today, instrumented impact tests measure E_{INT} by integrating the load vs. time graph over short time intervals and use the instantaneous velocity, such that equation 7 is used to calculate E_a.

$$E_a = v(t)\int_0^t P dt \qquad (9)$$

Since this is the most accurate way of measuring absorbed energy, any errors between E_{DIAL} and E_{INT} will be the result of errors besides improper energy calculations.

2.2.3 Modern Calibration

With the advancement in computer technology plus the development of the fabricated one piece integrated tups, errors due to amplifier characteristics plus unreliable bonding properties of the early tups have been either eliminated or minimized, and the existing discrepancies between energy values are now attributed to the geometry of the tup, position of strain gauges and compliance of the tup. Therefore several investigators have suggested potential calibration techniques[33, 37, 38, 39, 40] and variables that contribute to energy measurement errors.[35]

2.2.3.1 Tup Geometry

Fink[41], Kalthoff et al.[17], Naniwa et al.[34], Onizawa et al.[42], Nanstad et al.[43], Siewert and Vigliotti[44], Tanaka et al.[45] and Manahan and Stoneifer[46] have hypothesized that the geometry of the tup can result in measurement discrepancies. The geometry of the two primary tups used in studies includes those schematically shown in Figure 2-14.

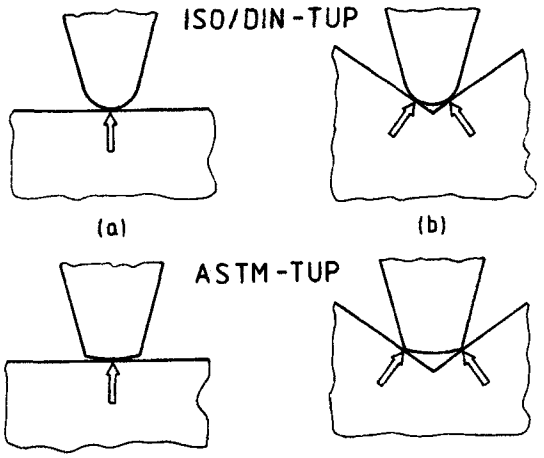

Figure 2-14. Schematic of the interaction of ASTM and ISO/DIN tups with specimens[32]

2.2.3.1.1 Effects on Dial Energy

E_{DIAL} discrepancies between ISO/DIN and ASTM tups have been shown by Fink[41] to increase with material toughness. His work is graphically depicted in Figure 2-15 with the dial energy of the ISO/DIN tup falling above a 1:1 correlation line with an ASTM tup, and the best-fit regression line being represented by:

$$(ISO) = 1.0420\ (ASTM) + 0.5160 \qquad (8)$$

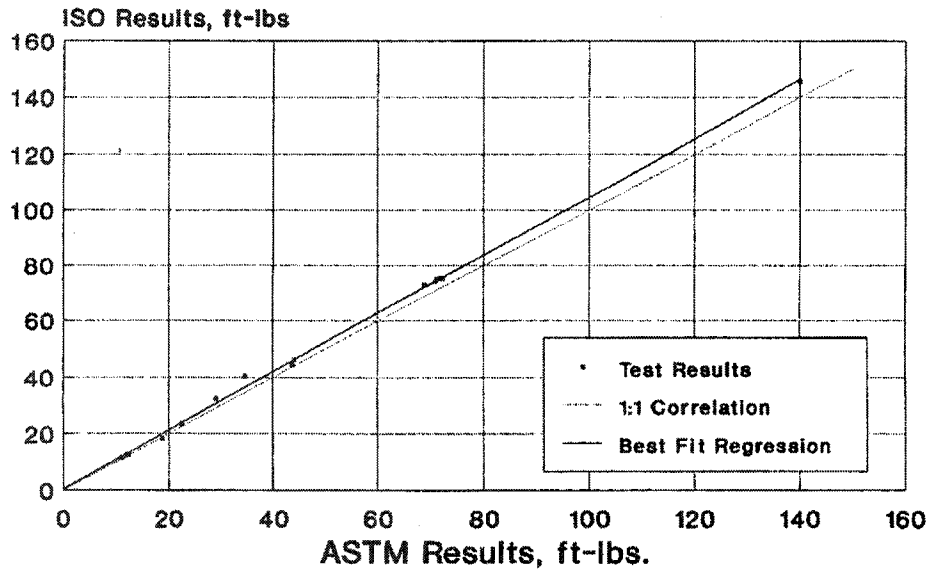

Figure 2-15. Correlation of ASTM and ISO Impact tests

Work by Naniwa et al.[34] confirms the results obtained by Fink[41], plus because he performed more tests it can be seen in Figure 2-16 that differences observed between the ISO (2mmR) and ASTM (8mm) tups are not significant until energy levels in excess of 200 J.

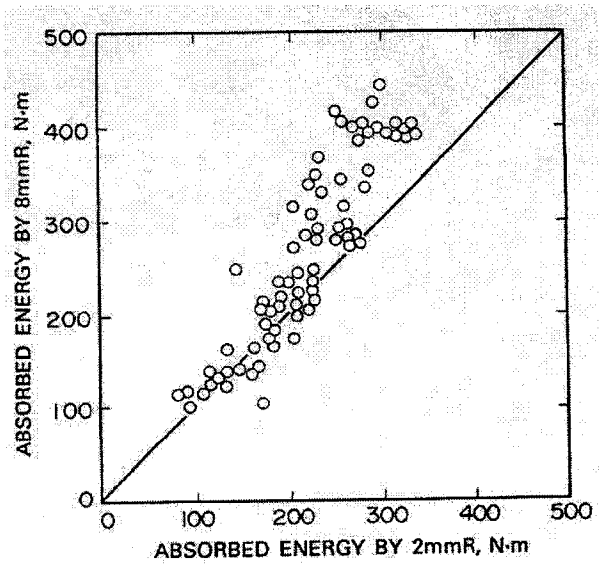

Figure 2-16. Comparison of absorbed energy between the ISO and ASTM Tups[34]

Fink concluded that the shape of the tup does have an effect on energy absorption because of frictional effects and/or increased Brinell deformation. These results are useful in showing that the Brinell deformation by the tup is greater with the ISO/DIN tup because of its smaller surface area, but since these tests were performed with low toughness materials the credibility of Equation 8 has to be questionable at a higher toughness (>250 J). This is because the frictional effects are not likely to result with materials of low toughness since the interaction time of the tup and the specimens are relatively low. Therefore at higher toughness levels the differences in energy absorption between an ISO/DIN an ASTM tup are unknown, but it is likely that increased frictional effects will be observed with the ASTM tup and increased Brinell deformation will be observed with the ISO/DIN tup.

2.2.3.1.2 Effects on Instrumented Energy Measurement

Although a tup's geometry affects the energy absorbed by a specimen, E_{INT} should equal E_{DIAL}. Work by Manahan and Stoneifer[46] have listed the discrepancies between E_{INT} and E_{DIAL} as being the result of:

1. elastic deformations of the striker and pendulum;
2. rotations of the striker due to pendulum rigid body rotation;
3. initial specimen machining tolerance on squareness (10 minutes);
4. wear of the striker, anvils, or supports;
5. plasticity in the specimen leading to force redistribution;

6. wrapping of the specimen around an 8 mm striker with plowing of the specimen surface and associated pinching of the striker nose;
7. specimens of different material elastic and plastic behavior;
8. specimen height;
9. non-symmetry in crack growth behavior.

As the ductility of a material increases the energy necessary to both initiate and propagate a crack increases: thus the interaction time between tup and specimen increases. The increased interaction time enables the specimens to wrap around the tup, and has been noted to result in a difference in force measurements.[32, 34]

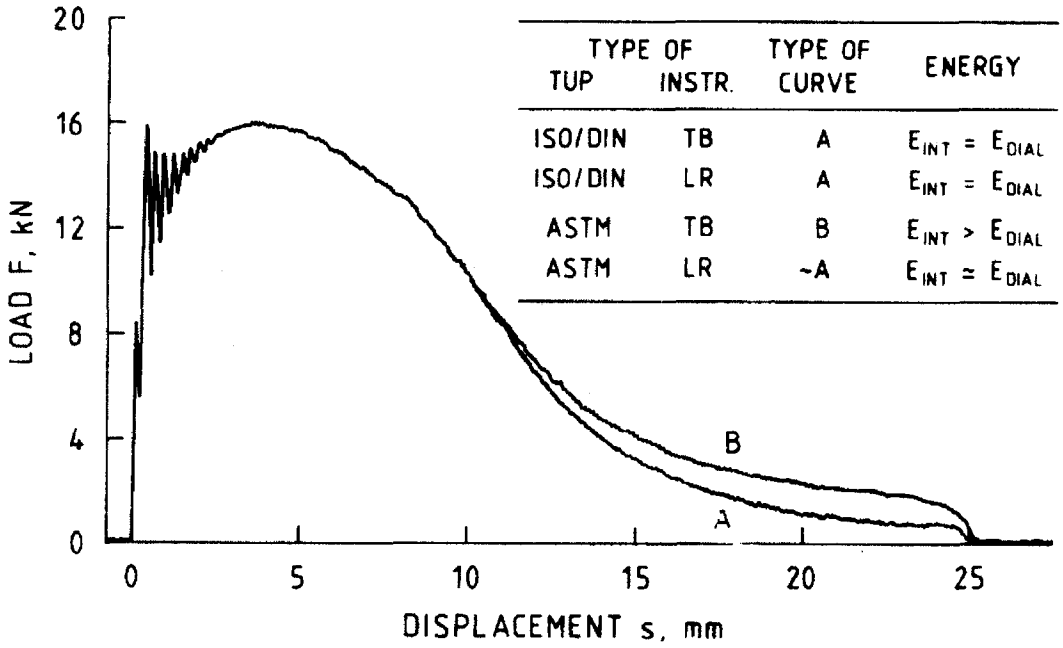

Figure 2-17. Results of pinching on different tup geometries and strain gauge positions[32]

The interaction results in a pinching effect, and it has graphically been shown for both the ISO/DIN (2mm R) and the ASTM (8mm R) tup by Naniwa et al.[34] in Figure 2-18.

Striker	8mm R (ASTM)	2mm R (ISO)
1 Maximum Load Point	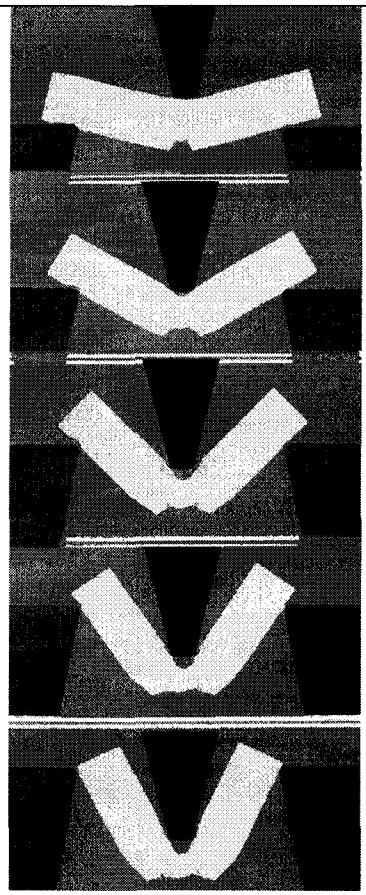	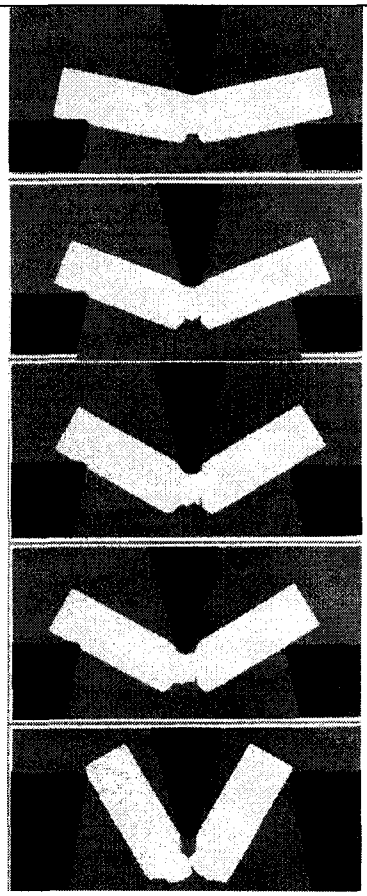
2		
3 Bending		
4		
5 Anvil Slip		

Figure 2-18. Interaction of tup and specimens under static loading[34]

Although the pinching effects exhibited in Naniwa's work was performed under static conditions, he used the pinching effect to explain the discrepancy between $E_{INT;ASTM}$ and $E_{DIAL,ASTM}$ is greater than $E_{INT,ISO}$ and $E_{DIAL,ISO}$.

Kalthoff et al.[32] however stated that the axis of rotation is relatively constant when tests are performed with an ISO tup since the force imparted by the tup does not deviate far from the initial impact point (point load - centerline). Conversely, with an ASTM tup,

the change from a point load to a distributed load occurs (increases the rotation axis). When increasing the rotation axis the larger contact lengths between specimen and tup will result in higher maximum load (initiation energy). Increasing or decreasing the contact length will increase or decrease the initiation energy, which has been subsequently proven by Etoh[32] with elastic dynamics. Force versus time graphs such as those obtained from Kalthoff et al.[32] work, as seen in Figure 2-19, confirms that tup geometry potentially influences the measured force.

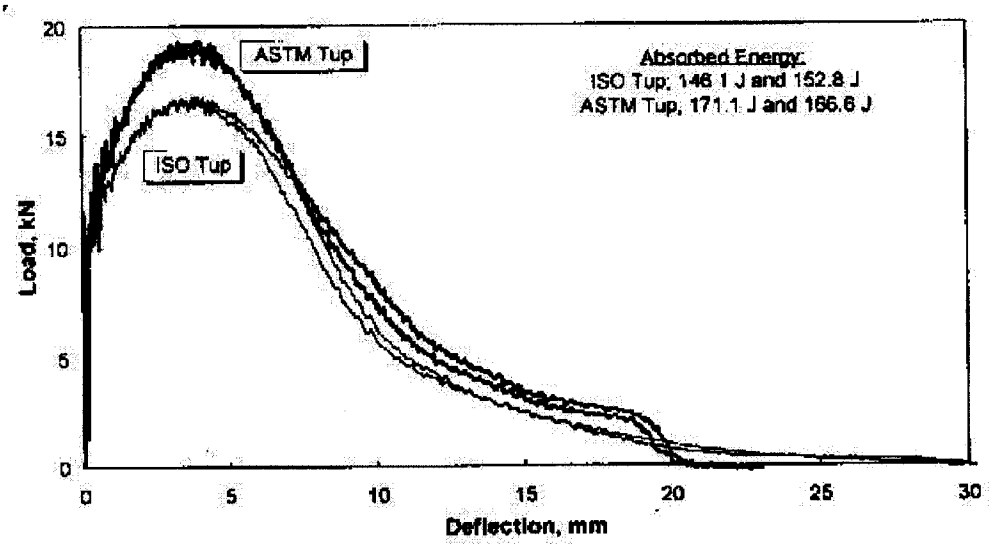

Figure 2-19. Load vs. Time graphs for ASTM and ISO/DIN tup[32]

Battelle's[36] work, shown in Figure 2-20, also resulted in erroneous load measurements revealing that the load measured by the tup is actually lower than the applied load which opposes Kalthoff's view, plus Battelle has shown that the error in energy measurement occurs following the maximum load. This occurs as the specimen wraps around the tup, when performed under quasi-static conditions so any calibration technique must consider the specimen-tup interaction through impact.

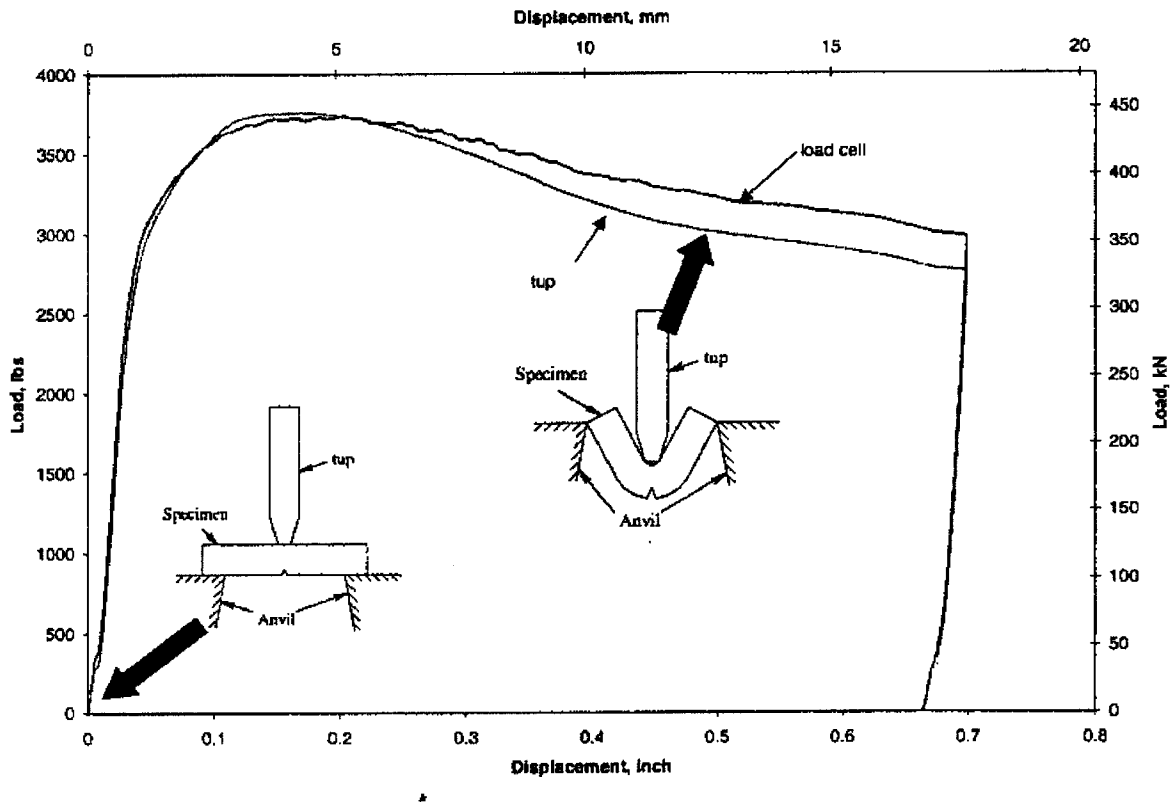

Figure 2-20. DWTT Instrumented tup vs. Optical Encoder[36]

According to work performed by Kalthoff et al., a difference exists between the recorded force measurement from an instrumented tup and the true applied force. The difference occurs as a Charpy specimen deforms around the tup as seen in Figure 2-21. This difference is notable with the ASTM tup as the forces become concentrated closely around two separate contact points as seen in Figure 2-14. With the use of an ASTM Top/Bottom tup, the F_{app} / F_{true} increases as the ASTM tup is subject to an increased inclination angle.

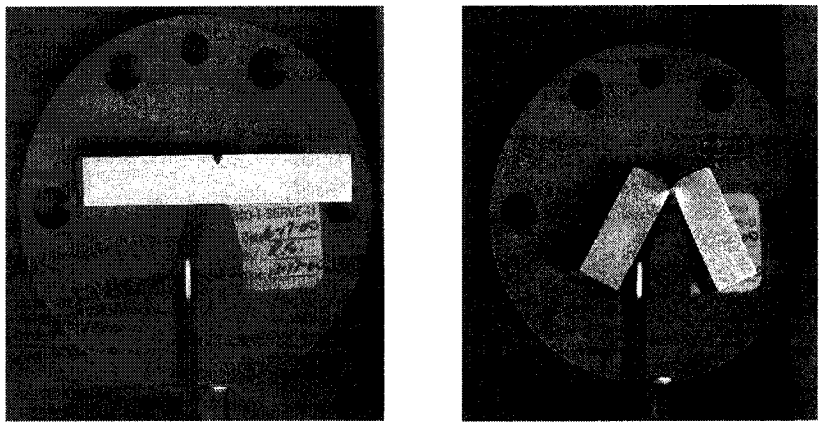

Figure 2-21. a) inclination angle = 0° b) inclination angle > 45°

Therefore, the error in force measurement has been corrected by determining how the measured force changes with the inclination angle. The method of calibration is as follows:

1. make four different calibration blocks, each with a different inclination angle
    b. 0° angle
    c. 22.5 ° angle
    d. 45.0° angle
    e. 67.5° angle
2. each of the specimens will be subjected to a range of different low blow forces
    a. 1kN
    b. 2kN
3. formation of a calibration curve
    a. F_{app} / F_{true} @ inclination angle of 0° = 1

b. F_{app} / F_{true} @ inclination angle of $22.5^{o} - 67.5^{o}$ =

i. $F_{app\ 22.5} / F_{app\ 0}$

ii. $F_{app\ 45.0} / F_{app\ 0}$

iii. $F_{app\ 67.5} / F_{app\ 0}$

4. after this calibration curve is determined for the instrumented tup, testing may commence, and the load measured during Charpy impact testing will be corrected according to the change in inclination throughout the period of the test

a. Newton second law of $S(t) = \int[v_o - 1/m \int P(t)\, dt]\, dt$

i. Corrected P(t) using calibration curve

ii. Measure S(t)

iii. Measure the inclination angle

iv. Using the above calculated inclination angle, proceed to the first step

This procedure was used to calibrate the instrumented tup for inclination angle errors.

2.2.3.2 Material Compliance and Strain Gauge positioning

Manahan et al.[46], Fink[41] and Kalthoff et al.[32] have shown that differences in energy measurements were not only the result of geometry, but also due to the positioning of the strain gauges and the tups compliance. With calibration blocks of increasing inclination angles the differences between F_{app} and F_{true} were shown to change with inclination angle. By manipulating both the strain gauge positioning and the compliance of the tup, Kalthoff et al. determined how each variable affected the force measurements. Since the inclination increases in conjunction with the toughness of a material, the most accurate

force measurements would be provided with a tup that minimizes the area over which the forces are transferred. Therefore, he suggested that the ISO/DIN tup would be a better choice with high toughness materials because two inclined contact forces as seen in Figure 2-14 will be spread over a smaller area.

Both top-bottom and left-right positioning of strain gauges also result in a difference of force measurements. A top-bottom orientation results in an overestimate of the force applied while a left-right orientation of the strain gauges will underestimate the force applied but will also have a lower percent error. The lower error is likely due to the closer proximity of the strain gauges to the actual force as the inclination angle increases, and thus positioning of the strain gauges in a L-R orientation may be considered the best choice.

2.2.3.2.1 Material Compliance

Testing both titanium and steel tups has shown that the material selection of a tup does affect force measurements with high toughness materials. Experiments have shown that steel tups will result in a more accurate force measurement than the titanium counterpart, which is due to the larger compliance of the titanium tup.

2.3 Literature Review Summary

When considering all of the aforementioned variables, Kalthoff et al.[32] believes the tup that provides the most accurate force measurement is an ISO/DIN tup made from steel with the strain gauges in a L-R orientation.

There is no doubt that errors do exist when measuring absorbed energy with strain gauges, thus energy measured with an instrumented tup needs to be examined further. Although several solutions have been proposed for an energy measurement correction, the loads measured by strain gauges in the tup are still difficult to measure correctly. Since the energy absorbed by a specimen is measured by the area under a load-displacement curve, any errors in the load measurement that either over or under estimate the energy absorbed will result from higher or lower measured loads respectively.

Energy measurement errors have been suggested to be due to compliance, pinching effect, inertial effect and strain gauge orientation. These errors do definitely have an effect on the energy measured by the specimens since they ultimately influence an inaccurate load measurement by the strain gauges.

Both Kalthoff et al. and Battelle explain the error in energy measurement as a result of the wrapping of the specimen around the tup. Because they overestimate and underestimate the energy measured, respectively, compliance, orientation and bonding of the strain gauges and tup geometry seem to affect energy measurement calculations on a case-by-case basis.

3 EXPERIMENTAL METHODS

3.1 Material and Specimen Extraction

The material tested included both a 36" X70 and 42" X80 pipeline steel provided by IPSCO. 930 cm^2 sections were removed from the pipe at equivalent distances from the ERW's as seen in Figure 3-1 with an oxy-acetylene torch.

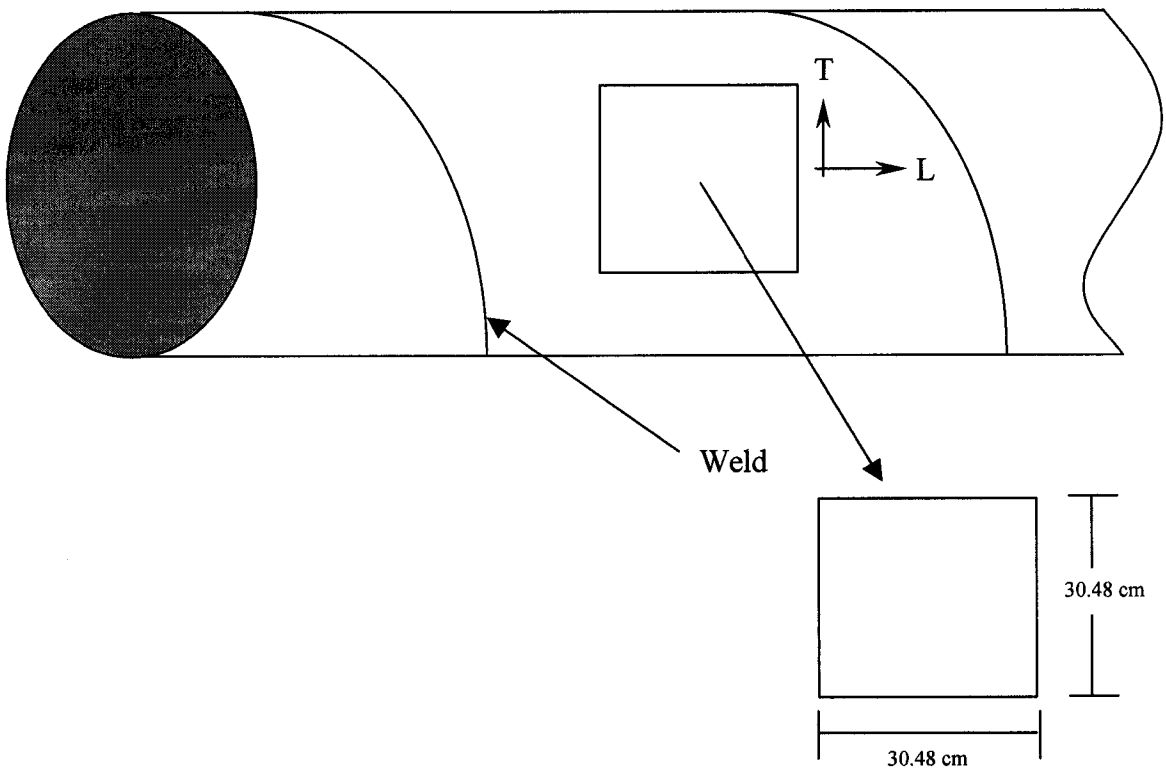

Figure 3-1. Sectioning of Pipe

Flattening of the specimens was necessary due to the curvature of the plates, and therefore all of the sections removed from the pipe were flattened in a three point bend setup with a 4.5 MN universal machine as seen in Figure 3-2.

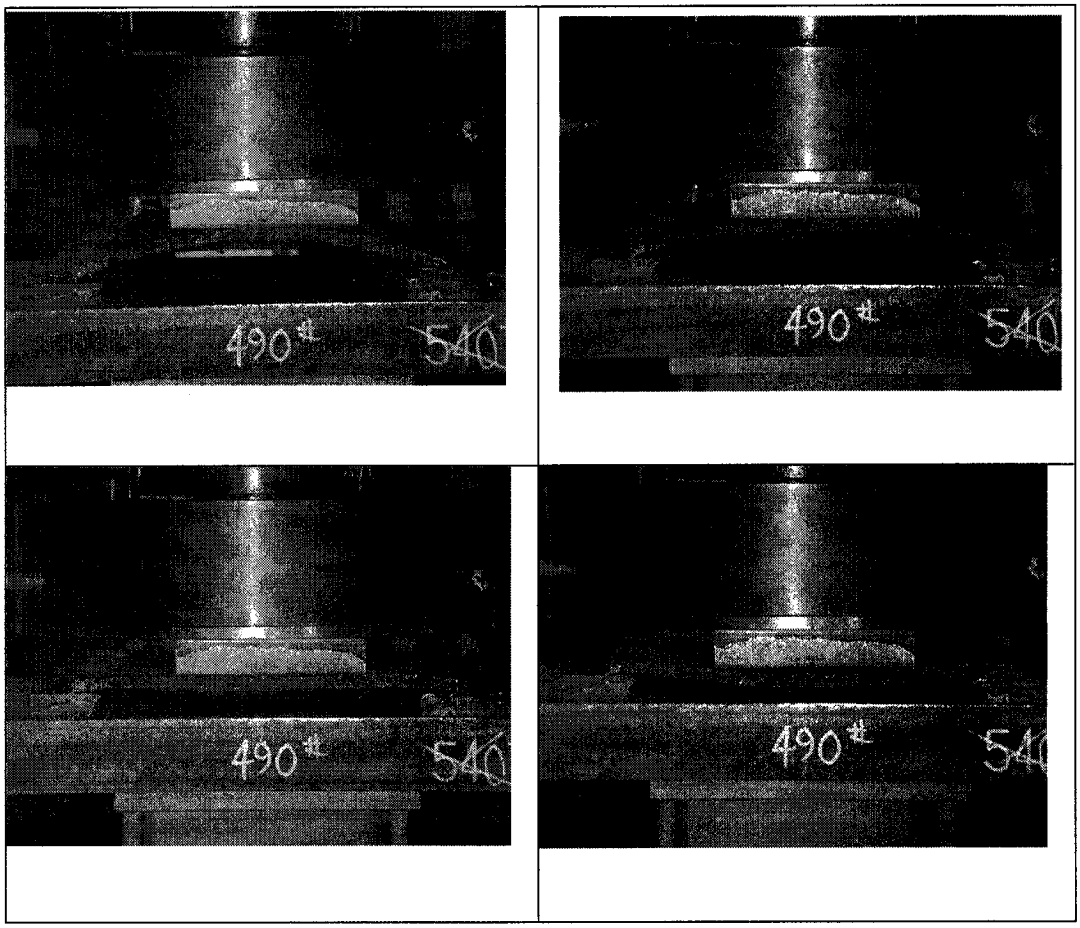

Figure 3-2. Flattening pipe

To minimize induced strain hardening in the specimens the plates were bent only slightly beyond flat such that elastic recovery of the material resulted in a flat plate.

Charpy and DWTT specimens were then removed from the plate so the crack orientation of the specimens are such that the crack would propagate in the longitudinal direction of the pipe as shown in Figure 3-3.

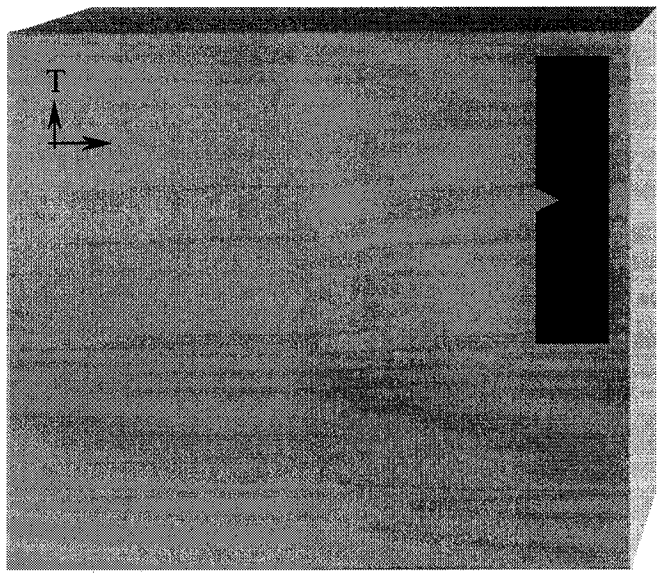

Figure 3-3 Orientation of specimens removed from plate sections

ASTM standards E436 and E23 were followed when fabricating the DWTT and Charpy specimens, respectively, and all dimensions met standard specifications.

3.1.1 DWTT Specimens

Every DWTT specimen, except the side grooved specimens, were fabricated to the ASTM E436 standard as shown in Figure 3-4. The side-grooved specimens still met these specified dimensions except for the additional side-grooves that were added.

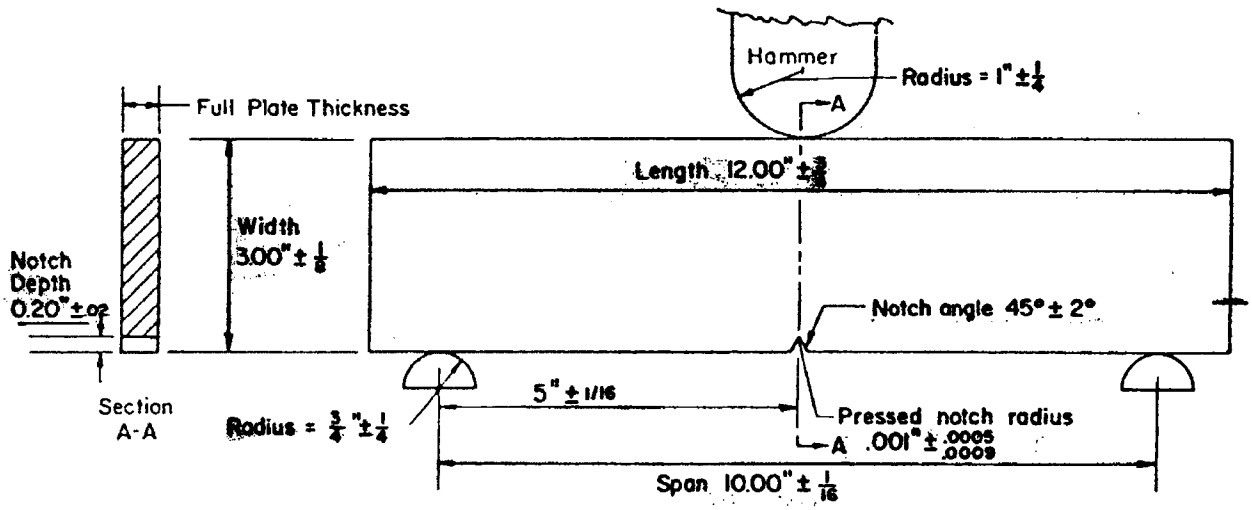

Figure 3-4. ASTM E436 DWTT specimen dimensions

The full wall thickness of each of the materials along with the different side groove depths used for each material is given in Table 3-1.

Material	Wall Thickness (mm)	Side Groove Depth (mm)	Side Groove Depth (mm)	Side Groove Depth (mm)	Side Groove Depth (mm)
X70	14.4	0	1.0	1.5	2.0
X80	13.4	0		1.5	2.0

Table 3-1. Side groove depth of DWTT specimens tested

The depth of the side grooves was to be increased until the absorbed energy per unit area for two given side groove depths were equal, and steady state crack propagation occurred.

3.1.1.1 Notch and Side Groove

To ensure that the side grooves start at the notch tip, a pressed notch was added to the specimen in accordance to ASTM E436 with a chisel as seen in Figure 3-5 followed by the addition of side grooves. This is the best method to ensure that side grooves start at the tip of the notch as shown in Figure 3-6.

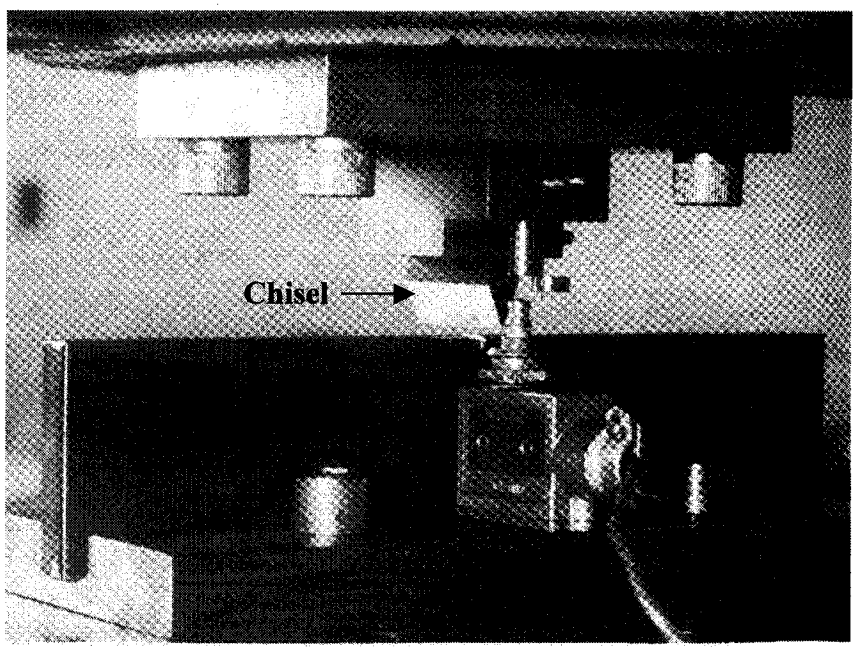

Figure 3-5. PN from Impact Testing of Metals

Figure 3-6. DWTT specimen with side grooves

A milling cutter with dimensions similar to a Charpy V-notch (45° , 0.25mm radius) was used to mill the side grooves into the DWTT specimens.

3.1.2 Charpy Specimens

Traditional Charpy specimen dimensions were made in accordance to ASTM E23 as shown in Figure 3-7, but some side grooved specimens were made and modified slightly from the traditional specimen through the addition of side grooves.

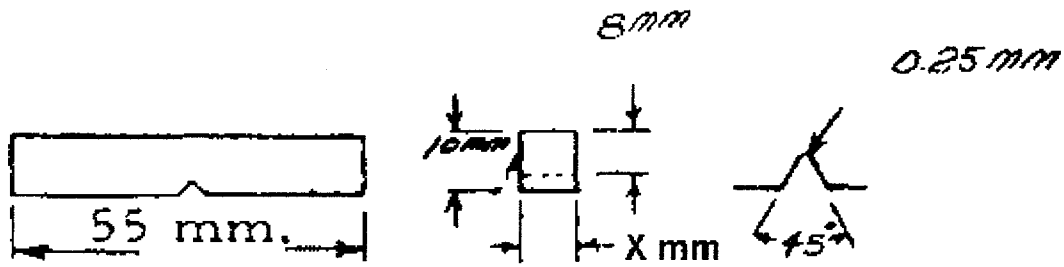

Figure 3-7. ASTM E23- Charpy Dimensions[47]

Since the fracture area of traditional Charpy specimens is 80 mm^2, this fracture area was kept constant in the side-grooved specimens by increasing the thickness of the specimens to compensate for the addition of side grooves. Hence, after the addition of side grooves the fracture area still equaled 80 mm^2 as the thickness of a side grooved specimens were made so they equaled 10mm + x where x is equal to one half of the side groove depth.

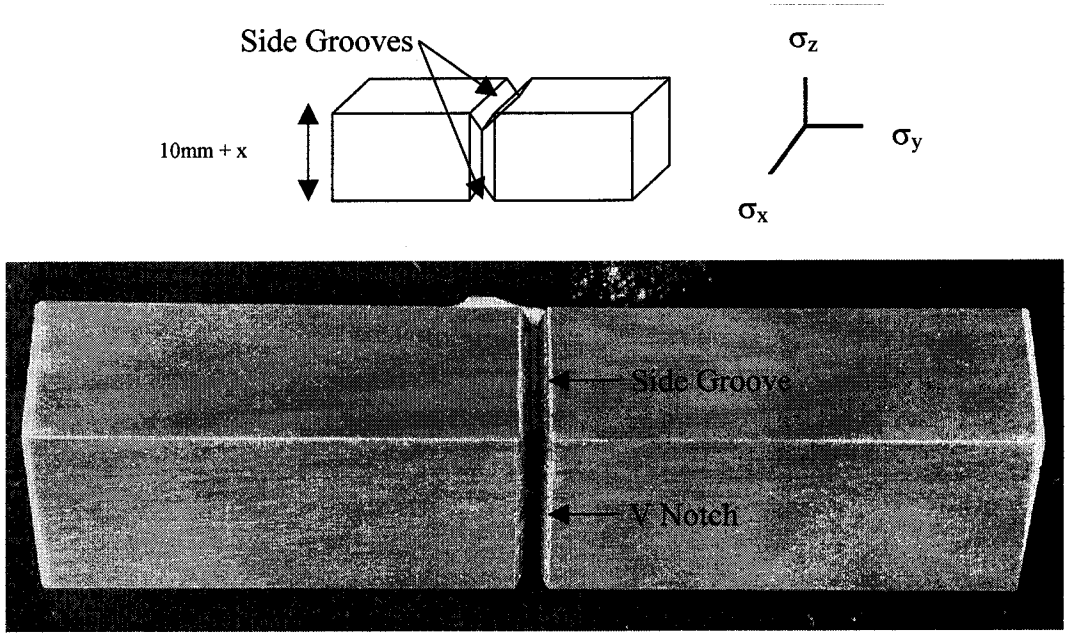

Figure 3-8. Charpy Specimen with Side Grooves

Material	Wall Thickness (mm)	Side Groove Depth (mm)
X70	10	0
X70	11	0.5
X70	12	1.0
X70	13	1.5
X80	10	0
X80	11	0.5
X80	12	1.0
X80	13	1.5

Table 3-2. Side groove depth of Charpy Specimens tested

3.1.2.1 Notch and Side Groove

Notches and side grooves added to all the specimens were made by broaching the specimens with a 45°, and 0.25mm radius broach in compliance with ASTM E23.

3.2 Energy Measurement

Energy measured by both the Charpy and DWTT instrumented tups are used as an indication of the energy absorbed by a specimen. The method is simple such that the total energy absorbed in each test can be calculated by measuring the area underneath the load-displacement curve as seen in Figure 3-9.

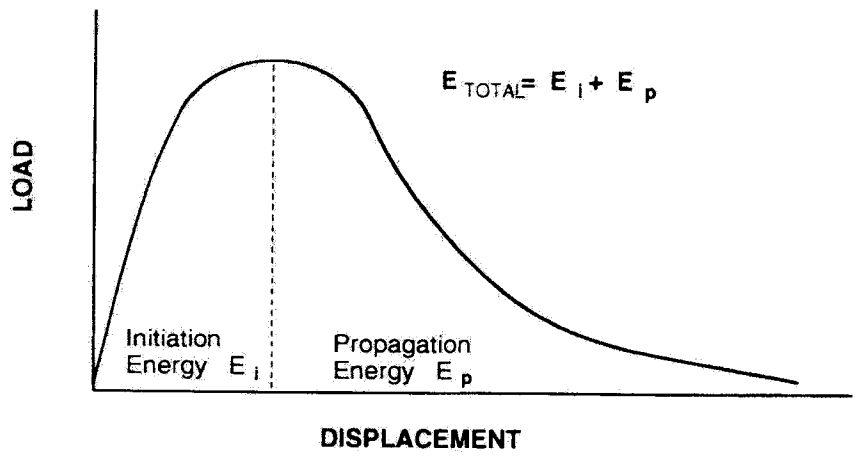

Figure 3-9. Separation of initiation energy from propagation energy[10]

The benefit of using this measurement technique is that either the initiation or propagation energy can be individually measured from the area prior to and following the maximum load point respectively. Since our focus is on propagation energy

measurement, the area following the peak load will be used for measuring and comparing the propagation energy between Charpy and DWT tests.

The constant slope that occurs following the maximum load in Figure 2-9 is very important and will be used in the analysis of DFP toughness because crack propagation in this region has been shown to propagate under steady state conditions and is therefore more accurate than Figure 3-9 for measuring the propagation energy of a material.

4 RESULTS AND DISCUSSION

Since the various attempts that have been used to relate Charpy energy to full scale crack propagation energy with high toughness controlled rolled steels were shown not to work, our attempt at relating Charpy propagation energy to DWTT propagation energy revolved about measuring energy with instrumentation. Unlike the previous energy relationships that used the total energy absorbed by a specimen to measure the propagation energy, the use of instrumentation allows for the direct measurement of propagation energy. Side grooves were added for the purposes of: minimizing plastic deformation, controlling the orientation of the fracture path, and easing the measurement process of energy absorption. With the use of side grooves and instrumented impact testing, measurement of the energy necessary to propagate a crack may be easily related to DWTT propagation energy. Therefore, if a correlation between Charpy and DWTT energy are to be obtained, the absorbed energy measurement by the instrumented tup must be evaluated.

Two issues that were focused on when attempting to compare the propagation energy of the Charpy specimens to the DWTT specimens were the validity of the energy measured by the instrumented tups, and determining the suitability of side grooving impact test specimens.

4.1 Validity of the Energy Measured by the Instrumentation

Prior to this experimental work the Charpy impact testing machine shown in Figure 4-1 only measured total absorbed energy with the dial gauge that measures the change in potential energy of the machine.

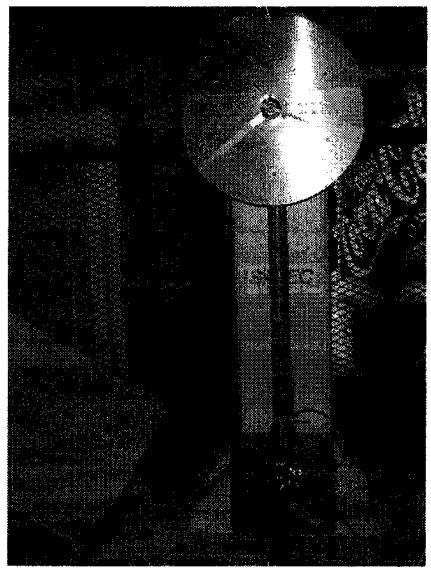

Figure 4-1. Satec Charpy Impact Tester

The mechanics of the test are such that the striker as induces a dynamic load upon the specimen shown in Figure 4-2.

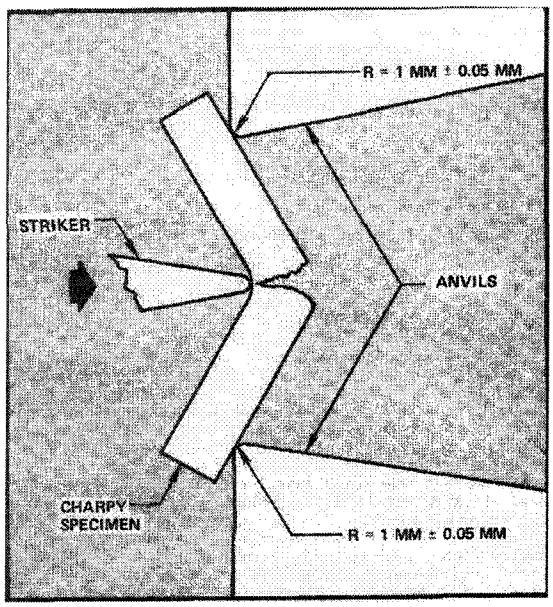

Figure 4-2. Charpy Test

However, as previously mentioned, for the purposes of measuring ductile fracture propagation in high strength pipeline steel this measurement method is not sufficient. The dial energy measurement is very important in other aspects though, because its value can be used as a benchmark for other measurement techniques. Since the energy measurements use the difference in the pendulum height from before and after impact for measuring the total energy absorbed by a specimen (E_{DIAL}) the potential sources of energy measurement errors are small. The machine used in our tests complied with ASTM E-23 and hence E_{DIAL} can be used as a reference value because it represents an accurate measure of the energy absorbed by a specimen.

After E_{DIAL} was determined to comply with ASTM E-23 it can be used to determine the accuracy of alternative energy measurement methods, which include the instrumented tup and linear tape/optical encoder method.

4.1.1 Instrumented Tup

An ASTM tup that included internally mounted and calibrated strain gauges as seen in Figure 4-3 was purchased from DYNATUP and installed on the Charpy impact tester.

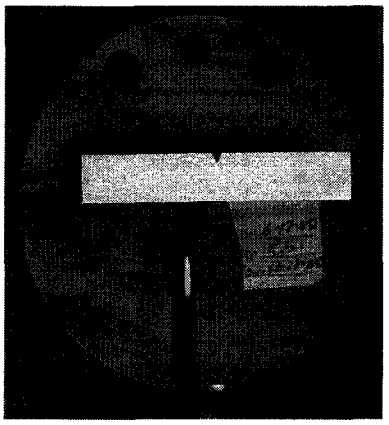

Figure 4-3. ASTM Instrumented Tup

Introduction of an alternate energy measurement method for Charpy testing has been developed for the separation of initiation and propagation energy. Use of alternate energy measurement methods has typically used the addition of strain gauges to the tup. Since this has been the primary alternative energy measurement method that has been in use since the 1970's, the method was initially implemented as the means to separate crack initiation energy from crack propagation energy. With the recent implementation of British Standard: BS EN ISO 14556:2000 for an ISO tup, the accuracy of energy measurement with an instrumented tup was expected to be high. Since there is no current ASTM standard for instrumented impact testing, this experimental setup and analysis relied on the British Standard and ASTM E-23. However, impact tests that followed these standards revealed that there is a definite discrepancy between E_{DIAL} and E_{INT}.

The usefulness of E_{DIAL} as a benchmark was appreciated in the first round of tests, as the energy measured by the instrumented tup (E_{INT}) was found to be incorrect as shown in Table 4-1.

Side Groove Depth	E_{DIAL} (J)	E_{INT} (J)	Difference (J)
0.5mm	208	234	26
1.0mm	155	180	25
1.5mm	121	141	20

Table 4-1. Average energy values of E_{DIAL} and E_{INT}

The instrumented tup was selected on the assumption that the forces and energy measured by it would give an accurate representation of the energy transfer during a test.

All the energy comparisons between E_{DIAL} and E_{INT} revealed in Table 4-1 showed discrepancies, which questioned the validity of using strain gauges for energy measurements. Discrepancies in E_{DIAL} and E_{INT} energy values have been noted by investigators, however they only made comparisons between ISO and ASTM tups. The primary deductions from their research were that the ISO tup measured the energy absorption better than the ASTM tup because the energy discrepancy between the ISO tup and E_{DIAL} is much lower than its ASTM counterpart.

This could just be a coincidence though. Therefore, an alternative energy measurement method was developed, which calculates absorbed energy by measuring the displacement of a specimen rather than through an electrical signal obtained by strain gauges. It is believed that comparing the ISO to the ASTM tup is an inappropriate method of determining errors, and hence an alternative energy measurement method should be used. The use of a linear tape and optical encoder method to measure the velocity of the pendulum at any instant through impact, which can be used to measure the energy absorbed by a specimen, is proposed.

The energy measurement errors can be attributed to several different sources, which include strain gauge position, material compliance, pinching effects, and inertial effects and v_o measurement errors. Unfortunately the only error that can be eliminated by proper setup is the initial velocity measurement error. Analysis of one set of instrumented Charpy data revealed that the initial velocity measurement was incorrect, but this error in energy measurement can be simply corrected either prior to or following testing but correction prior to testing is preferable. In a Charpy impact test the initial velocity error can be the result of either an incorrect placement or a bent flag tape, because the flag tape is used to measure the initial velocity measurement. The initial velocity will be greater than the theoretical value if the flag tape spacing is shortened and less if the length is increased. To correct this error both the theoretical velocity and the velocity measured by the flag tape are needed. The theoretical velocity prior to impact of the SATEC SI-1K3 is 5.18m/s, and can be used to determine the accuracy of the measured flag tape initial velocity. If an error exists, it can be corrected by either getting a new flag

tape or by physically bending the flag tape and performing free fall runs until the velocity measured by the flag tape equals the theoretical velocity of the Charpy machine. However, if the integrated energy data is measured with an incorrect initial velocity, some adjustment can be made to the data to correct the energy measurement error as a result of an incorrect initial velocity reading.

Because there was still a discrepancy between E_{DIAL} and E_{INT} after this correction, it was evident that energy measurement errors were present and inevitable when using strain gauges under dynamic loading conditions, thus an alternative energy measurement technique that used an optical encoder and linear tape was introduced.

4.1.2 Optical Encoder and Linear Tape

An optical encoder and linear tape were added to both the DWTT and Charpy machines in attempts to resolve energy measurement errors observed in the instrumented tup energy measurements. This method has been proven to be successful when used on the Charpy machine because of its pendulum motion, but data obtained from DWTT was not consistent.

The principles of the proposed method like the instrumented tup can utilize Newton's Second law of motion for determining the unmeasured force and displacement. Alternatively, the change in kinetic energy of the hammer can be used to evaluate the energy absorbed by the specimens.

The technique that is being proposed consists of measuring the displacement of the pendulum during the impact period and subsequently converting this measurement to an instantaneous velocity and applied force for the given test period. By measuring the deceleration rate of the impact head during the impact period, the force being applied to the impact head and that applied to the specimen can be determined. The initiation energy and propagation energy can be measured by using kinetic energy equations. Accurate displacement and time measurements are necessary for accurate force or energy measurements. The accuracy of the energy measured by this method can be checked again the dial energy on the Charpy machine.

Other measurement techniques were examined for measuring the displacement of the impact equipment, but the optical encoder/linear tape method seemed to be the best and easiest method.

4.1.2.1.1 Equipment

With the optical encoder measurement method an 80 MHz counter/timer board from National Instruments as seen in Figure 4-4 is used to measure the time between two successive reference points. The reference points are obtained by passing the linear tape as seen in Figure 4-5 through an optical encoder as seen in Figure 4-6.

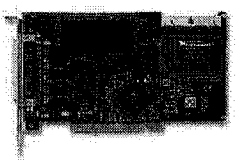

Figure 4-4. National Instruments 80 MHz Counter/Timer Card

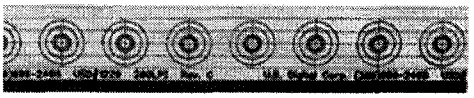

Figure 4-5. Linear Tape

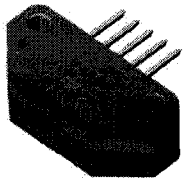

Figure 4-6. Optical Encoder

4.1.2.2 Setup

The measurement setup was installed on both the Charpy and DWTT machines to both determine the sources of error of the strain gauges and attempt to use this method as an alternative energy measurement technique.

Setup of the equipment is shown in Figure 4-7 where the encoder is rigidly attached to the floor and the linear tape is attached directly to the pendulum.

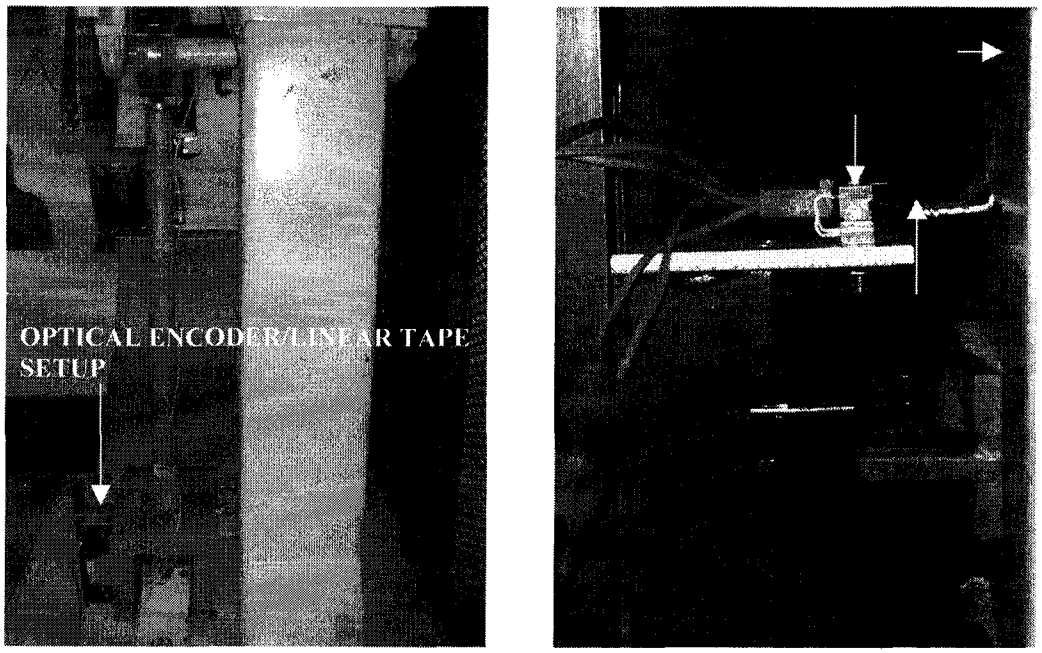

Figure 4-7. Optical Encoder / Linear Tape Setup

The linear tape must be placed in the same plane as the point of impact between the tup and the specimen or the measured velocity will be incorrect. However, velocity corrections can be made by using the angular velocity of the pendulum if the linear tape can not be placed in the impact plane. To make the correction the angular velocity (ω) is calculated by using the linear tape's position from the pendulums center of rotation (r). The velocity of the impact point can then be calculated by multiplying the angular velocity by the distance between the impact plane and the pendulum's center of rotation.

$$v = \omega * r \qquad (9)$$

4.1.2.2.1 Gate and Source Signals / Calculations

Since the theoretical velocity calculation is performed for the pendulum's center of percusion (CP) it is important to correct for the difference in position between CP and the linear tape's position.

Instantaneous velocity measurement by using Equation 10 at the linear tapes position is possible since the distance between two given points on the linear tape is known as shown in Figure 4-8, and the time (dt) to traverse two successive points is measured using a 80 MHz counter.

$$v(t) = ds/dt \qquad (10)$$

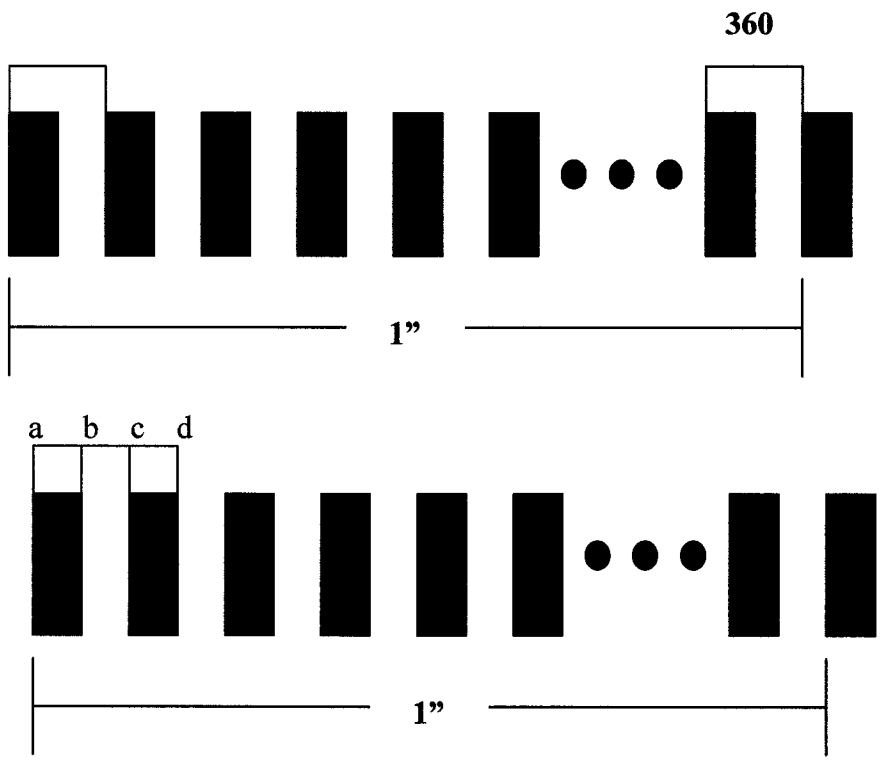

Figure 4-8. Linear Tape Resolution

The tape must be set up to acquire data prior to impact, so the velocity can be measured prior to and through impact, and then a constant (ω) can be calculated with Equation 9 to use to calculate the proper CP velocity values.

Successive counts are produced and stored in a database for each d_{a-c} position traversed as shown in Figure 4-8. An example of how the data is used to calculate velocity, acceleration and applied force is shown in below, where d_{a-c} is constant and t_{a-c} is calculated by dividing the counts produced by the frequency of the counter used. In this case a pulsing frequency of 80 MHz is used and therefore the count is divided by 80000000 to determine the time it takes to traverse d_{a-c}.

360 CPI ; V_o = 5.1975m/s Clock Speed = 80MHz

d_{a-b} = 1/720"

= 1.39×10^{-3} inches

= 0.03528 mm

t_{a-b} = 6.78745 μs

d_{a-c} = 0.07054 mm

t_{a-c} = 13.5749 μs

Source = 1086

A buffered periodic event counting is used to obtain the data. This method of counting requires both a gate and a source signal as shown in Figure 4-9, where each is provided by the encoder and the counter timer card respectively.

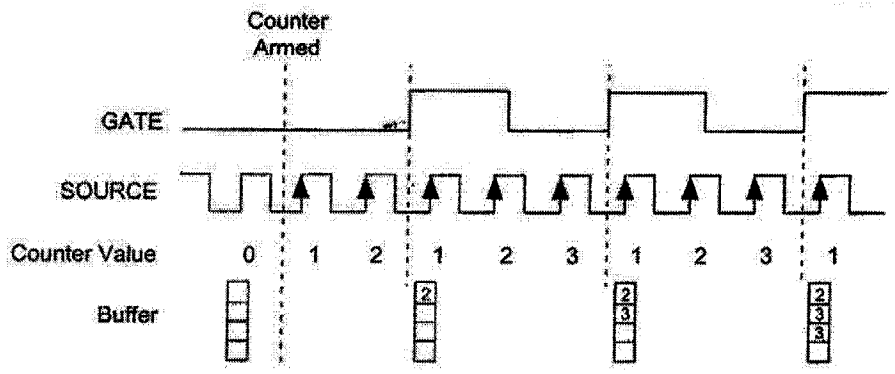

Figure 4-9. Gate signal produced by the optical encoder and the source signal produced by the counter/timer card

The Gate signal is converted to the digital signal seen from an analog signal with an internal optoschmidt trigger. Its signal indicates the boundary between consecutive counting intervals where the rise of the gate signal occurs at the start of each line on the linear tape. The distance between each rise of the gate signal will always be constant for any given linear tape resolution, and for this set of experiments, a resolution of 180 CPI or a distance of 141.1μm between successive gate rise signals is used.

As shown in Figure 4-10 the source signal measures the time interval between events on the Gate signal, so only a source signal is required for a velocity measurement. By using a National Instruments 80 MHz counter/timer card thousands of source signals are produced for each gate signal.

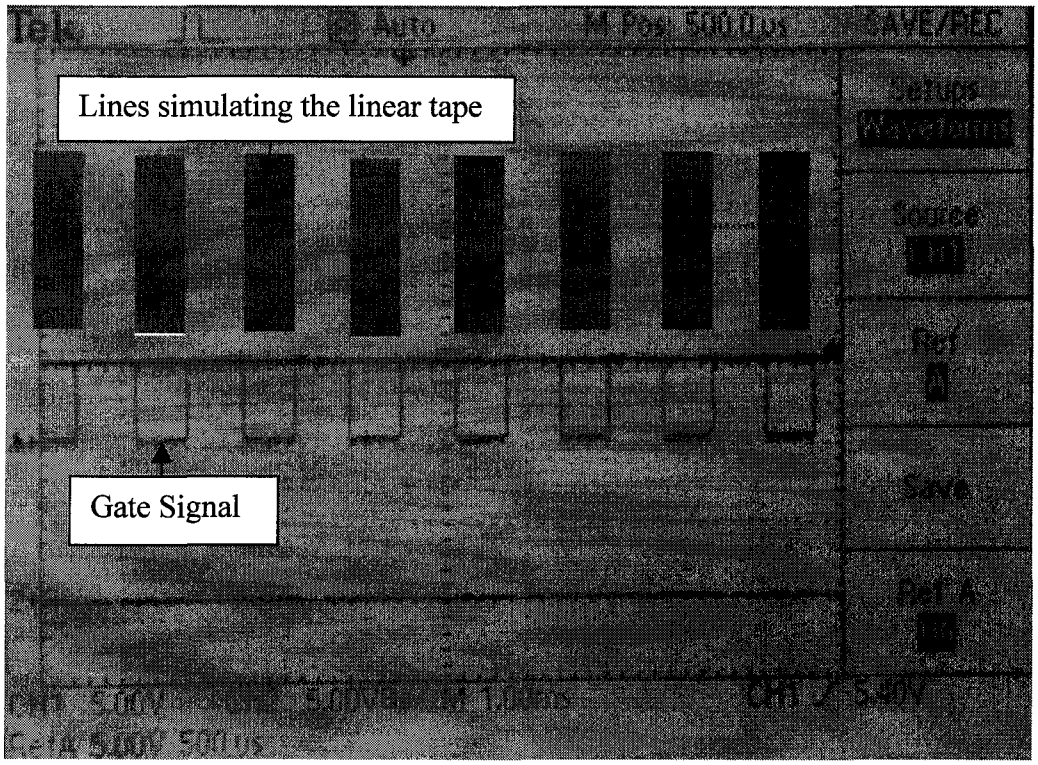

Figure 4-10. Gate signal produced on a scope from a linear tape passing through an encoder

Once the instantaneous velocities are calculated using equation 10, both acceleration and applied force can be calculated using Newton's 2nd law:

$$a(t) = dv/dt \qquad (11)$$

$$F(t) = m*a(t) \qquad (12)$$

4.1.2.2.2 Errors

Since velocity, acceleration and force value are all dependent on an accurate position and time measurement, potential errors will be examined.

Potential sources of error include position measurement, counter/timer, and optical encoder errors.

4.1.2.2.2.1 Position

Resolution of the linear tape was checked with an optical microscope and image analysis software. After the image analysis software was calibrated with a calibration slide shown in Figure 4-11 the linear strip was measured as seen in Figure 4-11 and confirmed to have a resolution of 180 CPI, therefore the linear tape can be eliminated as a potential error source.

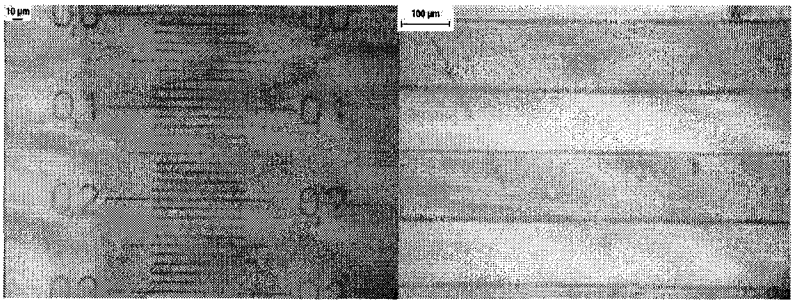

Figure 4-11. Calibration Slide **Figure 4-12. Linear Tape 180 CPI resolution**

4.1.2.2.2.2 Counter/Timer

Acquiring the gate signal from the optical encoder is subject to measurement errors due to 'Crystal Oscillator Error' and 'Measurement Error', and the total error involved with frequency measurement is equal to the sum of each of these. National Instruments 6602 has a maximum source frequency of 80 MHz and the crystal oscillator can potentially have an error up to 4000 Hz since the crystal is rated at 50 parts per million stability over temperature. Measurement error is the result of experimental setup of the frequency measurement, and therefore a setup that minimizes error should be chosen.

The setup can include either a period measurement, counting the number of pulses in a known time, or measurement of the time of a known number of cycles. A potential measurement for each of these will be based on having a linear strip with a resolution of 180 that has a maximum frequency of 40 kHz during maximum velocity.

Measuring the period with an 80 MHz time base and a 40 kHz frequency should return a count of 2000. The specifications of the card yield that this count may be off by +/- 1 due to sampling errors, and therefore a count of 1999, 2000, and 2001 will be returned with a corresponding frequency of 40.02 kHz, 40 kHz, and 39.98 kHz respectively. The respective sampling error is then 2003, 2004, and 2005 ppm.

Example:

40 kHz * 1/x = 2.5 E-5 s

2.5 E-5 s * 80 MHz = 2000 counts

By having both a counter with a fast time base and a linear strip with a low resolution the sampling error can be kept low. However, the benefits of decreasing the sampling error with a low-resolution strip are offset by a reduced number of data points. Since a high rate counter of 80 MHz will be used, the error is only reduced by varying the resolution of the linear strip, and encoder.

4.1.2.2.2.3 Encoder

Table 4.2 lists the minimum, typical and maximum error over a full rotation of an optical rotary encoder that is used under recommended operating conditions. The conditions that the optical encoder was used under during impact testing included ambient temperature (20°C), 5 Volts, ~ 40 – 80kHz count frequency. According to Table 4-2, testing conditions do fall within the recommended operating parameters.

Parameter	Min.	Max.	Units	Notes
Temperature	-40	100	°C	
Supply Voltage	4.5	5.5	Volts	Ripple < than 100mV P-P
Load Capacitance	-	100	pF	
Count Frequency	-	100	kHz	rpm/60 x cycles/rev.

Table 4-2. Encoders recommended operating conditions[48]

Parameter	Note	Symbol	Min.	Typ.	Max.	Units
Cycle Error	-	-	-	3	5.5	°e
Symmetry	-	-	150	180	210	°e
Quadrature	-	-	60	90	120	°e
Index Pulse width	-	Po	60	90	120	°e
CH. I rise after CH. B or CH. A fall	-	t1	-300	100	250	ns
CH. I fall after CH. A or CH. B rise	-	t2	70	150	1000	ns

Table 4-3. Values are for the maximum error over a full rotation and within the recommended operating range[48]

Cycle, quadrature, and symmetry errors have to do with how precisely the electronics in the module responds to the edges of the lines on the linear tape. One complete electrical square wave cycles is generated out of both the A and B channels, as seen in Figure 4-13, each time there is movement of the strip equal to the leading edge of one line to the leading edge of the next line.

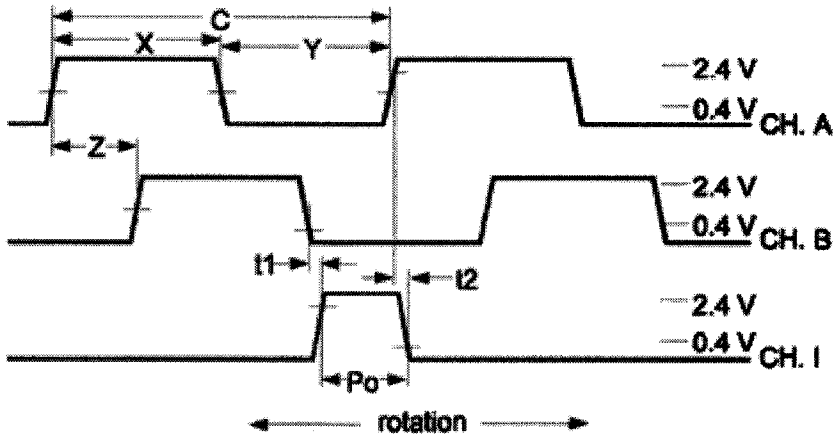

Figure 4-13. Gate Signal[48]

On a 180 CPI strip, this distance is going to be 1 divided by 180 or 0.0055556". Each electrical square wave cycles has 360 electrical degrees in it. So each electrical degree corresponds to 0.0055556" divided by 360 or 0.00001543". So if the typical cycle error is stated to be +/-3 electrical degrees, that would be equal to +/-0.00004629".

In a perfect world, a 180 CPI linear encoder would generate 180 perfectly even electrical square wave cycles for each inch of travel. Each electrical square wave cycle would last for 1/180th of an inch. The cycle error is telling us that the module isn't quite perfect, it will typically introduce up to +/-3 electrical degrees (+/- 0.00004629" for a 180 CPI strip) of error into an individual cycle's length. Some cycles may be short by that amount, and some cycles may be long by that amount. The errors do cancel each other out after one complete rotation of the disk, because it always returns to the same beginning point in one revolution. For every cycle that was short in duration, there were other cycles that were long to compensate for it. The same thing is true for symmetry errors (the high time

vs. low time of each cycle), and quadrature errors (the 90 electrical phase shift of A in relation to B).

Theoretical errors due to position accuracy, the counter/timer and encoder, encompass less than a 1% error. Thus if the equipment is setup properly, measuring the time between any two successive points during impact should be done with a high degree of accuracy.

4.1.2.2.2.4 Electrical Noise

If the lengths of the cables are longer than 6ft it is suggested to have a noise reducer to minimize electrical noise. Since it is a digital signal that is being produced by the optical encoder by the optoschmitt trigger, neglecting to meet this criterion will just result in the lack of a signal being produced.

4.1.2.3 Encoder Verification on Charpy Machine

Optimization of the optical encoder / linear tape method can be improved upon by lowering the cycle error. Although this error exists in every test and produces scatter in the data, the high sampling rate increases the curve fit accuracy. Ideally it would be best to have no scatter at all, and this should easily be achieved in the future as optical encoders improve and the cycle errors are minimized.

Velocity versus displacement graphs from optical encoder data show initially showed that the velocity of the pendulum head increased part way through the test as seen in Figure 4-14. The increase in velocity was originally thought to occur as the result of stored elastic energy in the pendulum arm. Although it is inevitable that some energy will likely be stored and lost in the pendulum arm as elastic energy as noted by Manahan[49], data gathered like that in Table 4-1 were considerably different from the dial gauge energy. Manahan noted that up to 1.5 J of energy could be lost to the pendulum arm as a result of different CP to CM within ASTM parameters, but Table 4-1 and other results from initial optical encoder tests were revealing up to a 20 J difference when measuring the energy difference between v_{max} and v_{min}. The discrepancy between Manahan's work and our encoder results questioned the validity of the either the encoder data or Manahan's work.

4.1.2.3.1 Velocity Increase

While measuring the displacement of the pendulum head with the optical encoder and linear tape on a Charpy impact tester, a significant amount of elastic energy was initially assumed to be stored in the pendulum as a result of the increase in velocity of the pendulum as shown in Figure 4-14.

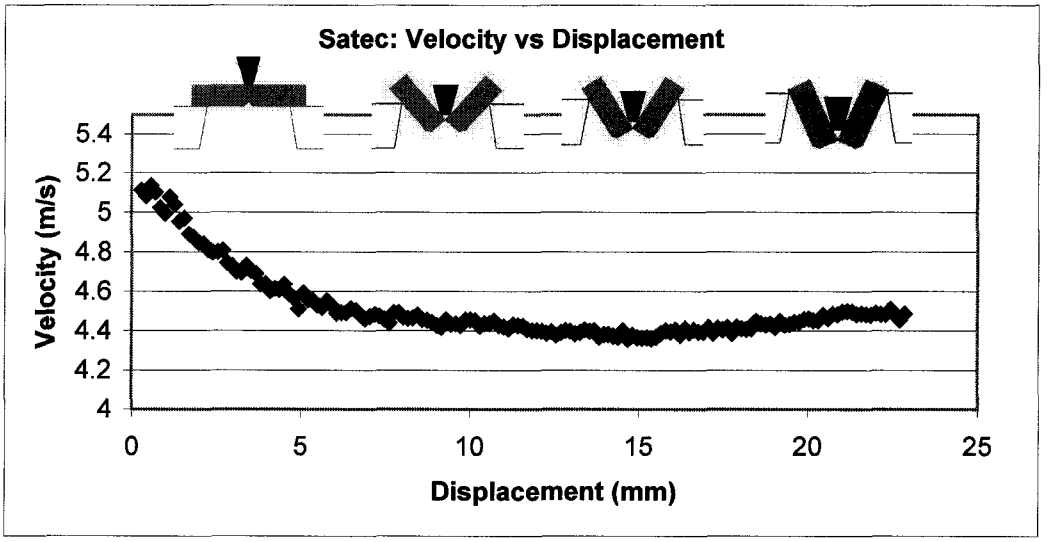

Figure 4-14. Measured velocity of pendulum with optical encoder and linear tape

The difference between the dial energy and the energy measured by the optical encoder were calculated to be up to 20 J. The energy difference was calculated by using the change in kinetic energy between the initial velocity and the lowest velocity obtained with the velocity displacement curve shown in Figure 4-14. Velocity displacement curves that showed this increase in velocity always display a lower absorbed energy than should exist according to the dial energy, and thus it was initially believed that more energy could be lost to the pendulum than Manahan[49] indicated.

Many basics of Charpy impact testing suggest that specimens are subjected to a three-point bend with a "rigid" pendulum arm. Theory that suggests that the pendulum is a rigid body is based on having the pendulums center of strike (CS) in the same plane as the center of percussion (CP).

Hence, elastic energy can only be stored in the pendulum if the center of mass of the pendulum and the impact specimens do not fall in the same plane. Free body diagrams in Figure 4-15 shows how induced moments would affect the pendulum for the three different specimen/center of mass interaction scenarios.

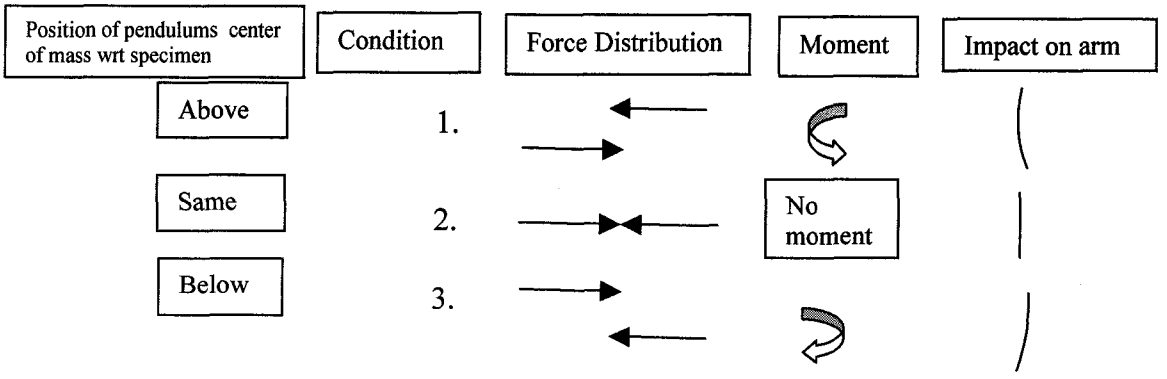

Figure 4-15. Effects of induced moments on the pendulum

Although CS and CP should be like condition 2 in Figure 4-15 (according to ASTM E23 within 1%), if the center of mass is changed and all other conditions are kept constant (mass, v_o, arm length, specimen) the velocity profiles for the other (1&3) "force distribution" conditions would differ.

The resulting moment in condition 1 results in the pendulum storing elastic potential energy similar to a compressing spring. Elastic energy that is stored in the pendulum should theoretically be released following the maximum load, which occurs well before the point of increasing velocity. Since the maximum deflection of the pendulum arm occurs when the applied load is maximum and as the load decreases the stored elastic

energy in the pendulum will be released as energy giving the pendulum head an added force in the forward direction. The point where there is an increase in the velocity of the pendulum was thought to occur as a result of anvil slip because the material resistance of the test specimen becomes overpowered by the elastic energy stored in the pendulum. This seemed to be a possibility as all of the X70 and X80 pipeline steels that were tested in the upper shelf region on the SATEC SI-SK1 initially showed that an increase in velocity of the specimens occurred at the deflection point of about 15 mm.

Storing of energy in the pendulum arm seemed inevitable and these initial results suggested that up to 20 J of energy were being stored in the pendulum arm and released as elastic energy. The 20 J noted in these measurements were significantly different from the maximum 1.7 J that Manahan[49] suggested could potentially be stored in the pendulum arm and therefore the optical encoder / linear tape setup was tried on a few different machines to determine if the increase in velocity was a potential error.

Additional encoders were placed on the pendulum arm as shown in Figure 4-16 in attempts to show that the pendulum arm would deflect as thought and could be measured because the arm and head would travel at different angular velocities if there was any deflection in the pendulum.

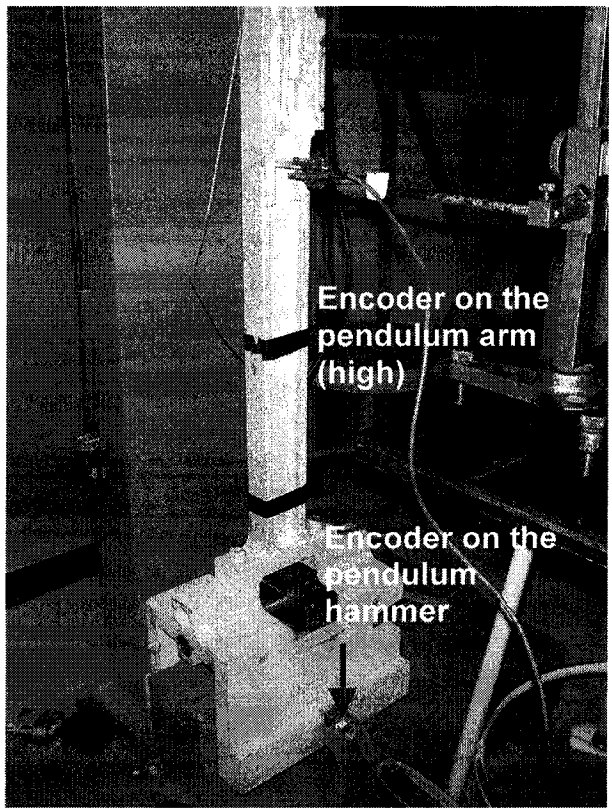

Figure 4-16. Addition of multiple encoders to the pendulum

The expected results were not obtained but rather the pendulum arm was shown to vibrate as shown in Figure 4-17 and Figure 4-18 as suggested by Kobayashi.[35]

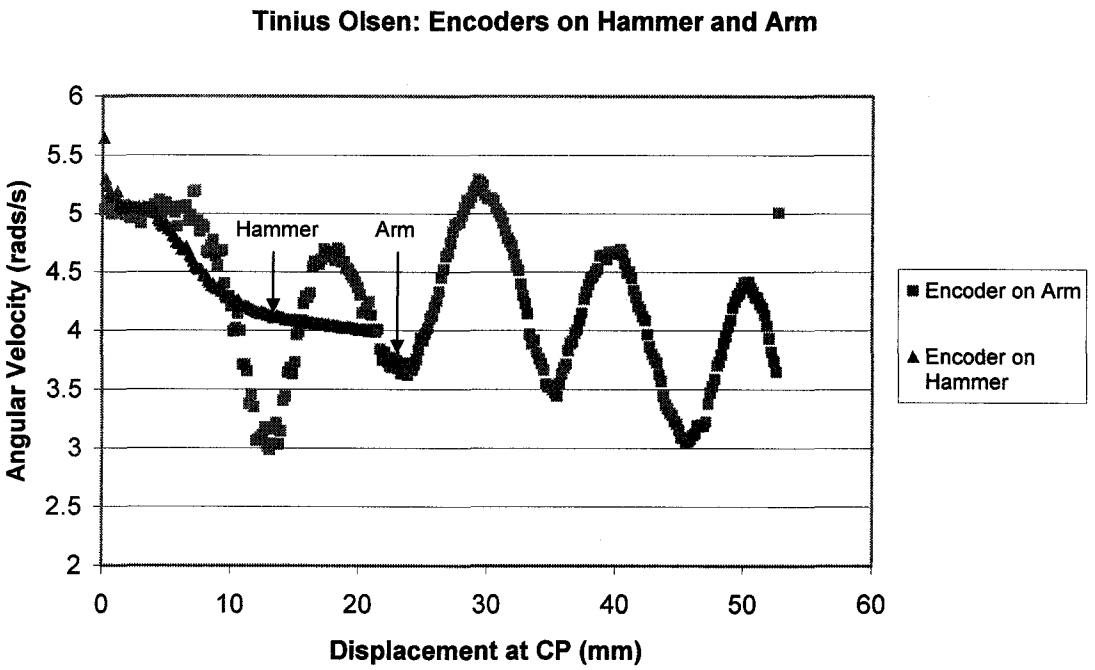

Figure 4-17. Angular velocity measurement of pendulum at two different positions

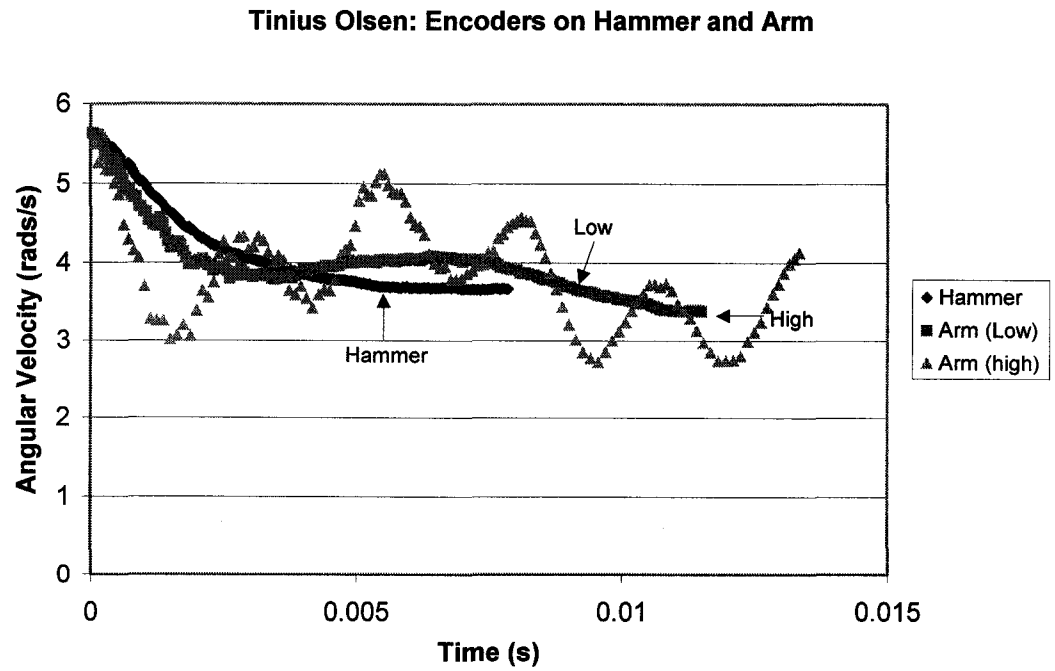

Figure 4-18. Angular velocity measurement of pendulum at three different positions

In addition to determining that the pendulum oscillates rather than deflecting, as initially predicted in Figure 4-15, no increase in velocity at the hammer position was observed in Figure 4-18 like that observed in Figure 4-14, which suggested that the initial increase in velocity could be due to setup errors. Setup errors were indeed confirmed as subsequent calculations of the hammer encoder data from the setup used in
Figure 4-17 and Figure 4-18 resulted in an energy measurement error of less than 2 J when compared to the dial gauge energy.

Since the velocity of each of the encoders is measured while the pendulum is primarily in the vertical position the velocity of the pendulum through a free fall should be relatively constant, but a slight decrease in velocity may be observed with larger arc lengths. Free fall tests performed on the setup used in Figure 4-18 confirmed that the encoder on the hammer and the lower encoder on the arm were setup correctly while the higher encoder on the arm had setup errors as indicated by the measured velocity increase shown in Figure 4-19.

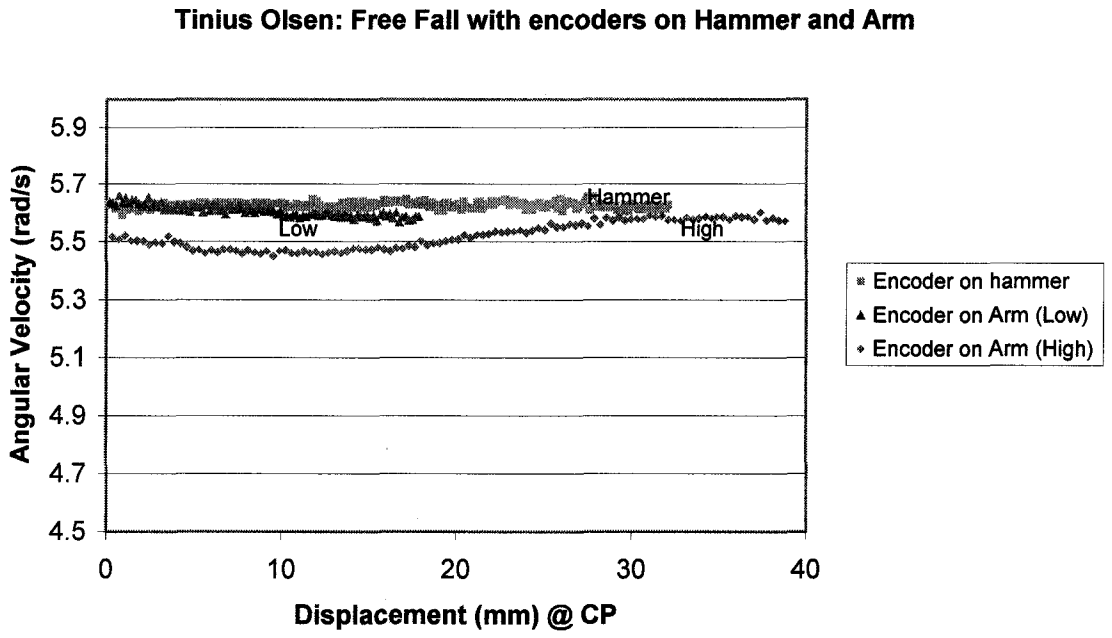

Figure 4-19. Free fall velocity measurement with encoders placed at three different positions on the pendulum

Free fall tests have therefore shown their importance in determining if the setup of the optical encoder and linear tape are correct, because in no way should there be an increase in velocity observed in a Charpy impact test if the pendulum is in the vertical position or in the upswing position.

The accuracy of the encoder velocity measurements for properly setup encoders was checked at several points during and after impact as shown in Figure 4-20. Since the theoretical velocity can be determined at different heights by equating potential energy to kinetic energy, the three encoders were placed in series at different heights, and the theoretical velocity was then compared to the velocity measured by the encoders.

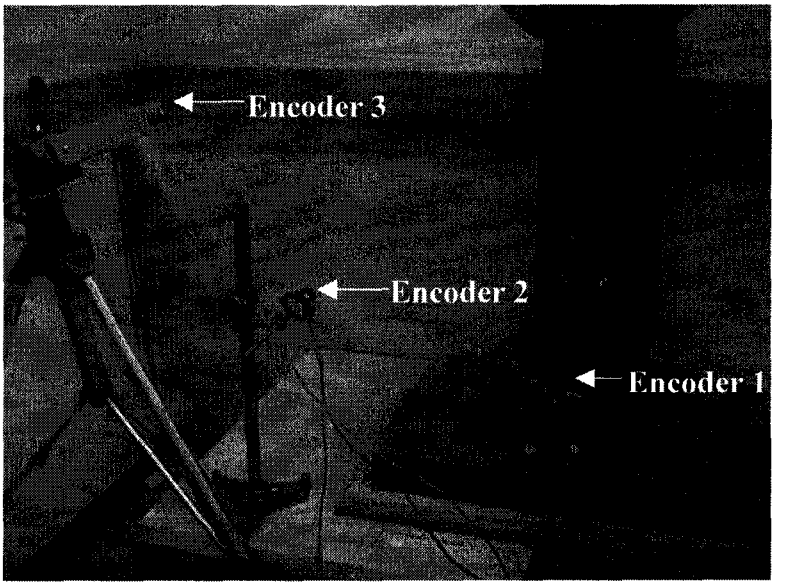

Figure 4-20. Setup of encoder velocity measurement at three successive points

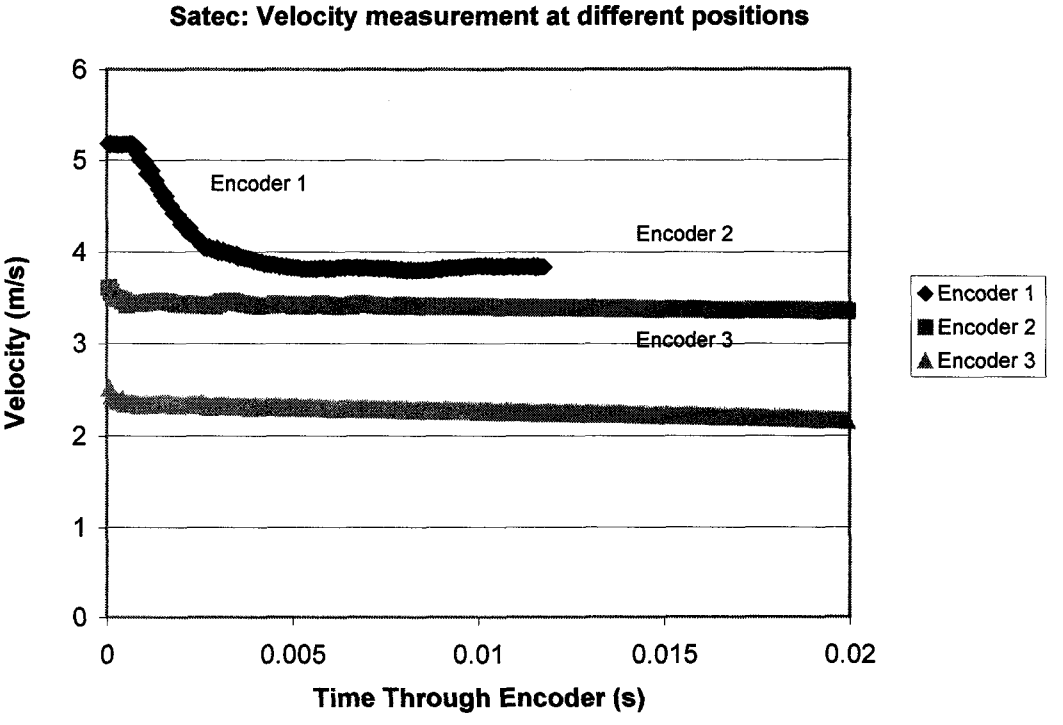

Figure 4-21. Encoder velocity measurement at CP at three successive points

Comparison of the velocity after fracture (v_f) and the velocities at encoders 2 and 3 to the theoretical velocity at each encoder were equal, and therefore the significant velocity rise in Figure 4-14 at 15 mm was confirmed to be the result of setup errors because tests performed on both Tinius Olsen and a Satec Charpy impact testers showed that a minimal or no increase in velocity occurs during the test as seen in Figure 4-18 and Figure 4-21, therefore initial optical encoder data had errors. With proper setup, the velocity of the pendulum just after the specimen breaks was shown to be equal to the total energy absorbed by the specimen during impact ($KE = \frac{1}{2} m (v_o^2 - v_f^2)$), which confirms the accuracy of the optical encoder and linear tape measurement method.

Since all the optical encoder data available for analysis measured an incorrect velocity due to setup errors, the Charpy propagation energy will be selected from the instrumented tup data. Although the energy measured by the instrumented tup has been shown to provide incorrect data, the steady state propagation energy measured by the instrumented tup is out by a specific factor as indicated by the similar slopes in Figure 4-22.

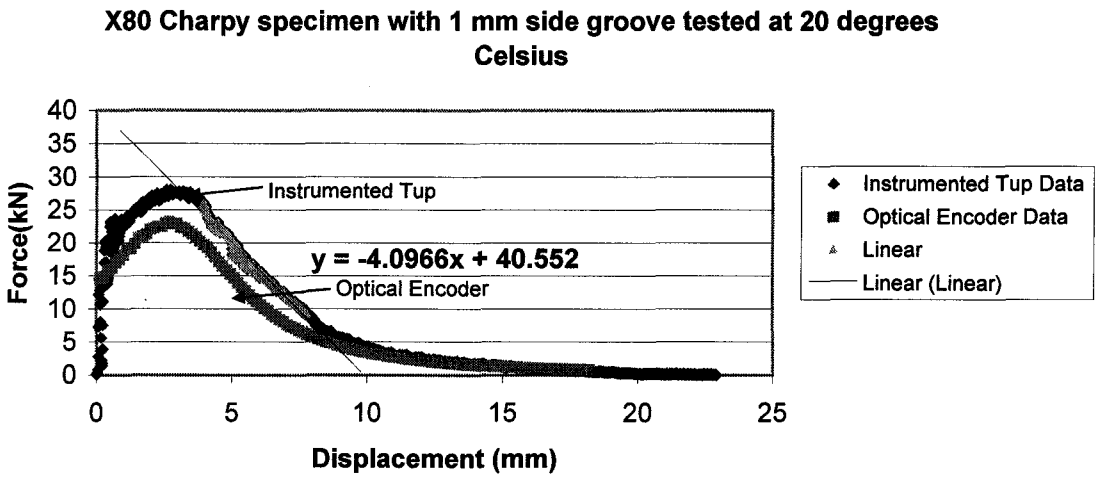

Figure 4-22. Optical encoder vs. instrumented tup data

4.1.2.4 DWTT

Unlike the Charpy machine, the DWTT machine cannot account for the energy absorbed during impact with differences in potential energy before and after impact. Therefore an instrumented tup must be used on the Dynatup 8100F drop weight tear tester to measure the energy absorbed by the DWTT specimens. The energy absorbed by the specimen is calculated from the area under the load-displacement curve from initial impact complete fracture (where the load returns to zero). Since the absorbed energy by the DWTT specimen cannot be confirmed with direct potential energy measurements as with the Charpy machine the absorbed energies are assumed to be correct if proper calibration factors are used. The strain gauges in the tup ensure that consistent load measurements are obtained and thus reliable values can be obtained in the quality assurance / control of materials. Even though tup measured energy values are consistent, the current use of

static calibration factors to obtain actual energy values absorbed by the DWTT specimens under dynamic conditions may be wrong. Therefore an alternative energy measurement has been attempted and tested to confirm or contradict the energy values that are obtained with the instrumented tup.

The setup for this measurement is seen is Figure 4-23, and the method for measuring the absorbed energy uses the potential energy of the weights that impact the DWTT specimen and be explained according to Equation 13.

$$PE = KE + \text{Energy Absorbed} \qquad (13)$$

Where: PE – Potential Energy of the hammer to the point where the crack has completely propagated through the specimen

KE – Kinetic Energy of the hammer at the point where the crack has completely propagated through the specimen

Energy Absorbed - Fracture
- Friction (anvils and tup)
- Elasticity (negligible)

Although the potential energy can be measured prior to impact, the energy absorbed by the specimen can only be measured once the crack completely propagates through the specimen.

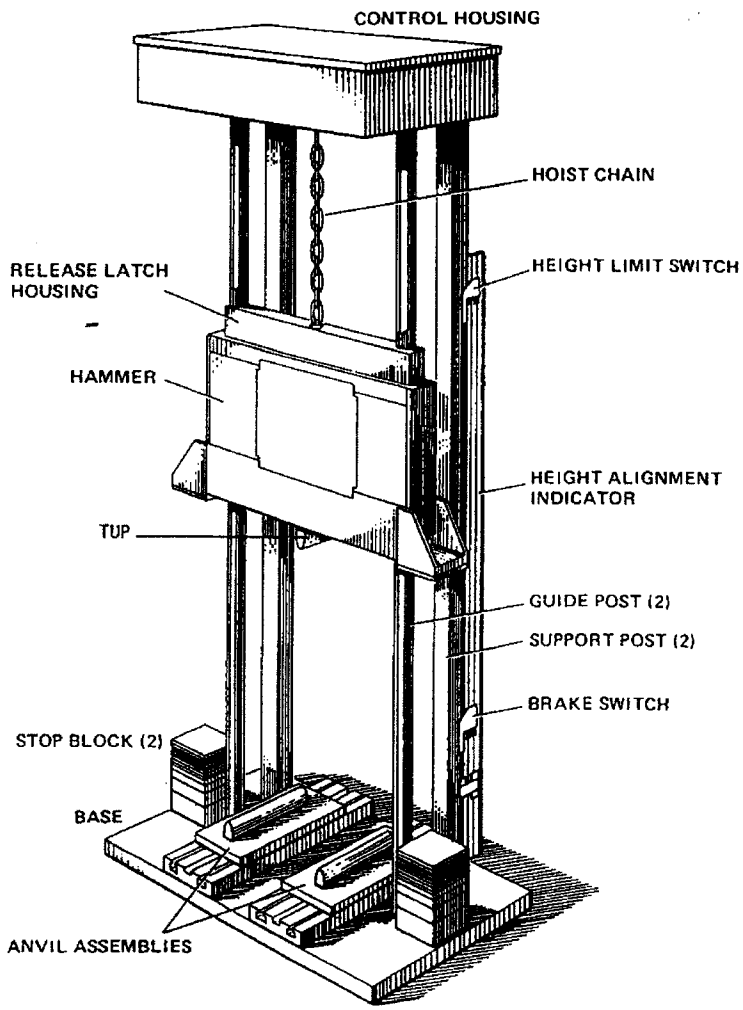

Figure 4-23 DWTT machine[50]

The results from the encoder/linear tape energy measurement show a large amount of scatter. Scatter in the counts between two consecutive points are considerably higher than expected from error calculations, which is likely the result of the encoder and linear tape vibrating during impact. The vibrations are the result of a 1000-kilogram mass

impacting the test specimen at a velocity of 5.9 m/s, which exaggerated the expected counts between points. Figure 4-24 shows the difference between counts measured during a free fall and that from an impact test with X80 pipeline steel.

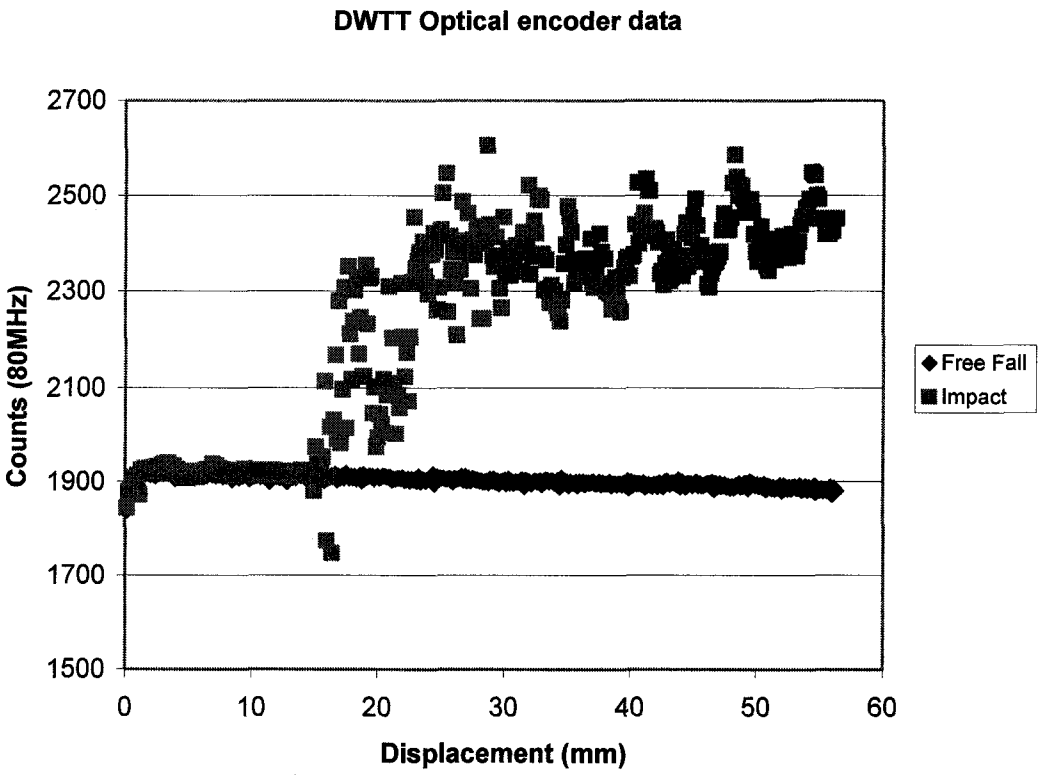

Figure 4-24. Attempted energy measurement with optical encoder

From the slope of the free fall line we can conclude that the encoder/linear tape method can measure the velocity with reasonable accuracy if encoder vibration is minimal since the velocity of 5.9 m/s is identical to the theoretical velocity calculated from the hammer's initial potential energy.

The problems that have contributed to the counting error can probably be eliminated with the use of a vibration pad if this is the source of error. Potentially the error in this can be

the result of setup error from vibrational effects but further testing would need to be done to confirm this.

4.2 Side Grooving

Energy absorption relationships that exist between traditional Charpy and DWT tests do not consider the different stress conditions that exist between specimens of different size. Because the larger thickness of a DWTT specimen produces a larger plane strain section than a thinner Charpy specimen, side grooves were added to both impact specimens to change and equalize the stress conditions and control the fracture path. Ideal stress conditions in the Charpy and DWTT specimens should eliminate or dramatically minimize the plane stress section by increasing restraint at the edge of the specimen.

4.2.1 DWTT Results

Analysis of the load displacement plots reveals that side grooves negatively affect the DWTT data such that typical steady state crack propagation does not occur. Addition of the side grooves to DWTT specimens changes the through thickness restraint conditions in the specimens, and since traditional DWTT data already resembles full scale pipeline behavior in stress conditions, fracture morphology, transition temperature, and energy absorbed, the addition of side grooves results in an inability to measure a comparative full scale energy with DWTT specimens. As seen in Figure 4-25 and Figure 4-26, steady state crack propagation does not occur in specimens with side grooves as indicated by the lack of a traditional linear region.

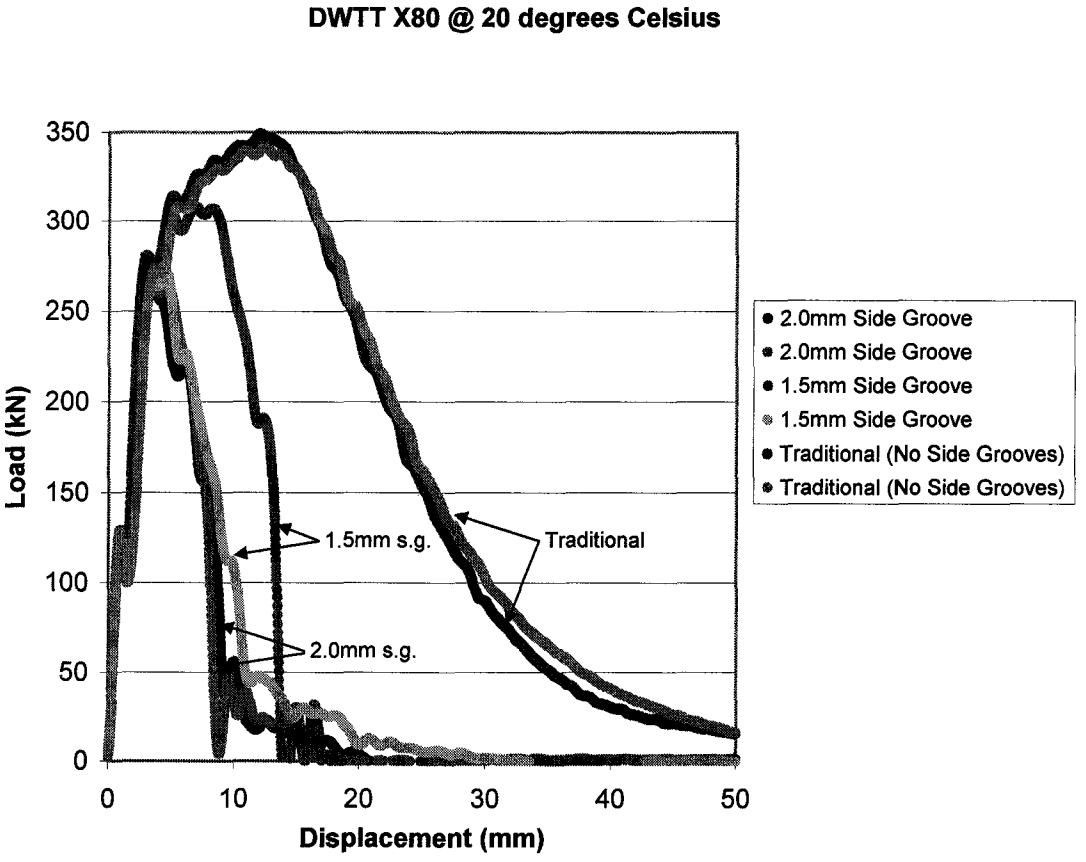

Figure 4-25. Comparison of DWTT load vs. displacement data for X80 specimens in the upper shelf region

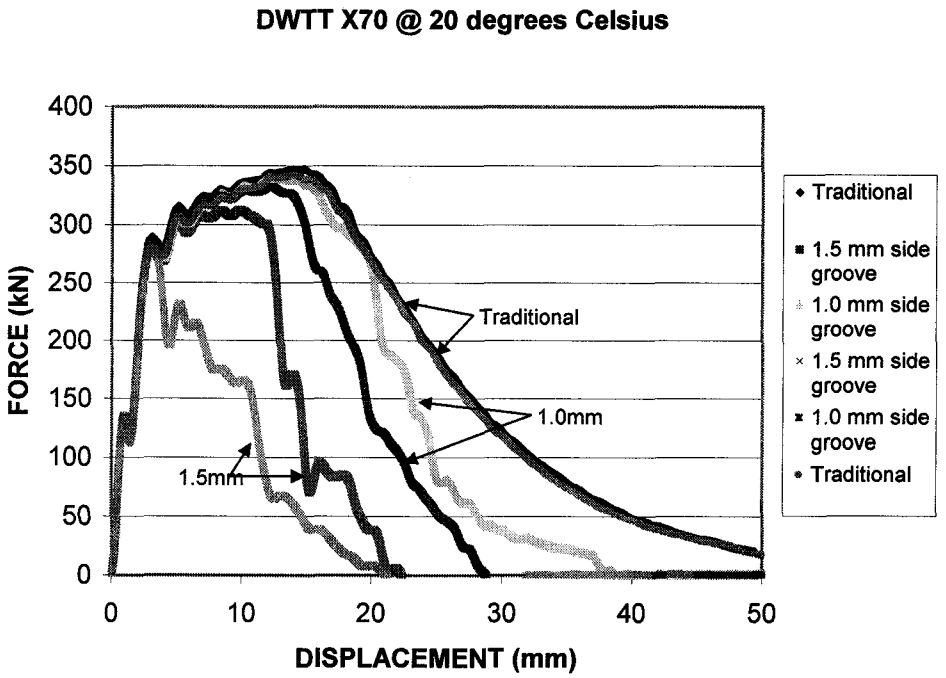

Figure 4-26. Comparison of DWTT load vs. displacement data for X70 specimens in the upper shelf region

Since the traditional specimens have a measurable linear region on a load versus displacement curve, steady state crack propagation is assumed to occur only in traditional specimens, as shown by Wilkowski in Figure 4-27.

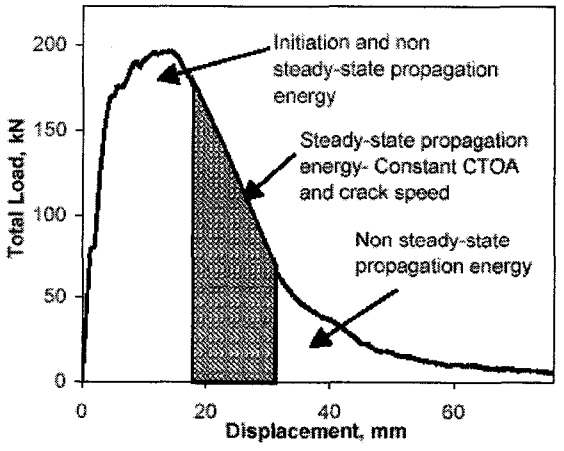

Figure 4-27. Steady state crack propagation region[51]

4.2.2 Charpy Specimens

A Charpy's short ligament length and thickness will result in a ductile fracture that results in failure and a significant amount of plastic deformation as shown by the shear lips in Figure 4-28.

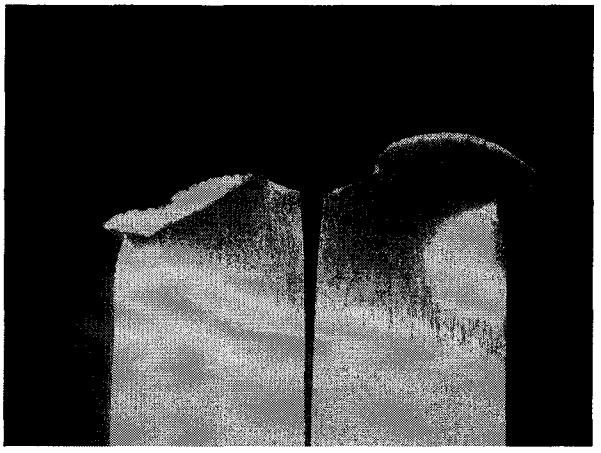

Figure 4-28. X80 – Traditional Charpy specimen

Side grooves have been added to the Charpy specimens to manipulate the stress conditions and induce steady state crack propagation. Attempts to induce steady state conditions with side grooves are necessary because steady state crack propagation has been shown not to occur in traditional Charpy specimens as shown in Figure 2-10. Since the side groove depth necessary to induce plane strain conditions in a Charpy specimen is material dependent, determining an appropriate side groove depth for the X70 and X80 materials is necessary. Increasing the side groove depth beyond a certain minimum depth has no effect on the stress conditions or energy, and thus different side groove depths were tested for each material and compared against traditional data to determine if steady state crack propagation can be inferred from force vs. displacement curves on X70 and X80 materials.

Side grooves added to Charpy specimens does get rid of the shear lips as shown in Figure 4-29 and the deeper side grooves results in less plastic deformation because of the change of stress condition at the edge of the specimen.

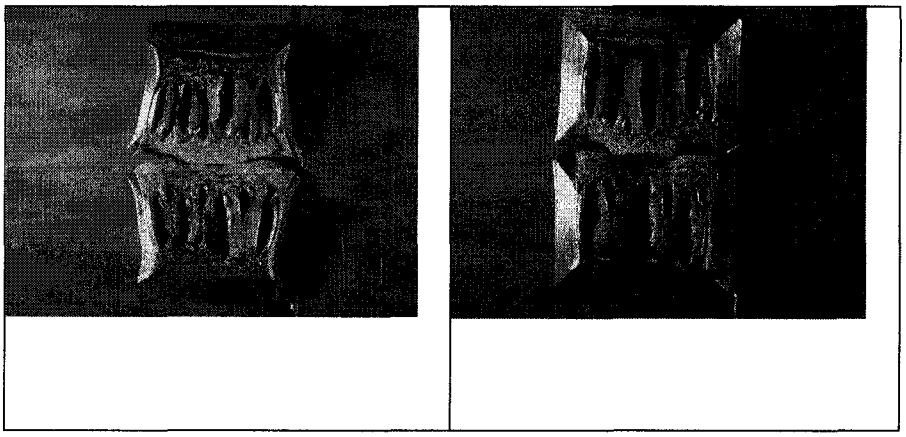

Figure 4-29. X80 Charpy specimens with 0.5 mm and 1.5 mm side grooves

The percentage of plane strain definitely increases with deeper side groove depths as indicated by the decreasing lateral expansion. Measuring the amount of lateral expansion in the specimens is a method that can be used to show augmented plane strain conditions with side groove depth. Minimizing the amount of lateral expansion in the specimen signifies the plane strain conditions existing in a specimen can be maximized, and Figure 4-30 shows how increasing side groove decreases the plastic deformation in Charpy specimens.

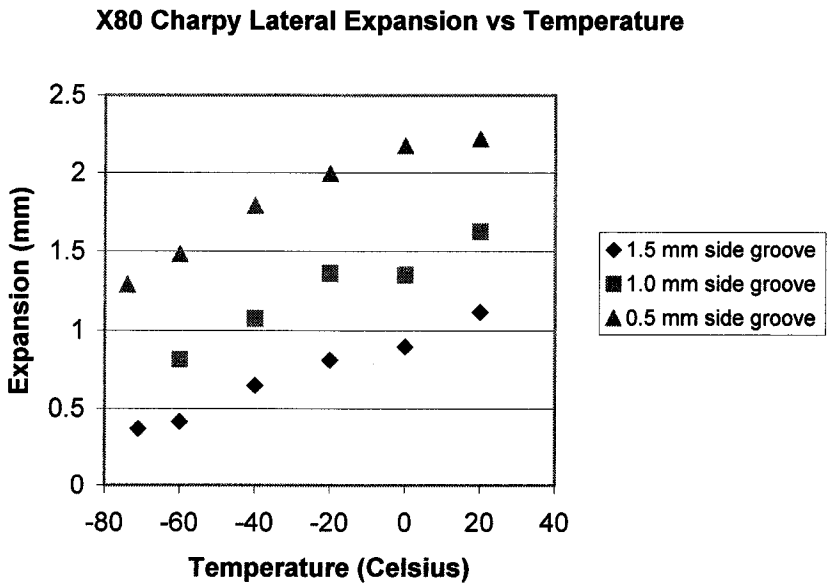

Figure 4-30. Lateral expansion of side grooved specimens

There is a definite decrease in plastic deformation of the specimens with increasing side groove depth and the changing stress conditions do affect the propagation toughness measurement. An appropriate side groove depth must be determined, which will be material dependent.

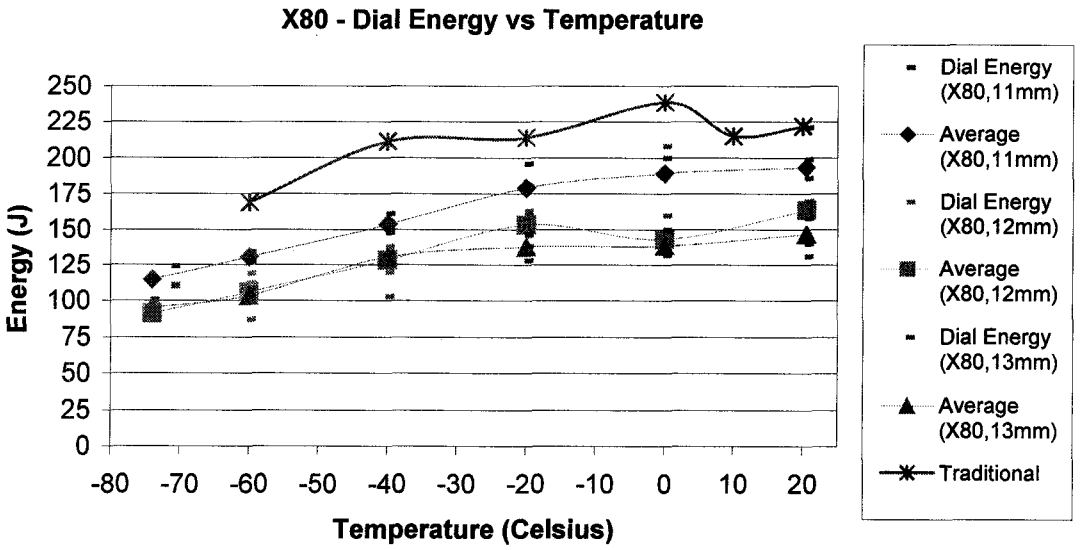

Figure 4-31. X80 Charpy transition curve

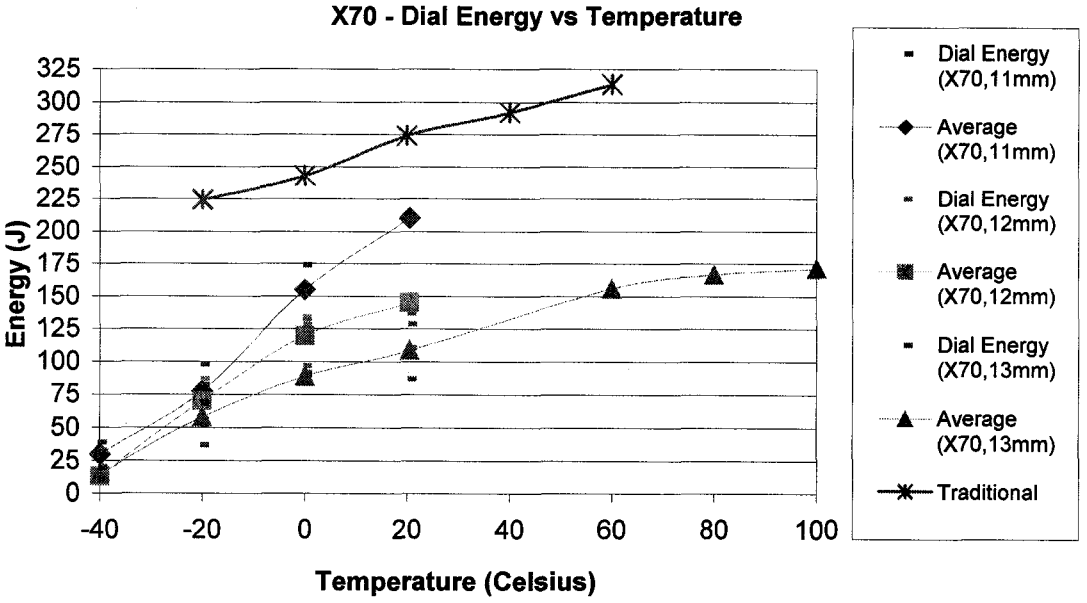

Figure 4-32. X70 Charpy transition curve

4.3 Measuring Propagation Energy

Because we could not measure the CTOA directly with high-speed video cameras, a value representative of steady state crack propagation was measured in the linear region of the load versus displacement curve. The purpose of obtaining instrumented data from both Charpy and DWT tests is to measure the energy necessary to propagate a crack directly from load-displacement curves, and thus the slope of the linear region will be examined and compared between Charpy and DWTT data.

Since it is known that non-steady state crack propagation exists both prior to and following the linear region in a load-displacement curve, the technique that was used to quantify the steady state propagation energy properties of the Charpy and DWTT specimens simply involved determining the slope of the linear region on the load-displacement curves. Steady state crack propagation exists only in the linear region of the curve in DWTT specimens and hence the slope of the curve could describe the material resistance of the specimens under dynamic conditions. It is already known that with brittle materials the slope of the curve would be vertical ($-\infty$), and therefore as the toughness of the material increases the slope of the curve increases from negative infinity.

4.3.1 DWTT

The slope of the load-displacement curve for the DWTT specimens is easily measured as the cracks propagate under steady state conditions because of its longer ligament length

and the resulting stress conditions under which failure occurs. The slopes of the DWTT curves were measured by manipulating the data in an excel spreadsheet and the result for both the X70 and X80 materials are shown in Table 4-4, Table 4-5, Figure 4-33, and Figure 4-34.

X70 Steady State Propagation			
Temperature	Equation of Load/Displacement	Slope (kN/mm)	Average
20	load = -17.318 * displacement + 619.09	-17.318	
20	load = -17.282 * displacement + 613.4	-17.282	-17.3
10	load = -18.117 * displacement + 660.07	-18.117	
10	load = -19.937 * displacement + 780.47	-19.937	-19.027
-5	load = -18.855 * displacement + 708.56	-18.855	-18.855

Table 4-4. Slope of steady state region for X70 DWTT specimens

X80 Steady State Propagation			
Temperature	Equation of Load/Displacement	Slope (kN/mm)	Average
20	load = -16.718 * displacement + 580	-16.718	
20	load = -17.788 * displacement +593.53	-17.788	-17.253
10	load = -18.218 * displacement + 587.91	-18.21	
10	load = -17.945 * displacement + 595.16	-17.945	-18.0775
-5	load = -21.915 * displacement + 740.49	-21.915	
-5	load = -19.401 * displacement + 674.27	-19.401	-20.658

Table 4-5. Slope of steady state region for X80 DWTT specimens

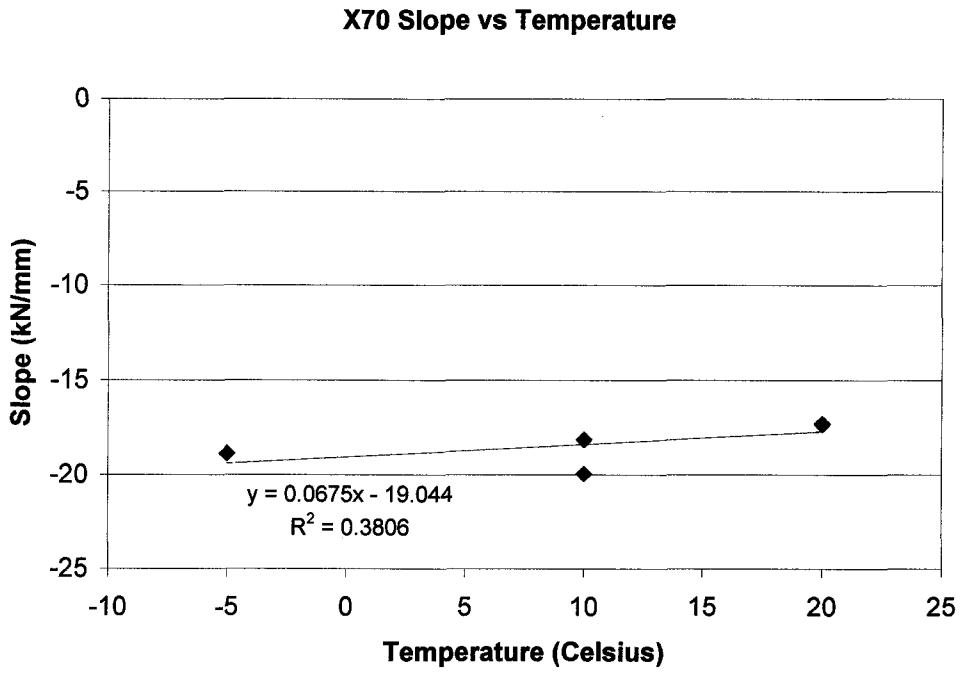

Figure 4-33. DWTT X70 values representative of steady state crack propagation

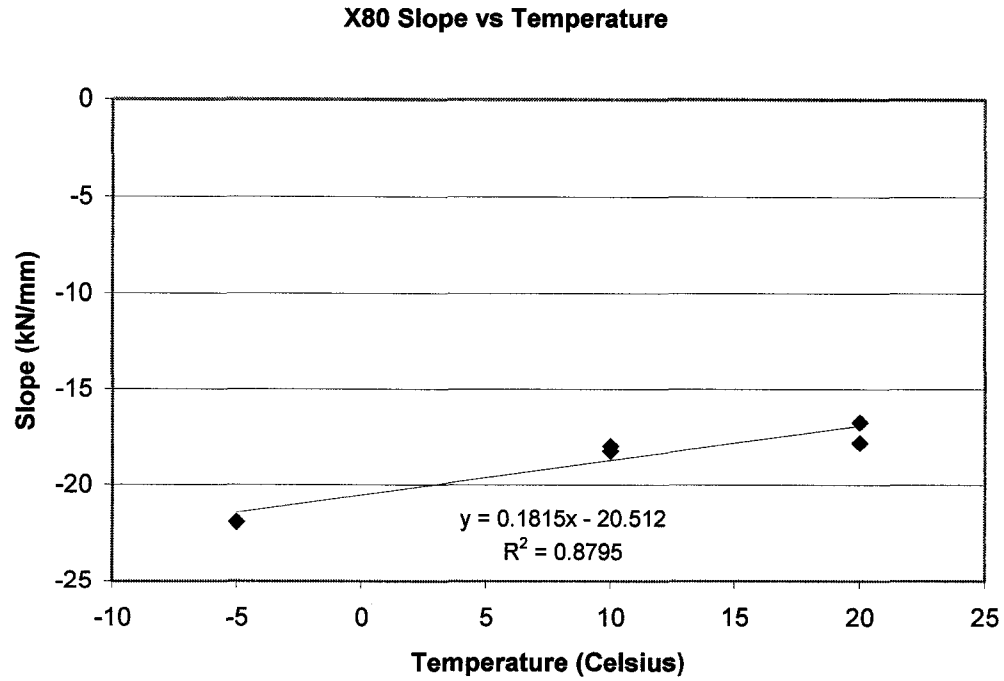

Figure 4-34. DWTT X80 values representative of steady state crack propagation

The decreasing slope with temperature indicates that the propagation toughness of both the X70 and X80 materials decreases with temperature. The decreasing slope with temperature, and high-speed video camera tests by Wilkowski confirmed that there is a decrease in CTOA with temperature. This indicates that the slope of a PN-DWTT load-displacement curve is a feasible method of measuring the propagation toughness of higher toughness pipeline material.

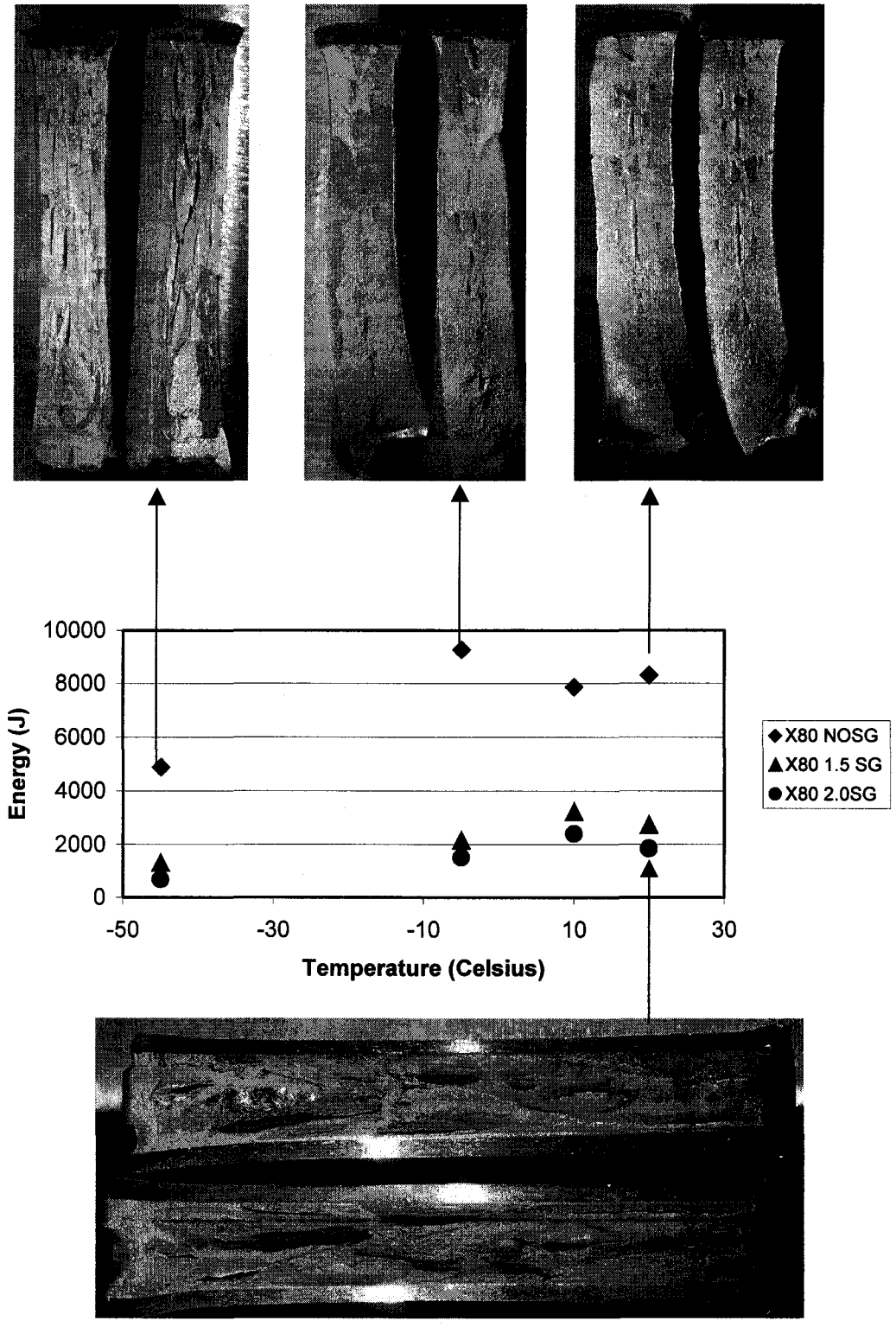

Figure 4-35. Transition Curve of X80 DWTT specimens and fracture morphology

4.3.2 Charpy

4.3.2.1 X80

When measuring the propagation toughness of the X80 material, steady state crack propagation occurs in all of the specimens except the traditional specimen, as evident by the lack of linear region during crack propagation of the traditional specimens shown in Figure 4-36 and Figure 4-37. Steady state crack propagation does not occur in the traditional specimen because of crack tunneling and the resulting shear lips, but with the addition of side grooves to the specimens the material constraint is increased which induces steady state conditions in the specimens. And from the linear region of the load displacement trace a value representative of steady state crack propagation can be measured.

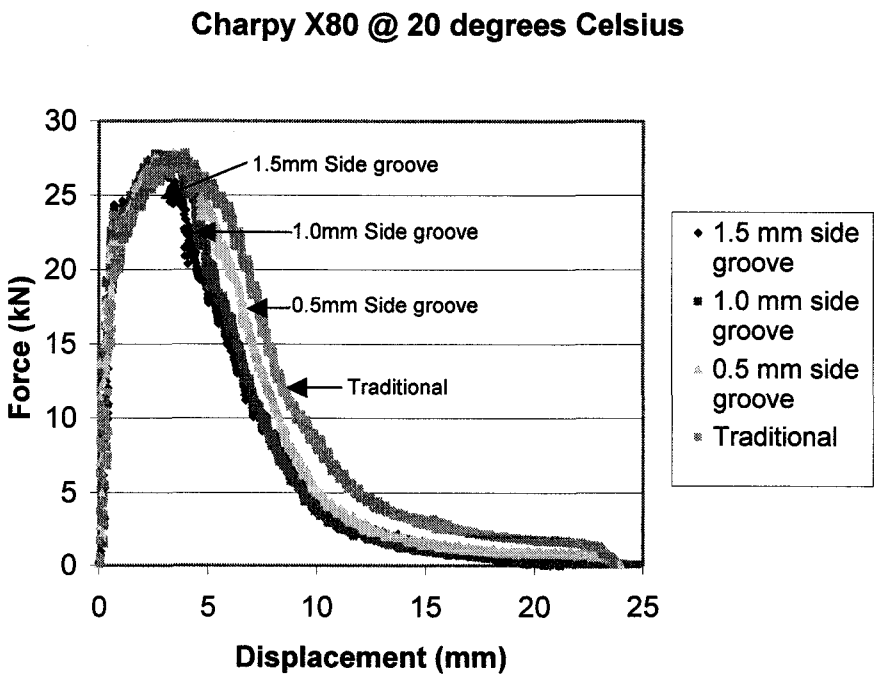

Figure 4-36. Load-displacement curve for X80 specimens tested at 20°C

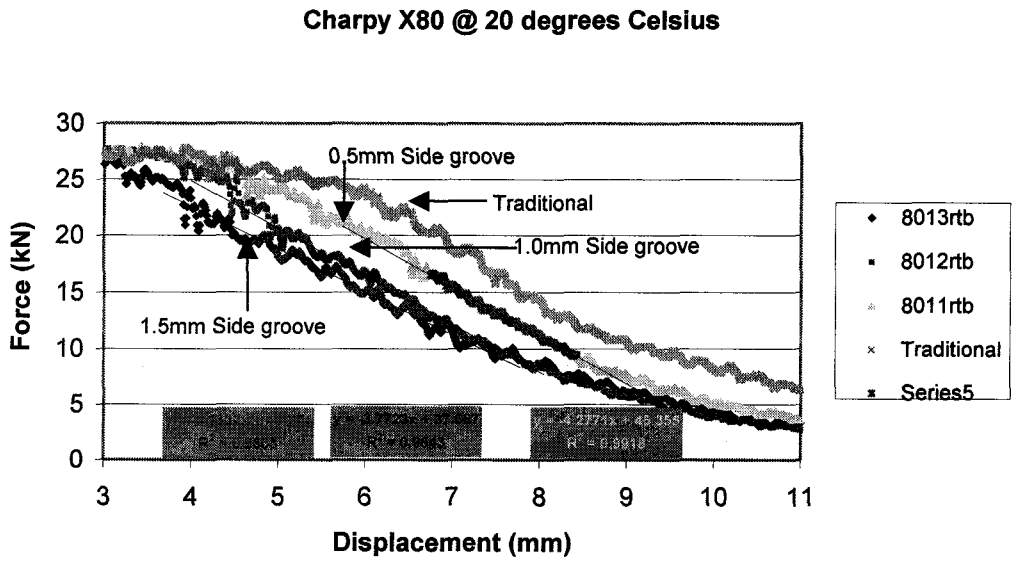

Figure 4-37. Propagation region of X80 specimens tested at 20°C

The traditional specimens, unlike the side-grooved specimens, do not exhibit a region of steady state crack propagation (as indicated by the non-linearity of its load-displacement curve). The non-linearity is the result of the plane stress conditions that exist at the edges of the specimens and result in the presence of the shear lips as shown in Figure 4-38.

Figure 4-38. X80 Charpy specimens with splitting

However, by adding side grooves to the specimens plane strain conditions are induced and the cracks achieve steady state crack propagation for a finite time as indicated by the linear region of the load-displacement curve. Table 4-6 & Table 4-7 show that both the 1.0 mm and 1.5 mm side groove depths result in similar values representative of steady state crack propagation, and therefore either side groove depth would be appropriate in obtaining steady state values but the deepest side groove depth would be the best selection.

X80 with 1.5 mm side grooves			
Temperature	Equation	Slope	Average
20	load = -4.5564 * displacement + 40.09	-4.5564	
20	load = -3.6355 * displacement + 36.843	-3.6355	
20	load = -4.0688 * displacement + 40.372	-4.0688	-4.0869
0	load = -6.0051 * displacement + 47.716	-6.0051	
0	load = -4.9801 * displacement + 40.528	-4.9801	
0	load = -5.1356 * displacement + 46.061	-5.136	-5.37373
-20	load = -5.9441 * displacement + 47.075	-5.9441	
-20	load = -5.482 * displacement + 41.628	-5.482	
-20	load = -6.6171 * displacement + 53.246	-6.6171	-6.0144
-40	load = -7.4172 * displacement + 60.707	-7.4172	
-40	load = -6.5719 * displacement + 49.17	-6.5719	
-40	load = -7.309 * displacement + 43.231	-7.309	-7.09937
-60	load = -10.783 * displacement + 56.276	-10.783	
-60	load = -6.7107 * displacement + 39	-6.7107	
-60	load = -8.9622 * displacement + 52.37	-8.9622	-8.81863

Table 4-6. Slope of steady state region for X80 Charpy specimens with 1.5 mm side grooves

X80 with 1.0 mm side grooves			
Temperature	Equation	Slope	Average
20	load= -4.1385 * displacement + 42.916	-4.1385	
20	load = -4.6576* displacement + 44.522	-4.6576	
20	load = -4.0966 * displacement + 40.552	-4.0966	-4.29757
0	load = -5.6077 * displacement + 46.431	-5.6077	
0	load = -5.0835 * displacement + 43.032	-5.0835	
0	load = -5.3846 * displacement + 45.346	-5.3846	-5.3586
-20	load = -6.3639 * displacement + 51.206	-6.3639	
-20	load = -5.5583 * displacement + 49.659	-5.5583	
-20	load = -5.7764 * displacement + 49.474	-5.7764	-5.89953
-40	load = -7.8812 * displacement + 54.569	-7.8812	
-40	load = -7.721 * displacement + 50.459	-7.721	
-40	load = -6.385 * displacement + 49.212	-6.385	-7.32907
-60	load = -10.143 * displacement + 48.076	-10.783	
-60	load = -9.3688 * displacement + 57.993	-9.3688	
-60	load = -7.9805 * displacement + 50.734	-7.9805	-9.37743

Table 4-7. Slope of steady state region for X80 Charpy specimens with 1.0 mm side grooves

4.3.2.2 X70

The significance of the side grooves in manipulating the plane strain to plane stress ratio in the X70 specimens is more pronounced as the traditional specimens crack does not propagate under steady state crack propagation but rather the crack tears open slowly through impact and propagates under unsteady state conditions as evidenced by the significant load through impact as shown in Figure 4-39.

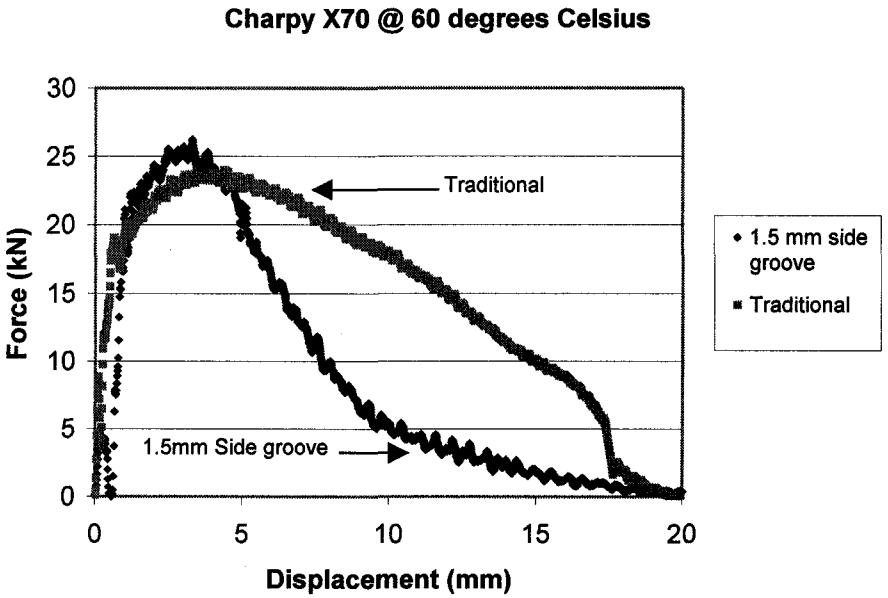

Figure 4-39. Load-displacement curves for X70 Charpy specimens tested at 60°C

The higher toughness of the traditional specimens and its effects on notch blunting results in the inability of the crack front to propagate under steady state conditions.

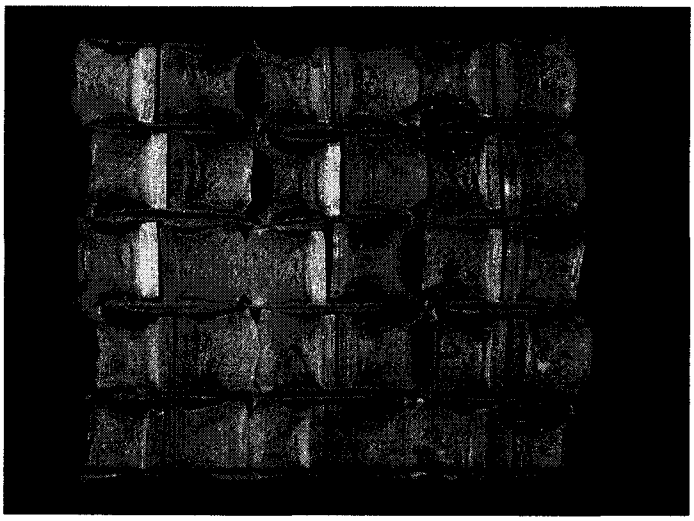

Figure 4-40. X70 Charpy specimens with no splitting

For specimens tested in the rising shelf region as shown in Figure 4-41, measurement of steady state crack propagation also could not be measured, as no linear region existed. Different energy values of unsteady state crack propagation exist in the three specimens tested at the 20°C as a result of different values of %SA fracture existing in all three specimens.

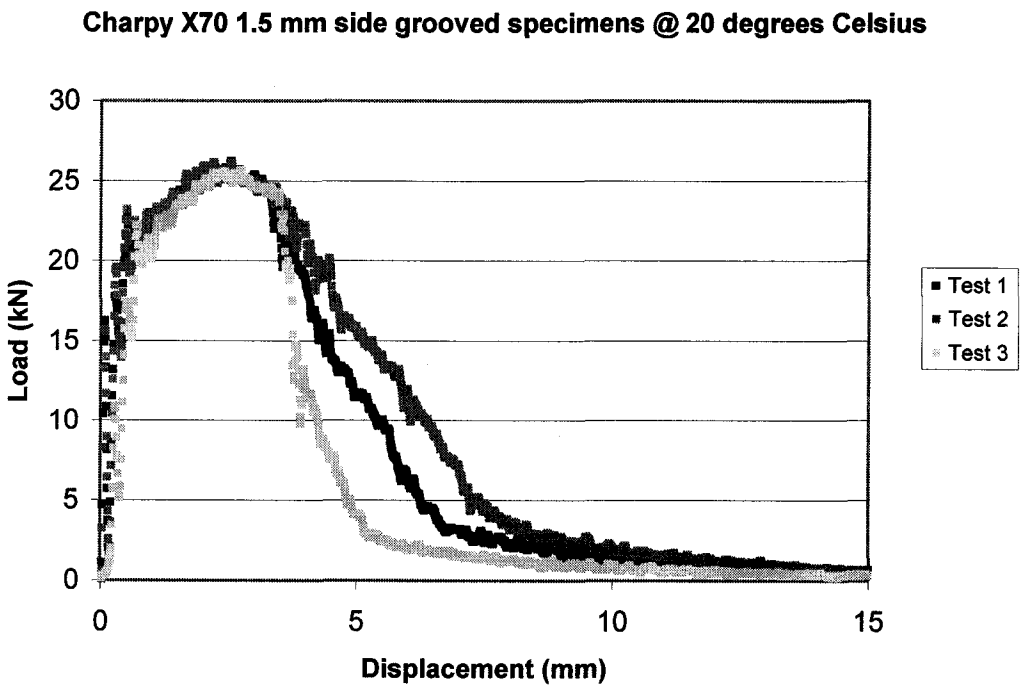

Figure 4-41. Load-displacement curves for X70 Charpy specimens with 1.5mm side grooves tested at 20°C

Hence further investigation of the side-grooved specimens was performed on X70 specimens with 1.5 mm side grooves tested in the upper shelf region at 80°C. Figure 4-42 displays similar toughness values for all the specimens tested at 80°C, this occurs as

a result of the 100% SA fracture occurring all three specimens tested in the upper shelf region.

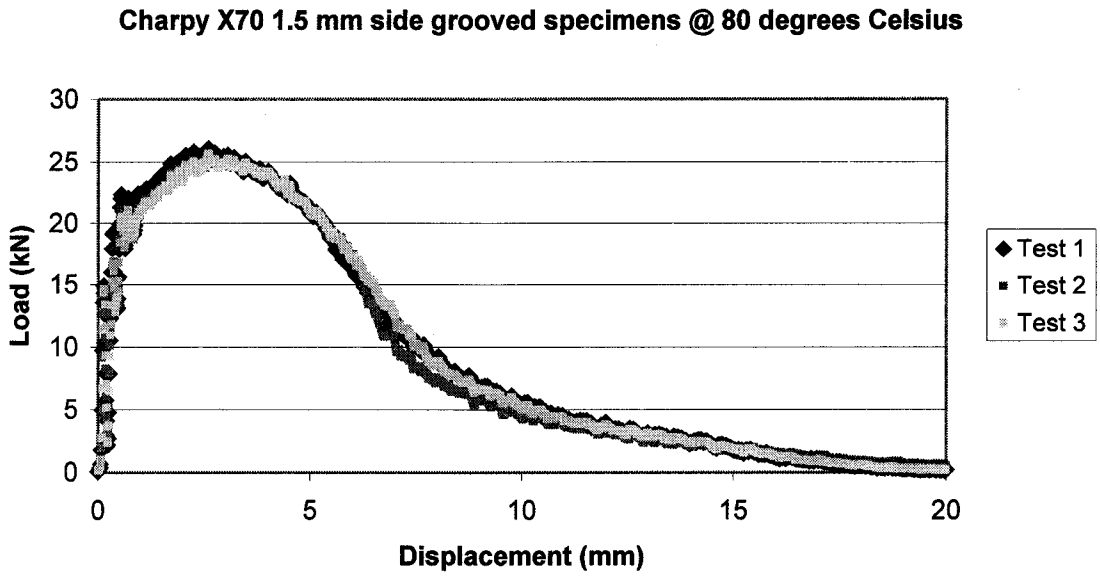

Figure 4-42. Load-Displacement Curves for X70 Charpy specimens with 1.5mm side grooves tested at 80°C

However, no region of steady state crack propagation exists with the X70 specimens tested in the upper shelf region as shown in Figure 4-43. Therefore, further tests may be necessary with specimens with deeper side grooves.

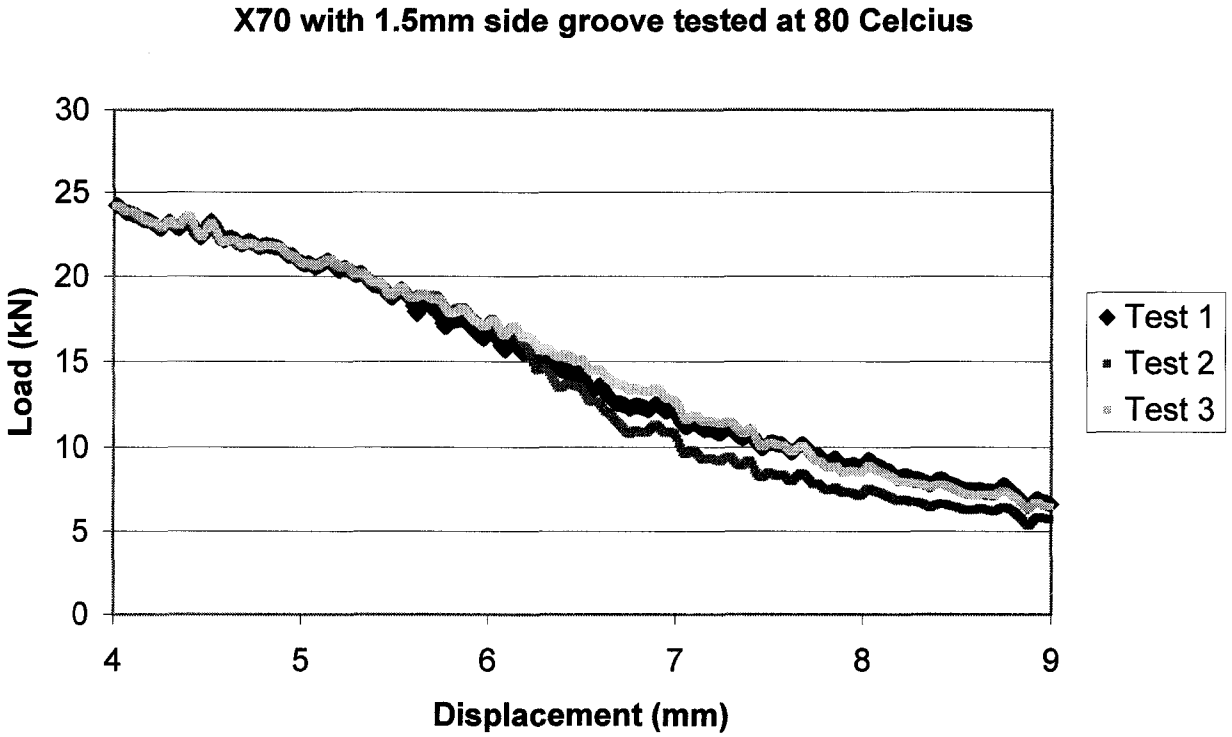

Figure 4-43. Propagation Region of X70 specimens tested at 80°C

A deeper side groove depth is definitely needed with the X70 Charpy specimens as fracture is dominated by notch blunting and no steady state crack propagation occurs as a result of X70's high toughness.

4.3.3 Conclusion measuring propagation energy

Measuring propagation energy has been shown to be successful with both the traditional DWTT X70 and X80 materials and the X80 Charpy specimens, and values representative of steady state crack propagation for each are shown in Figure 4-44. However, deeper

side grooves are necessary for the X70 Charpy specimens to increase the material constraint so steady state conditions will occur.

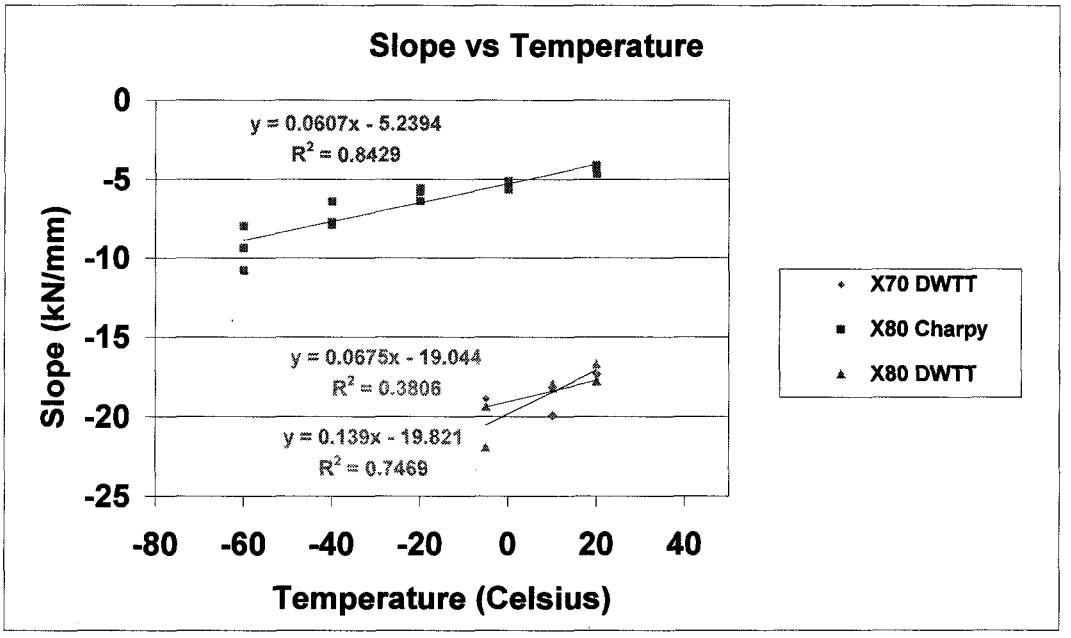

Figure 4-44. Values representative of steady state crack propagation

4.4 Splitting

Splitting has been shown to occur in steels where the finishing rolling temperature is below the Ar_3[52] due to the resulting segregation effects. And there is only a small reduction in the CV100 values. The splits seen in the fracture surface are the result of the segregation during the casting and forming processes, but only occur in the rising and initial upper shelf regions as seen in

Figure 4-45. The increase in temperature eliminates splitting by allowing the matrix to become sufficiently ductile such that it is able to more fully absorb the impact energy without any de-lamination between phases (splitting).

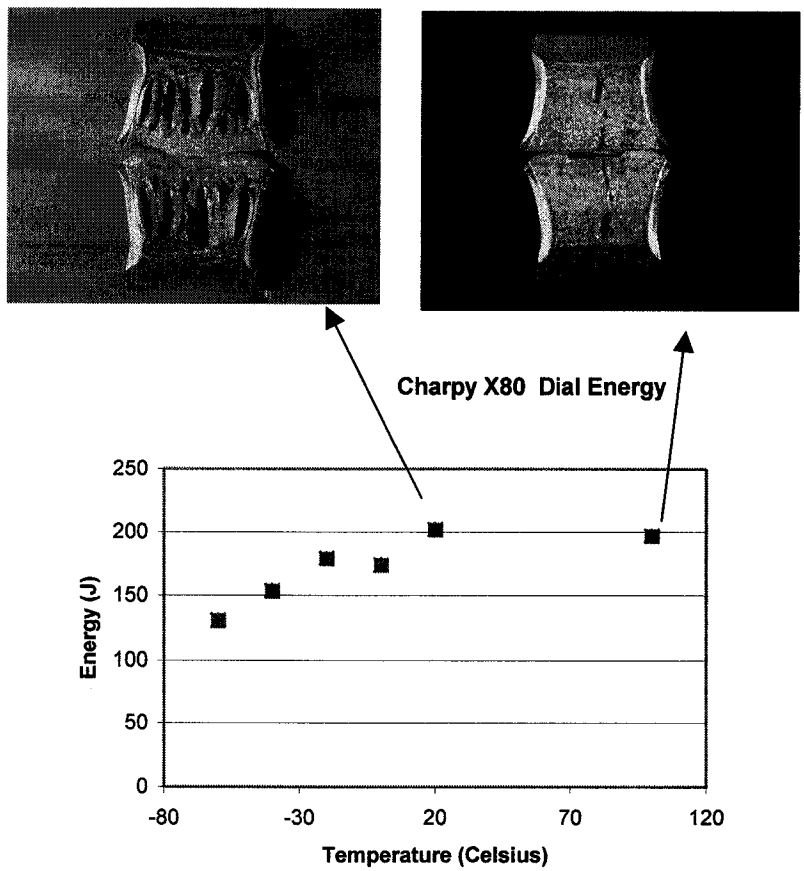

Figure 4-45. Energy absorbed by X80 Charpy specimen with 0.5 mm side grooves

4.5 Microstructure

The splitting that is often seen in the Charpy samples is a direct result of the microstructure of the steel. Microstructural analysis of the X80 material reveals a non-polygonal ferrite microstructure with a finely dispersed second phase. Etching the specimens with a modified La Pera's etch reveals the martensitic and feritic microstructures as the etch colors the ferrite tan, martensite and retained austenite white and bainite/carbide black as seen in Figure 4-46. The second phase was found to be more concentrated along the centerline but its distribution occurs throughout the thickness and these results agree with Sharma's work.[53]

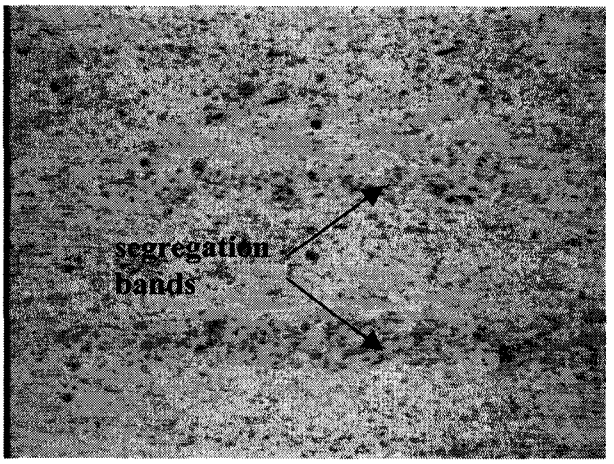

Figure 4-46. X80 Segregation bands

SEM work on a LaPera etch X80 specimen better revealed the distribution of the martensitic phase throughout the ferrite matrix. Interpretation of the photomicrograph reveals different phases are present, so an EDX spectrum was taken on the different area as seen in Figure 4-48 to check if different chemistries exist between the two phases. Analysis of the chemistry was inconclusive but the finely dispersed phase was assumed to be primarily martensitic because of its hardness.

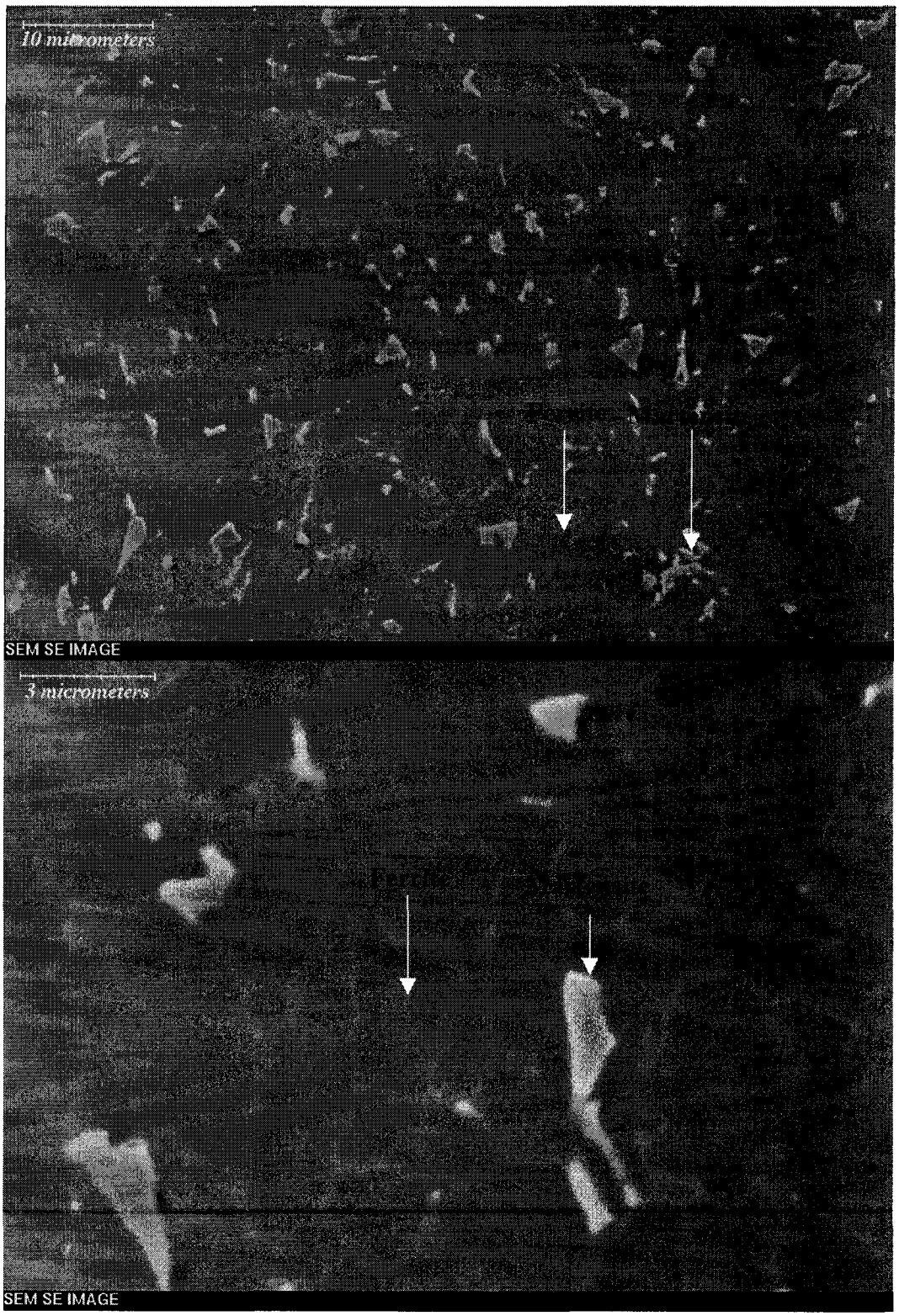

Figure 4-47. SEM micrograph of ferrite/martensite phases

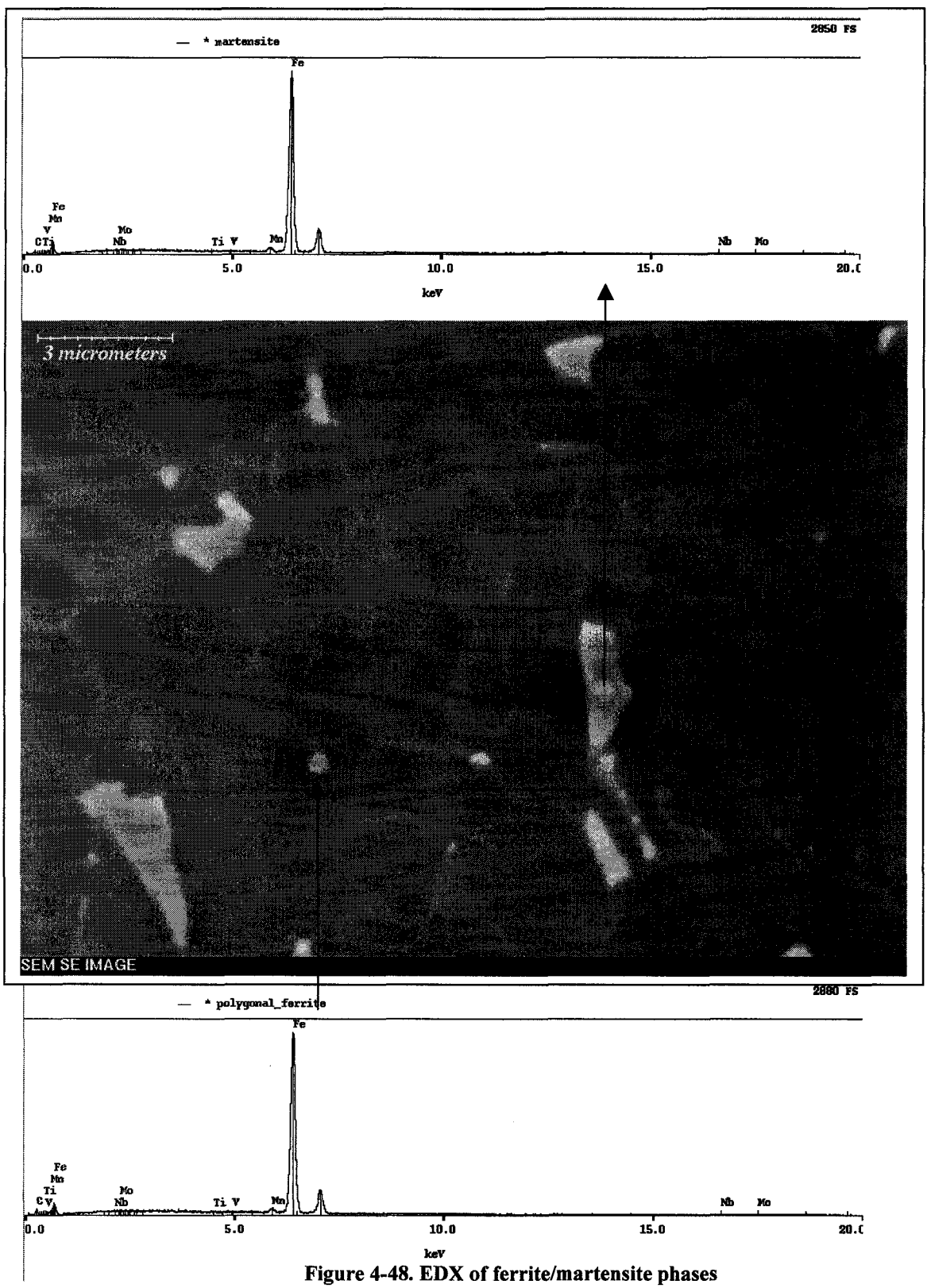

Figure 4-48. EDX of ferrite/martensite phases

Because the EDX analysis was inconclusive, a nano-hardness tester was subsequently used to determine the difference in hardness between the two phases. The size of the finely dispersed phase made it difficult to hit one individual phase, thus a cluster of the phase was selected to do a hardness test on. Figure 4-49 shows a photomicrograph of the indent that revealed the finely dispersed phase had a average hardness of HV320 while Figure 4-50 shows the average hardness of the ferrite matrix as being ~ HV210.

Figure 4-49. Vickers indents of the finely dispersed phase in the ferrite

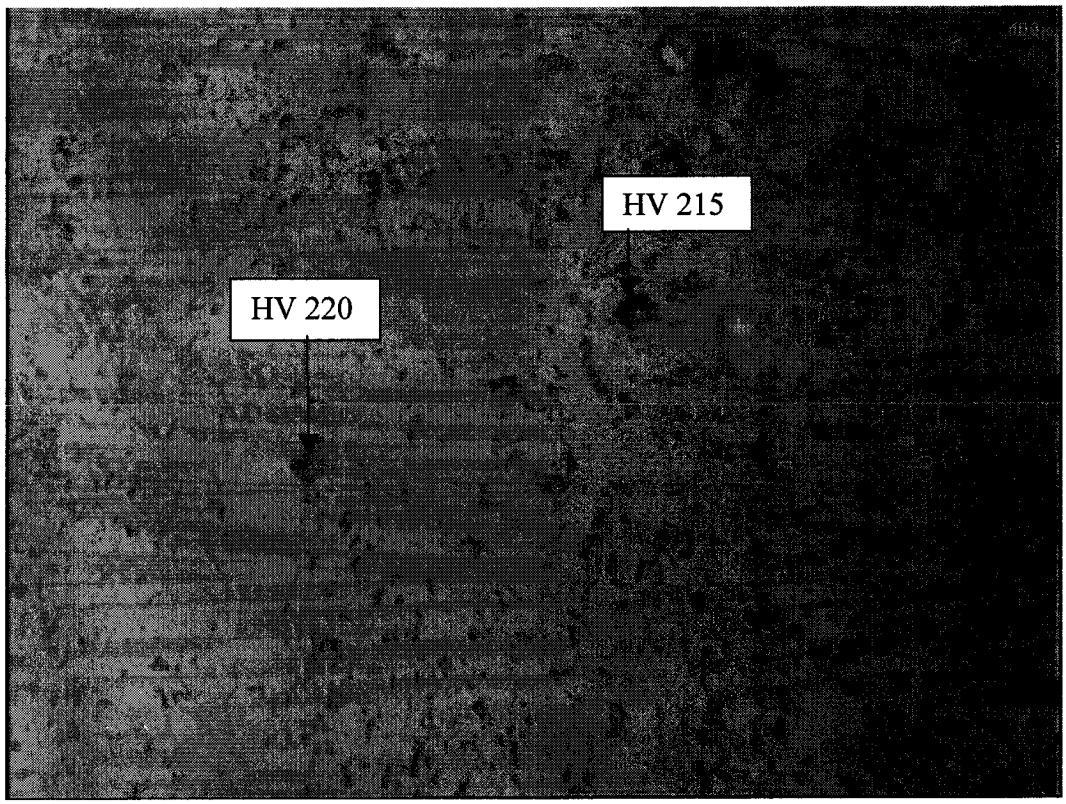

Figure 4-50. Vickers indents of ferrite phase

HV320 is the maximum hardness for martensite at about 0.15% as shown in Figure 4-51. Since the global carbon content of X80 is 0.033%, minimal segregation of carbon and some micro alloying elements is necessary.

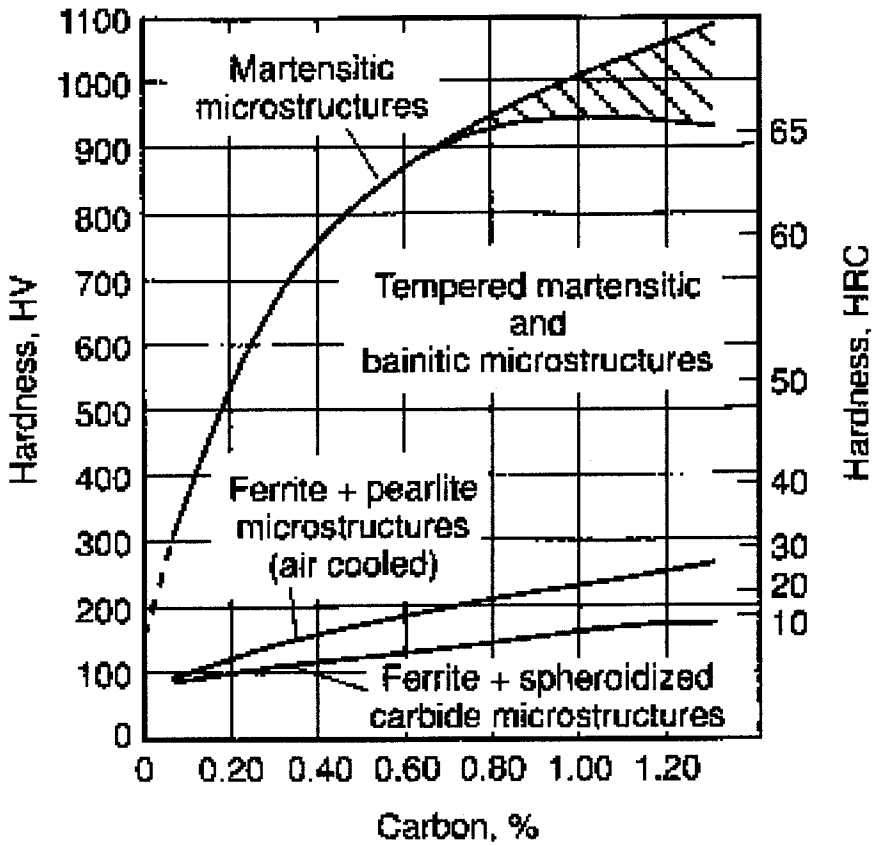

Figure 4-51. Hardness vs. carbon content[54]

Knowing that the white phase must be either martensite or retained austenite, the high hardness value of the white phase suggests it must be martensite as austenite cannot have such a high hardness values.

Splitting in the X-80 material occurs in a ductile manner by micro void coalescence as shown in Figure 4-52.

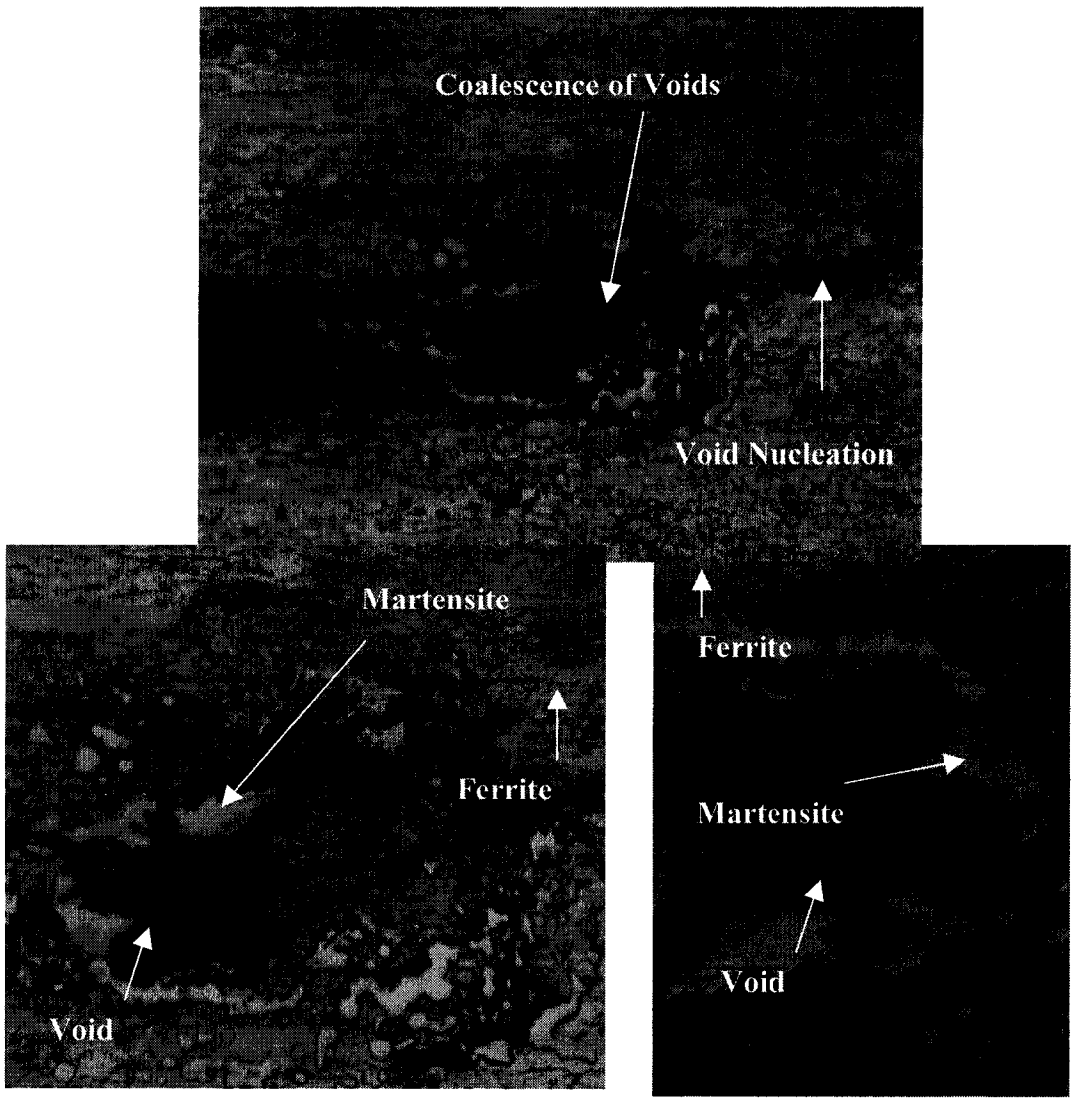

Figure 4-52. Photomicrographs of the fracture tip of the splits etched with Modified La Pera etch

The splits form in pipeline steels that have been rolled below the Ar_3[55] temperature. This type of themomechanical processing results in an aligned polygonal ferrite structure with dispersed martensitic or bainitic bands[56], which enables splitting. The nucleation of voids occurs either as a result of decohesion between the martensitic islands and the ferrite matrix or cracking within the brittle martensitic grain. These voids ultimately coalesce and result in the splitting features that are seen at lower temperatures.

During fracture, the splits separate the matrix into a number of thin platelets prior to the main fracture, which relieves the through-thickness restraint.[55] Because splitting relieves the through thickness restraint, it would be expected that deeper side groove depths would be required to increase the amount of material restraint to increase the plane strain conditions. However, the testing has shown that the X80 material achieves steady state propagation with the addition of side grooves as shown in Figure 4-36. Although the X70 specimens do not achieve steady state propagation with the addition of 1.5 mm side grooves as shown in Figure 4-39, increasing side groove depth increases the potential of steady state crack propagation occurring.

5 CONCLUSIONS AND RECOMENDATIONS

5.1 Conclusions

Based upon the work carried out in this study, the following conclusions about measuring the dynamic ductile fracture toughness of X70 and X80 pipeline steels:

1. With the use of instrumentation during impact tests, propagation energy can be separated from initiation energy. More importantly, the propagation energy can be separated into two regions: a) region of unsteady state crack propagation, b) region of steady state crack propagation.
2. Steady state crack propagation exists and can be measured on both the X70 and X80 DWTT specimens.
3. Lack of through thickness constraint in traditional Charpy specimens affects their ability to obtain steady state conditions. The required side groove depth for achieving steady state conditions is material dependent.
    a. With the X80 specimens a side groove depth of 1.0 mm will induce steady state propagation.
    b. With the X70 materials fracture with even the deepest side groove depth (1.5 mm) does not entirely induce steady state propagation although deeper side grooves do improve crack propagation characteristics.
4. The optical encoder and linear tape method is an improved alternative measurement method for measuring the energy absorbed in impact tests.
    a. Velocity measurement of a free fall DWTT can be measured with the DWTT. Excessive vibrations during specimen impact in the DWTT

affects the velocity measurements though, and hence the velocity during impact could not be measured with this test for the setup used.

b. Velocity measurement with an optical encoder during Charpy impact was shown to be a successful energy measurement tool.

5.2 Recommendations

1. Test deeper side grooved X70 Charpy specimens (2 mm), and check to see if this would be a deep enough side groove depth to induce steady state crack propagation.
2. Improve the optical encoder and linear tape measurement method by using an encoder that has a low electrical degree error (<3 ^{o}e).
3. Install the optical encoder and linear tape measurement system on a pendulum type DWTT machine to see if encoder measurement methods can be improved. If errors still exist install the encoder setup on a vibration-free pad.

REFERENCES

Literature Cited

[1] Buzzichelli, G., 2000, "Designing against ductile fracture propagation in very high strength steel gas pipelines: a review", Fracture Mechanics: Applications and Challenges (UK) , pp 235-252

[2] Afaganis, A.J., Mitchell, J.R., Carlson, L., Gilroy-Scott, A., 2000, "Design, development and confirmation of a high toughness gas line pipe for alliance pipeline at Camrose pipe company", *2000 International Pipeline Conference: IPC 00-0244,* pp 1-8

[3] Eiber, R.J., Maxey, W.A., 1979, "Fracture propagation control methods", *6th Symposium on Line Pipe Research* pp L1-L16

[4] Maxey, W.A., 1981, "Dynamic crack propagation in line pipe", *Sijthoff and Noordhoff* pp 109-123

[5] Wilkowski, G.M., Maxey, W.A., Eiber, R.J., 1978, "Ductile fracture propagation resistance of rising shelf controlled-rolled steels", *What Does the Charpy Test Really Tell Us?*, pp108-132

[6] Killmore, C., Barbaro, F., Williams, J., Rothwell, B., 1997, "Limitations of the Charpy test for specifying fracture propagation resistance", *International Seminar on Fracture Control in Gas Pipelines,* pp 1-17

[7] Pussegoda, N., Malik, L., Dinovitzer, B., Graville, A., Rothwell, B., 2000, "An interim approach to determine dynamic ductile fracture resistance of modern high toughness pipeline steels", *2000 International Pipeline Conference,* pp 239-245

[8] Demofonti, G. et al, 1995, "Step by step procedure for the two specimen CTOA test", *Pipeline Technology*, Vol. 2, pp 503-512

[9] Wilkowski, G.M. Rudland, D.L., Wang, Y.Y., Horsely, D., Glover, A., Rothwell, B., 2002, "Determination of the region of steady-state crack growth from impact tests", *Proceedings of IPC'02: IPC2002-27132,* pp 1-7

[10] O'Donoghue, P.E, Kanninen, M.F., Leung, C.P., Demofonti, G., Venzi, S., 1997, "The development and validation of a dynamic fracture propagation model for gas transmission pipelines", *Int. J. Pres. Ves. & Piping,* Vol 70, pp 11-25

[11] Jones, R., Rothwell, B., 1997, "Alternatives to Charpy Testing for Specifying Pipe Toughness", *Proceedings of the international seminar on fracture control in gas pipelines,* WTIA. June3, 1997.

[12] Bonomo, F., Buzzichelli, G.,Demofonti, G,., 1986, "Evaluation of ductile fracture propagation resistance in high grade (>=X70) pipeline steels with full scale and laboratory tests", *Boll. Tec. Finsider,* pp 126-129

[13] Pussegoda, L.N., Verbit, S., Dinovitzer, A., Tyson, W., Glover, A., Collins, L., Carlson, L., Beattie, J., 2000, "Review of CTOA as a measure of ductile fracture toughness", *2000 International Pipeline Conference,* pp 247-254

[14] Demofonti, G., Rizzi, L., 1991, "Experimental Evaluation of CTOA in Controlling Unstable Ductile Fracture Propagation", *Defect Assessment in Components – Fundamentals and Applications,* ESIS/EGF9, pp 693-703

[15] Mannucci G., Buzzichelli G., Eiber, R., Salvini, P., Carlson, L., 2000, "Ductile Fracture Arrest Assessment in a Gas Transmission Pipeline using CTOA", *2000 International Pipeline Conference*, pp 315-320

[16] Wilkowski, G.M. Maxey, W.A., Eiber, R.J., 1980, "Use of the DWTT energy for predicting ductile fracture behavior in controlled-rolled steel line pipes", *Canadian Metallurgical Quarterly*, Vol.19, pp 59-77

[17] Wilkowski, G.M., Mihell, J.N., 1998, "Ductile fracture arrest methodology for current and future grades of linepipe steels", *Materials for resource recovery and transport,* pp 267-295

6[18] Nanstad, R.K., Sokolov, M.A., 1995, "Charpy impact test results on five materials and NIST verification specimens using instrumented 2-mm and 8-mm strikers", *Pendulum Impact Machines: Procedures and specimens for verification: ASTM STP 1248,* pp.111-139

[19] Sokolov, M. A., Merkle, J. G., 2000, "Estimation of NDT and Crack-Arrest Toughness from Charpy Force-Displacement Traces", *Pendulum Impact Testing: A Century of Progress: ASTM STP 1380*

[20] Towers,O.L, 1986 "Testing Sub-Size Charpy Specimens. I. The Influence of Thickness on the Ductile/Brittle Transition", *Metals Construction*, vol. 18, no. 3, pp. 171R-176R

[21] Towers,O.L, 1986 "Testing Sub-Size Charpy Specimens. II. The Influence of Thickness on the Ductile/Brittle Transition", *Metals Construction*, vol. 18, no. 4, pp. 254R-258R

[22] Zhang, X.P., Shi, Y.W., 1995, "The reasonable design of Charpy-size specimen for fracture toughness test in nuclear surveillance", *International Journal of Pressure Vessel and Piping,* Vol 62, pp 219-225

[23] Smith, E., Patchett, B.M., 1975, "Effects of Notch Acuity and Side Grooving on Fracture Toughness", Vol. 54, No. 6, pp 169s-177s

[24] Smith, E., Patchett, B.M., 1975, "Effects of Notch Acuity and Side Grooving on Fracture Toughness", Vol. 54, No. 7, pp (7), pp 226s-233s

[25] Neale, B.K., 1982, "The influence of side-grooving on pre-cracked charpy specimens in bending", *International Journal of Pressure Vessels and Piping*, pp 375-398

[26] Anderson, T.L., 1994, "Fracture Mechanics: Fundamentals and Applications" *CRC Press, Boca Raton, FL*

[27] Broek, D., 1974, "Elementary Engineering Fracture Mechanics", *Noordhoff International Publishing*

[28] Wilkowski, G.M., Rudland, D.L., Wang, Y.Y., Horsley, D., Rothwell, B., Glover, A., 2002, "Development of a procedure for the calculation of J-R curves from pressed-notched drop weight tear test specimens", *Proceedings of IPC'02: IPC2002-27028,* pp 1-9

[29] Leis, B.N., 2002, "Evolution of line-pipe steel and its implications for transmission pipeline design", *Proceedings of IPC'02: IPC2002-27015,* pp 1-12

[30] Leis, Brian N., and Eiber, Robert J., 1998 "Fracture Propagation Control in Onshore Transmission Pipelines", *2nd International Onshore Pipelines Conference,*

[31] Ireland, D.R., 1973, "Procedures and problems associated with reliable control of the instrumented impact test", *Instrumented Impact Testing: ASTM STP 563,* pp 3-29

[32] Kalthoff, J.F., van Walle, E., Wilde, G., 1996, "Variations of the sensitivity of instrumented ISO/DIN and ASTM Tups and their influences on the determination of impact energies in tests with ductile steels", *Evaluating Material Properties by Dynamic Testing: ESIS Publication 20*, pp 25-35

[33] Sreenivasan, P.R., 1996, "Instrumented impact testing-accuracy, reliability and predictability of data", *Trans. Indian Inst. Met.,* Vol. 49, No. 5, pp 677-696

[34] Naniwa, T., Shibaike, M., Tanaka, M., Tani, H., Shiota, K., Hanawa, N., Shiraishi, T., 1990, "Effects of the striking edge radius on the charpy impact test", *Charpy Impact Test: Factors and Variables*, pp 67-80

[35] Kobayashi, T., Yamamoto, I., Niinomi, M., 1987, "On the accuracy of measurement of dynamic elastic-plastic fracture toughness parameters by the instrumented charpy test", *Engineering Fracture Mechanics,* Vol. 26, No. 1, pp 83-94

[36] Battelle, 1999, Pipeline Dynamic Fracture Testing Program, Vol 2

[37] Lenkey, G. B, Major, Z., Viehrig, H., 1992, "The dynamic calibration problems in instrumented impact testing", *ECF 9 Reliability and structural integrity of advanced materials*, pp 321-324

[38] Toropov, A.I., Grosso, M., 1998, "Dynamic Calibration of Impact Test Instruments", *Journal of Testing and Evaluation,* Vol. 26, No. 4, pp 315-319

[39] Kishimoto, K, Hirotsugu, I., Shibuya, T., 2000, "Dynamic force calibration for measuring impact fracture toughness using the charpy testing machine", *Pendulum Impact Testing: A Century of Progress: ASTM STP 1380,* pp 253-266

[40] Winkler, S., Vob, B., 1996, " Static Force Calibration of Charpy Impactors", *Evaluating Material Properties by Dynamic Testing,* pp 37-44

[41] Fink, D.A., 1990, "Quantitative Comparison and Evaluation of Various Notch Machining Methods and How They Affect ASTM E23 and ISO R442 Testing Equipment Results", *Charpy Impact Test: Factors and Variables,* pp 94-119

[42] Onizawa, K., van Walle, E., Nanstad, R.K., Sokolov, M., Pavinich, W., 1998, "Critical analysis of results from the ASTM round-robin on reconstitution", *Small Specimen Test Techniques,* pp 383-410

[43] Nanastad, R.K., Sokolov, M.A., 1995, "Charpy Impact Test Results on Five Materials and NIST Verification Specimens Using Instrumented 2-mm and 8-mm Strikers", *Pendulum Impact Machines: Procedures and Specifications for Verification,* pp 111-139

[44] Seiwert, T.A., Vigliotti, D.P., 1995, "The Effect of Charpy V-Nothch Striker Radii on the Absorbed Energy", *Pendulum Impact Machines: Procedures and Specifications for Verification,* pp 140-152

[45] Tanaka, M., Yoshinobu, O., Horigome, H., Tani, H., Shiota, K., Misawa, A., 1995, "Effects of the Striking edge Radius and Asymmetical Strikes on Charpy Impact Test Results", *Pendulum Impact Machines: Procedures and Specifications for Verification,* pp 153-167

[46] Manahan, M.P., Stoneifer, R.B., 2002, "Studies toward optimum instrumented striker designs", *From Charpy to Present Impact Testing (UK),* pp 221-228

[47]Welding Inspection, 1968, *American Welding Society,* New York, pp 146

[48] US Digital HEDS Encoder manual

[49] Manahan, M.P., Stonesifer, R.B., 2000, "The difference between total absorbed energy measured using an instrumented stiker and that obtained using an optical encoder", *Pendulum Impact Testing: A Century of Progress*, pp 181-197

[50] Snell, S.G., "Evaluation of Dynatup 8100F Drop-Weight Tester", *Ipsco Internal*

[51] Wilkowski, G.M., Rudland, D.L., Wang, Y.Y., Horsely, D., Rothwell, B., Glover, A., 2002, "Investigation Into the Use of a Single Specimen For the Determination of Dynamic Steady State Propagation Resistance in High Toughness Line-Pipe Steels", *Proceedings of IPC'02: IPC2002-27029,* pp 1-5

[52] http://www.cbmm.com.br/portug/sources/techlib/report/metall/metall.htm

[53] Sharma, U., 2000, "Microstructural characterization of microalloyed linepipe steel". Mater's Thesis, Department of Chemical and Materials Engineering, University of Alberta

[54] G. E. Krause: 'Properties and Selection: Irons, Steels and High Performance Alloys', 1990, Metals Park, Ohio, pp 127

[55] Eiber, R. J., Maxey, W. A., 1977, "Full-scale experimental investigation of ductile fracture behavior in simulated arctic pipeline", *Fracture in simulated arctic pipeline*, pp 306-319

[56] Wilkowski, G., Wang, Y. Y., Rudland, D., 1999, "Summary of recent efforts on characterizing propagating ductile fracture resistance of linepipe steels" *Proceedings of the International Conference on Advances in WeldingTechnology: Pipeline Welding and Technology*

Un-cited Literature

Bonomo, F., Buzzichelli, G.,Demofonti, G,., 1985, "Ductile Fracture Propagation in Gas Pipelines: an up-to-date survey of the "Italian Group" activity on high grade HSLA pipe materials", *HSLA Steels: Metallurgy and Applications,* pp743-751

Bernardo, G., Salvini, P., Mannucci, G., Demofonti, G., 2000, "On Longitudinal Propagation of a Ductile Fracture in a Buried Gas Pipeline: Numerical and Experimental Analysis", *2000 International Pipeline Conference,* pp 287-294

Lorriot, T., 2000, "Specimen Loading Determined by Displacement Measurement in Instrumented Charpy Impact Test", *Engineering Fracture Mechanics,* Vol. 65, pp 703-713

Morland, E., 1988, "Fracture Toughness in the transition regime for A533B-1 Steel: The effect of specimen sidegooving", *Fracture Mechanics Twenty-First Symposium: ASTM STP 1074*, pp 215-237

Radon, J.C., Turner, C.E., 1969, "Fracture Toughness Measurements by Instrumented Impact Testing", *Engineering Fracture Mechanics*, Vol. 1 Issue 3, pp 411-428

Turner, C.E., 1969, "Measurement of Fracture Toughness by Instrumented Impact Test", *Impact Testing of Metals: ASTM STP 466*, pp 93-114

Venzi, S., Priest, A.H., May, M.J., 1970, "Influence of Inertial Load in Instrumented Impact Tests", *Impact Testing of Metals: ASTM STP 466*, pp 165-180